NASA TM X-1087

TRANSONIC AERODYNAMIC CHARACTERISTICS OF A LIFTING REENTRY VEHICLE HAVING A DELTA PLANFORM AND A FLAT BOTTOM

By Charles D. Harris and Arvo A. Luoma

Langley Research Center
Langley Station, Hampton, Va.

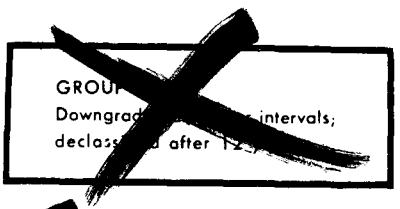

NATIONAL AERONAUTICS AND SPACE ADMINISTRATION

TRANSONIC AERODYNAMIC CHARACTERISTICS OF A LIFTING REENTRY VEHICLE HAVING A DELTA PLANFORM AND A FLAT BOTTOM*

By Charles D. Harris and Arvo A. Luoma
Langley Research Center

SUMMARY

An investigation was made in the Langley 8-foot transonic pressure tunnel of the static longitudinal and lateral stability and control characteristics of a 1/10-scale model of a lifting-body reentry vehicle, designated as Space Vehicle 5 (SV-5), having a 77° swept delta planform, a blunt nose, a flat bottom, and extensive boattailing. The investigation was made at Mach numbers from 0.50 to 1.20 and through an angle-of-attack range from approximately -2° to 24° at fixed angles of sideslip of approximately 0.4°, -3.4°, and -6.5°. The results include the effect on the aerodynamic characteristics of deflection of upper and lower trailing-edge flaps, of deflection of rudders on outboard vertical tails, and of model components.

The body-canopy configuration was longitudinally stable at the higher angles of attack and directionally unstable at all angles of attack. The outboard vertical tails made the configuration longitudinally stable at most test conditions and directionally stable at angles of attack up to about 18° at a Mach number of 0.50, up to only about 1° at a Mach number of 0.95, and up to about 9° at Mach numbers of 1.00 and 1.20. The directional-stability characteristics were improved by the central vertical tail and generally improved somewhat by the modified vertical tails. The canopy aggravated a loss in longitudinal stability at high angles of attack at high subsonic Mach numbers and generally had an adverse effect on directional stability. Large deflections of the upper and lower flaps improved the longitudinal-stability characteristics. The flaps were effective in changing the trim angle of attack. Uniform deflection of the rudders (as directional controls) produced substantial yawing moments but rather large adverse rolling moments. The effective-dihedral derivative of all configurations was usually negative in sign (that is, positive dihedral effect).

INTRODUCTION

Extensive studies of the aerodynamic characteristics of many types of lifting-body vehicles with a capability for reentry into and maneuverability

within the earth's atmosphere have been made by the National Aeronautics and Space Administration at Mach numbers ranging from hypersonic to low subsonic. (For example, see refs. 1 to 7.) Also included in such studies was a lifting-body reentry vehicle, designated as Space Vehicle 5 (SV-5), having a 77° swept delta planform, a blunt nose, a flat bottom, and extensive boattailing. Wind-tunnel investigations of this configuration were made at the Langley Research Center at subsonic, transonic, and supersonic speeds. The static longitudinal and lateral stability and control characteristics of a 1/10-scale model of this configuration were investigated at subsonic and transonic speeds in the Langley 8-foot transonic pressure tunnel, and these results are presented herein. Supersonic results are presented in reference 8.

The results from the present investigation include (1) the effect on the aerodynamic characteristics of upper and lower trailing-edge flaps uniformly deflected for pitch control and differentially deflected for roll control, (2) the effect on the aerodynamic characteristics of rudders on outboard vertical tails uniformly deflected for directional control and differentially deflected (trailing edges of rudders deflected outward) for stability improvement, (3) the incremental effect on the aerodynamic characteristics of outboard and central vertical tails, and (4) the incremental effect on the aerodynamic characteristics of a canopy. The investigation was made at Mach numbers from 0.50 to 1.20 and through an angle-of-attack range from approximately -2° to 24° at fixed angles of sideslip of approximately 0.4°, -3.4°, and -6.5°.

SYMBOLS

The lift and drag data are referred to the stability axes, the rolling-moment and yawing-moment data are referred to the body axes, and the side-force and pitching-moment data are referred to the common lateral axis of the stability and body axes (fig. 1). The origin of the stability and body axes is the moment reference point located longitudinally at model station 15.732 inches and vertically at model water line 2.640 inches. This location corresponds to 57 percent of the reference length of the body and 40 percent of the maximum height of the body.

b reference span used for computations; maximum width of body without outboard vertical tails (model value, 12.0 in.)

C_D drag coefficient, $\frac{\text{Drag}}{qS}$

C_L lift coefficient, $\frac{\text{Lift}}{qS}$

C_l rolling-moment coefficient, $\frac{\text{Rolling moment}}{qSb}$

$C_{l_\beta} = \frac{\Delta C_l}{\Delta \beta}$, per deg

C_m pitching-moment coefficient, $\frac{\text{Pitching moment}}{qSl}$

$C_{m_{\delta_l}} = \frac{\Delta C_m}{\Delta \delta_l}$, per deg

$C_{m_{\delta_u}} = \frac{\Delta C_m}{\Delta \delta_u}$, per deg

C_n yawing-moment coefficient, $\frac{\text{Yawing moment}}{qSb}$

$C_{n_\beta} = \frac{\Delta C_n}{\Delta \beta}$, per deg

$C_{p,1}$ pressure coefficient in balance chamber

$C_{p,2}$ pressure coefficient at base between left flaps

$C_{p,3}$ pressure coefficient at base between right flaps

C_Y side-force coefficient, $\frac{\text{Side force}}{qS}$

$C_{Y_\beta} = \frac{\Delta C_Y}{\Delta \beta}$, per deg

d diameter

L/D lift-drag ratio, C_L/C_D

$(L/D)_{max,trim}$ maximum value of trimmed lift-drag ratio

l reference length used for computations; distance from body nose to theoretical body base (model value, 27.6 in.)

M Mach number of undisturbed stream

q dynamic pressure of undisturbed stream

R Reynolds number based on model reference length l

r radius

S reference area used for computations; planform area of body to theoretical body base and without outboard vertical tails (model value, 1.62 sq ft)

X,Y,Z reference axes

α angle of attack measured relative to flat bottom surface

β angle of sideslip

δ_l lower-flap deflection measured with respect to stowed position and in plane perpendicular to hinge line; positive direction when trailing edge is down (Subscripts L and R refer to left or right flap when flaps differentially deflected; omission of L or R subscript indicates that flaps had same deflection.)

δ_u upper-flap deflection measured with respect to stowed position and in plane perpendicular to hinge line; positive direction when trailing edge is down (Subscripts L and R refer to left or right flap when flaps differentially deflected; omission of L or R subscript indicates that flaps had same deflection.)

δ_r rudder deflection (on outboard vertical tails) measured in plane perpendicular to hinge line; positive direction when trailing edge is to left (Subscripts L and R refer to left or right rudder when rudders differentially deflected; omission of L or R subscript indicates that rudders had same deflection.)

APPARATUS

Tunnel

The investigation was made in the Langley 8-foot transonic pressure tunnel. The test section of this tunnel is square in cross section with the upper and lower walls axially slotted to permit changing the test-section Mach number continuously from 0 to over 1.20 with negligible effects of choking and blockage. The total pressure of the tunnel air can be varied from a minimum value of about 0.25 atmosphere at all test Mach numbers to a maximum value of about 1.5 atmospheres at transonic Mach numbers and about 2.0 atmospheres at Mach numbers of 0.40 and less. The tunnel air is dried sufficiently to avoid condensation effects.

Model

The model used in the present investigation was a sting-supported 1/10-scale model of the SV-5 lifting-body reentry vehicle having a 77° swept delta planform, a blunt nose, a flat bottom, and extensive boattailing. The reentry vehicle had upper and lower flaps at the body base for longitudinal and roll

control, outboard vertical tails with rudders for directional stability and control, and a central vertical tail without a rudder for additional directional stability. A canopy was included in some of the configurations. A three-view drawing of the full-scale vehicle is given in figure 2 and the geometric characteristics of the model are given in table I.

Detailed drawings of the model are given in figures 3 to 5, but full-scale dimensions are used. The upper and lower flaps are presented in figure 3 and the basic outboard vertical tail with rudder in figure 4(a). The basic central vertical tail in side view was a projection of the basic outboard vertical tail (it should be noted that the exposed span and area were less for the central vertical tail), but differed in thickness, being essentially a flat plate. Modified outboard and central vertical tails were also investigated, and these differed only in the tip geometry from the basic vertical tails; the modification increased the area of the central vertical tail by about 11 percent and the area of each outboard vertical tail by about 8 percent. (See fig. 4(b).) External dummy support rods (fig. 5), which simulated the rods used to support the model in an investigation made in another wind tunnel, were tested in the present investigation in order to determine the interference effects of the rods on the aerodynamic characteristics.

Various combinations of the body (including the upper and lower flaps) with the other model components were investigated, and these configurations are identified herein as follows:

Configuration	Canopy	Vertical tails		External dummy support rods
		Outboard	Central	
1	On	Off	Off	Off
2	On	Basic	Off	Off
3	On	Basic	Basic	Off
4	Off	Basic	Basic	Off
5	Off	Modified	Modified	Off
6	Off	Basic	Basic	On

Instrumentation

Aerodynamic force and moments were measured with a six-component internal strain-gage balance. The model and balance were supported by a 1.375-inch-diameter sting which, in turn, was attached to a remotely controlled three-position sideslip mechanism. Three base static-pressure orifices, one located in the chamber surrounding the strain-gage balance, the second between the upper and lower left flaps, and the third between the upper and lower right flaps, were connected to pressure transducers. The overall forces and moments on the model, the angle of attack, the angle of sideslip, the static pressure in the chamber surrounding the strain-gage balance, and the static pressures at the body base between the upper and lower left and right flaps were recorded electronically on punch cards.

TESTS, CORRECTIONS, AND ACCURACY

Tests

The investigation was made at Mach numbers from 0.50 to 1.20, at a total pressure of approximately 1 atmosphere, and at a stagnation temperature of 120° F. The Reynolds number of the investigation is shown in figure 6. The tests were made at angles of attack from approximately -2° to 24° at the fixed angles of sideslip of approximately 0.4°, -3.4°, and -6.5°. The actual values of the angles of sideslip for the various configurations are given in figure 7.

The investigation included tests to determine the effect on the aerodynamic characteristics of the upper and lower flaps uniformly deflected for pitch control and differentially deflected for roll control, the effect on the aerodynamic characteristics of the rudders on the basic outboard vertical tails uniformly deflected for directional control and differentially deflected (trailing edges of rudders deflected outward) for stability improvement, the incremental effect on the aerodynamic characteristics of the outboard and central vertical tails, and the incremental effect on the aerodynamic characteristics of the canopy. Modifed outboard and central vertical tails with undeflected rudders were tested in an attempt to improve the directional stability. The various combinations of model components, upper-flap deflection, lower-flap deflection, and rudder deflection investigated are listed in table II. The combination of flap deflections of -30° on the upper flaps and 20° on the lower flaps was taken to be the basic flap setting in the present investigation since earlier investigations had shown that this combination of deflections provided more satisfactory longitudinal stability and trim characteristics than combinations of lower values of deflections. The configuration with and without the external dummy support rods, however, was investigated at an upper-flap deflection of -10° and a lower-flap deflection of 0°; for these tests, also, the trailing edges of the rudders were deflected 10° inward. All tests were made with natural transition on the model.

Corrections

The data presented herein have not been corrected for base pressure. The values of the base-pressure coefficient in the balance chamber $C_{p,1}$, between the left flaps $C_{p,2}$, and between the right flaps $C_{p,3}$ are included herein at all test conditions. The angle of attack and sideslip have been corrected for the deflection of the balance and sting support under aerodynamic load.

At subsonic and sonic Mach numbers, the interference effects of the tunnel boundary on the flow over the model in the slotted test section are considered negligible. At a Mach number of 1.20, the data presented herein are considered free of tunnel-boundary interference for angles of attack up to approximately 10°. At angles of attack greater than approximately 10°, however, schlieren photographs indicate that the reflection of the model bow wave from the upper boundary of the tunnel impinged on the upper rearward portions of the model. The effect of this impingement on the data has not been evaluated. The data at

angles of attack greater than approximately 10° at a Mach number of 1.20 therefore should be considered to be of questionable validity as a result of boundary interference; particularly suspect would be the drag results, which usually can be expected to be too low in magnitude when the reflected shock impinges in the vicinity of the model base. Even though the magnitudes and slopes of the data at the high angles of attack may have been modified by boundary interference, the general trends shown by these data may still be correct. In the belief that these data may be useful, they are included herein uncorrected for boundary interference.

Accuracy

The accuracy of the data, based primarily on the static calibrations and the repeatability of the data, is estimated to be as follows:

For all Mach numbers:	
α, deg	±0.10
β, deg	±0.15
M	±0.005
For Mach numbers of 0.90 and above:	
C_L	±0.005
C_D	±0.0015
C_m	±0.0003
C_n	±0.0005
C_l	±0.0003
C_Y	±0.002
$C_{p,1}$, $C_{p,2}$, and $C_{p,3}$	±0.01

For Mach numbers less than 0.90, for which the dynamic pressures were substantially less than those at the higher Mach numbers, the accuracy of the data expressed in aerodynamic-coefficient form was correspondingly poorer than that listed.

PRESENTATION OF RESULTS

The basic longitudinal aerodynamic data are presented in figures 8 to 21 as plots of aerodynamic coefficients against angle of attack for fixed values of angle of sideslip. The results of figures 14 to 21 have been arranged into groupings which make possible a more direct comparison of the effects of model components and control deflections; this arrangement necessitated the presentation of the results for some of the configurations more than once.

Summary longitudinal aerodynamic characteristics are shown plotted against Mach number in figures 22 to 24. The flap effectiveness parameters $C_{m_{\delta_u}}$ and

$C_{m_{\delta_l}}$, where $C_{m_{\delta_u}}$ is the average value for upper-flap deflections from -40° to -20° and $C_{m_{\delta_l}}$ is the average value for lower-flap deflections from 10° to 30°, are presented in figure 22 at an angle of attack of 15°; this value of angle of attack was selected as being representative of those at which $(L/D)_{max,trim}$ occurred. Trim values of $(L/D)_{max}$, with trim being obtained by using either the upper flaps or the lower flaps, are presented in figures 23 and 24, respectively.

The basic lateral aerodynamic data are presented in figures 25 to 32. The arrangement of presentation is similar to that used for the basic longitudinal aerodynamic data.

Summary lateral-stability derivatives are shown plotted against angle of attack in figures 33 to 37 and against Mach number at an angle of attack of 15° in figures 38 to 41. The value of the lateral-stability derivatives shown was taken as the average slope for angles of sideslip from approximately -3.4° to 0.4° for the data of figures 33 to 36 and 38 to 40 (except for the flagged data of fig. 36); and from approximately -6.5° to 0.4° for the flagged data of figure 36 and for the data of figures 37 and 41. The flagged and unflagged results at a rudder deflection of 0° shown in figure 36 give an indication of the linearity of the variation of the lateral coefficients with angle of sideslip.

The results of this investigation are presented as follows:

DISCUSSION

As mentioned previously, the basic flap setting in the present investigation was taken to be -30° on the upper flaps and 20° on the lower flaps, and most tests, accordingly, were made with this flap setting. The base-pressure results (figs. 8 to 13) are made available herein for possible future analytical use, but are not discussed further.

Longitudinal Characteristics

Body-canopy configuration.- The body-canopy configuration (configuration 1) was investigated only at Mach numbers of 0.70, 0.90, and 1.00. The lift-curve slope of this configuration generally increased with angle of attack. (See fig. 14(a).) The configuration was longitudinally unstable at the lower angles of attack but became stable at the higher angles of attack. (See fig. 14(c).) An increase in Mach number rotated the pitching-moment curves in a stable direction and, thereby, substantially decreased the angle of attack at which the configuration became stable. At a Mach number of 1.00, trim was realized at an angle of attack of approximately 20°.

Basic outboard vertical tails.- Addition of the basic outboard vertical tails to the body-canopy configuration (addition of basic outboard vertical tails to configuration 1 gives configuration 2) had a substantial effect on the longitudinal aerodynamic characteristics as shown by the results of

figure 14. As the drawing of figure 2 indicates, the outboard vertical tails were canted, or rolled out, 16° with respect to the plane of symmetry; this amount of cant resulted, as expected, in a component of force in the lift direction which contributed significantly to the lift and pitching-moment characteristics.

Although the trends are not readily apparent from a cursory inspection of the basic data of figure 14(a), these data show that at a given Mach number the increment in lift coefficient resulting from the addition of the outboard vertical tails first increased with angle of attack at the lower angles of attack, became a maximum at an intermediate value of angle of attack, and then decreased with further increase in angle of attack; this loss in lift increment at high angles of attack was probably due to flow separation on the inner surfaces of the outboard vertical tails and on the upper surface of the adjoining body. The effect of an increase in Mach number was to reduce the lift increment at all angles of attack and to cause the loss in lift increment to begin at a lower angle of attack.

The addition of the outboard vertical tails to the body-canopy configuration shifted the pitching-moment curves in a negative direction at all test conditions, and the amount of shift varied with angle of attack in a manner very similar to the variation with angle of attack of the incremental lift due to the outboard vertical tails. (See fig. 14(c).) In general, the configuration with the outboard vertical tails was longitudinally stable; however, at a Mach number of 0.95 for angles of attack near 0° and at a Mach number of 0.90 for high angles of attack the configuration was unstable; at Mach numbers of 0.95, 1.00, and 1.20 for high angles of attack the configuration showed some reduction in stability. The trim angle of attack was low at all Mach numbers and was, for example, about 5° at a Mach number of 1.00 and negative by a substantial amount at a Mach number of 1.20.

The drag coefficient was substantially increased at all test conditions by the addition of the outboard vertical tails, with the largest increase being evident at a Mach number of 0.70 at high angles of attack. (See fig. 14(b).) The maximum lift-drag ratio, however, was increased at all Mach numbers because of the higher lift-curve slope when the outboard vertical tails were on.

Basic central vertical tail.- The addition of the basic central vertical tail to the configuration consisting of body, canopy, and basic outboard vertical tails (addition of the basic central vertical tail to configuration 2 gives configuration 3) generally resulted in small decreases in lift and drag and essentially no change in maximum lift-drag ratio at all test conditions. (See figs. 14(a), 14(b), and 14(d).) The effect on pitching moment was a small change in trim, which resulted in a higher trim angle of attack and essentially no change in longitudinal stability (that is, in slope). (See fig. 14(c).) The trim angles of attack for the configuration with the basic central vertical tail at Mach numbers of 1.00 and 1.20, for example, were about 7° and -2°, respectively.

Modified outboard and central vertical tails.- Replacement of the basic outboard and central vertical tails on the canopy-off configuration (configuration 4) by the modified outboard and central vertical tails (configuration 5)

generally resulted in small increases in lift at subsonic Mach numbers and in drag at all Mach numbers at the low and intermediate angles of attack, and had negligible effect on maximum lift-drag ratios. (See figs. 15(a), 15(b), and 15(d).) The modified vertical tails generally shifted the pitching moments in a negative direction (for example, the trim angle of attack was reduced by about 3° to 5° at Mach numbers up to 0.90 and by lesser amounts at sonic and supersonic Mach numbers) and caused small decreases in stability at the highest angles of attack at some of the subsonic Mach numbers. (See fig. 15(c).)

Canopy.- Addition of the canopy to the configuration consisting of body, basic outboard vertical tails, and basic central vertical tail (addition of canopy to configuration 4 gives configuration 3) had a minor effect on lift, drag, and lift-drag ratio at all test conditions. (See figs. 16(a), 16(b), and 16(d).) The addition of the canopy generally shifted the pitching-moment coefficients in a positive direction, and this shift increased the trim angle of attack by about 2° at the low subsonic Mach numbers and at a Mach number of 1.20. (See fig. 16(c).) The addition of the canopy, however, aggravated the reduction in longitudinal stability and the longitudinal instability already evident at high angles of attack at the high subsonic and sonic Mach numbers.

Deflection of upper and lower flaps.- A limited amount of aerodynamic data was obtained in the present investigation at low values of deflection of the upper and lower flaps. These data, which are presented in figure 17, were obtained at Mach numbers from 0.50 to 0.80 for the canopy-off configuration (configuration 4) at an upper-flap deflection of -10°, a lower-flap deflection of 0°, and with the rudders differentially deflected $\pm 10^\circ$ (trailing edges of rudders were deflected inward). Also shown in figure 17 are the results (which will be discussed later) for the configuration with the external dummy support rods (configuration 6). As the figure shows, a definite break in the lift and pitching-moment curves occurred at an angle of attack which decreased as the Mach number was increased; the break in the pitching-moment curves was in an unstable direction and evidently was a consequence of the loss in lift. These unsatisfactory longitudinal-stability characteristics probably resulted from extensive flow separation on the inner surfaces of the outboard vertical tails and the upper surface of the adjoining body. Low values of deflection of the upper and lower flaps have appeared to be conducive to such separation; in addition, deflection of the rudders may have aggravated the problem.

Deflection of the upper and lower flaps to larger values has been found to have a beneficial effect on the longitudinal-stability characteristics. Accordingly, a more extensive investigation was made herein of the larger values of flap deflection. Figure 18 presents longitudinal aerodynamic characteristics at upper-flap deflections of -20°, -30°, and -40°, and figure 19, at lower-flap deflections of 10°, 20°, and 30°.

Deflection of the upper flaps from -20° to -40° while a constant deflection of the lower flaps of 20° was maintained shifted the lift in a negative direction by amounts which generally were substantial; however, the shift usually decreased at high angles of attack and at high Mach numbers. (See fig. 18(a).) A loss in lift (that is, a falloff in lift from a straight-line

variation with angle of attack), which was particularly evident at high angles of attack, occurred at a flap deflection of -20° and, to a much lesser extent, at deflections of -30° and -40°. The loss in lift at a deflection of -20°, however, was substantially less than the loss in lift at a lower deflection of the flaps noted previously and shown by the results of figure 17(a). These data indicate that deflection of the upper and lower flaps to large values resulted in a definite overall improvement in flow over the model.

Deflection of the upper flaps from -20° to -40° increased the drag at the lower angles of attack, generally decreased drag at the higher angles of attack, and, as a result of the higher minimum drag, reduced the maximum lift-drag ratio. (See figs. 18(b) and 18(d).)

Deflection of the upper flaps from -20° to -40° displaced the values of the pitching moment in a positive direction by amounts which usually decreased with increasing angle of attack at the high angles of attack and which substantially increased the trim angle of attack. (See fig. 18(c).) At a flap deflection of -40°, for example, the trim angle of attack was about 24° at a Mach number of 0.95, 18° at a Mach number of 1.00, and 12° at a Mach number of 1.20; this trim angle, it is to be noted, decreased considerably with Mach number at Mach numbers above 0.95. Deflection of the upper flaps from -20° to -40° usually increased the longitudinal stability somewhat at the intermediate and the higher angles of attack. The average value of the pitch effectiveness parameter $C_{m_{\delta_u}}$ for deflections from -20° to -40° is shown in figure 22(a) for an angle of attack of 15°, and it is seen that the pitch effectiveness generally decreased as the Mach number was increased. As figure 18(c) shows, at high angles of attack the pitch effectiveness was usually greater at flap deflections from -30° to -40° than that from -20° to -30°; for example, at a Mach number of 1.00 and at an angle of attack of 15° the pitch effectiveness was about 75 percent greater for deflections from -30° to -40° than that for deflections from -20° to -30°.

Deflection of the lower flaps from 10° to 30° while maintaining a constant deflection of the upper flaps of -30° increased the lift and drag by amounts which usually increased with angle of attack; this change in deflection also increased the maximum lift-drag ratios somewhat at Mach numbers of 1.00 and 1.20. (See figs. 19(a), 19(b), and 19(d).) Deflection of the lower flaps from 10° to 30° shifted the pitching-moment curves in a negative direction by substantial amounts, the amount of this shift usually increasing with angle of attack. The effect of flap deflection on the pitching moment was similar to the effect of flap deflection on incremental lift with increasing angle of attack; and, accordingly, the longitudinal stability generally increased with flap deflection. (See fig. 19(c).) As an example of the capacity of the lower flaps for changing trim, figure 19(c) shows that a change in flap deflection from 20° to 10° increased the trim angle of attack from about -2° to 15° at a Mach number of 1.20. The pitch-effectiveness parameter $C_{m_{\delta_l}}$ shown in figure 22(b) increased with Mach number up to a Mach number of 1.00, and then decreased at supersonic Mach numbers. The pitch effectiveness of the lower flaps at angles of attack near 15° and at near-sonic Mach numbers was somewhat greater at deflections from 10° to 20° than that from 20° to 30°. (See

fig. 19(c).) As figure 22 indicates, the pitch effectiveness of the lower flaps was greater than that of the upper flaps at high angles of attack at Mach numbers of 0.70 and above.

The maximum lift-drag ratio at trim conditions, when either the lower flaps or the upper flaps were used for obtaining trim, substantially decreased with Mach number, so that the maximum lift-drag ratios at a Mach number of 1.20 were about one-half of those at a Mach number of 0.50. (See figs. 23 and 24.) Somewhat higher lift-drag ratios were obtained throughout the Mach number range when the lower flaps were used for obtaining trim. The angle of attack at trim conditions fell within the range from 12° to 18°.

Differential deflection of the upper and lower flaps had some effect on the longitudinal aerodynamic characteristics as shown by figure 20.

Rudder deflection.- Uniform deflection of the rudders (as directional controls) on the basic outboard vertical tails usually had a small effect on the longitudinal aerodynamic characteristics. In particular, results show that the drag was generally increased, the maximum lift-drag ratio was reduced at low Mach numbers, and the 10° deflection resulted in some pitch-up tendencies at $\beta \approx -3.4^\circ$ at the high angles of attack at a Mach number of 0.70. (See fig. 15.)

Differential deflection of the rudders (with trailing edges of rudders deflected outward) increased the lift over most of the angle-of-attack range. (See fig. 21(a).) At the higher angles of attack there was a decrease in lift effectiveness due to differential deflection at $\beta \approx 0.4^\circ$ and $\beta \approx -3.4^\circ$ and actually a reversal in lift effectiveness for differential rudder deflections from $\pm 10^\circ$ to $\pm 20^\circ$ at $\beta \approx -3.4^\circ$ at subsonic Mach numbers. Differential deflection of the rudders increased the drag considerably and reduced maximum lift-drag ratios. (See figs. 21(b) and 21(d).) Differential deflection of the rudders shifted the pitching moments in a negative direction, and this shift resulted in substantial decreases in trim angle of attack; differential deflection also caused some decreases in longitudinal stability. (See fig. 21(c).)

External dummy support rods.- The external dummy support rods were investigated only at a Mach number of 0.50, and the results are presented in figure 17. The interference effects of the rods on the longitudinal aerodynamic characteristics were substantial. The rods worsened the unsatisfactory lift and pitching-moment breaks, which were characteristic of the configuration without the rods, by increasing the extent of the breaks and by causing these breaks to develop at somewhat lower angles of attack.

Lateral Characteristics

The basic lateral aerodynamic characteristics are presented in figures 25 to 32 and the summary lateral-stability derivatives are presented in figures 33 to 41. Most of the discussion of the lateral characteristics will be concerned with the summary lateral-stability figures.

Model components.- The body-canopy configuration (configuration 1) was directionally unstable at all test conditions. (See figs. 33(a) and 38.) Addition of the basic outboard vertical tails to this configuration (addition of basic outboard vertical tails to configuration 1 gives configuration 2) made the configuration directionally stable at a Mach number of 0.50 at angles of attack up to about 18°; at higher angles of attack, however, the configuration became unstable. (See fig. 33(a).) Increasing the Mach number up to 0.95 progressively reduced the range of angles of attack wherein the configuration was stable, so that at the Mach number of 0.95 the configuration was stable only at angles of attack up to about 1°. At Mach numbers of 1.00 and 1.20, however, the configuration regained directional stability at angles of attack up to about 9°. (See also fig. 38.)

Addition of the basic central vertical tail to the configuration consisting of body, canopy, and basic outboard vertical tails (addition of basic central vertical tail to configuration 2 gives configuration 3) improved the directional stability at all Mach numbers by extending the angle-of-attack range in which the configuration was directionally stable (by an amount which varied between approximately 2° and 8°) and by increasing the magnitude of the directional-stability derivative C_{n_β} in this angle-of-attack range. (See figs. 33(a) and 38.)

Replacing the basic outboard and central vertical tails on the canopy-off configuration (configuration 4) by the modified outboard and central vertical tails (configuration 5) had a variable although, at most, a small effect on the extent of the angle-of-attack range wherein the configuration was directionally stable; to be specific, this range was increased by about 1° or 2° at Mach numbers from 0.90 to 1.20 and the range was slightly decreased at the lower test Mach numbers. (See figs. 34(a) and 38.) The modified vertical tails also generally increased the magnitude of the derivative C_{n_β} within this angle-of-attack range at all Mach numbers; this increase was substantial at the low angles of attack.

Addition of the canopy to the configuration consisting of body, basic outboard vertical tails, and basic central vertical tail (addition of canopy to configuration 4 gives configuration 3) resulted in an unstable yawing-moment increment which at all Mach numbers except 1.00 reduced the angle-of-attack range wherein the configuration was stable (by an amount which varied between 2° and 5°) and which at all Mach numbers generally decreased by rather substantial amounts the magnitude of the derivative C_{n_β} in this angle-of-attack range. (See figs. 35(a) and 38.)

The effective-dihedral derivative C_{l_β} of all configurations was usually negative in sign (that is, positive dihedral effect) except in some cases at the highest angles of attack at some of the Mach numbers. (See figs. 33 to 37.) The modified vertical tails generally increased the magnitude of the derivative C_{l_β} at all angles of attack and Mach numbers. (See fig. 34(b).)

Control deflection.- Uniform deflection of the rudders (as directional controls) of either 10° or -10° on the basic outboard vertical tails resulted in values of the directional-stability derivative C_{n_β} which were somewhat different but which usually were not much different from those values at a rudder deflection of 0°. (See figs. 34(a) and 39.) These differences were perhaps due to diverse separation effects; it should be noted that the derivative shown is the average slope from $\beta \approx -3.4°$ to $\beta \approx 0.4°$. Uniform deflection of the rudders (as directional controls) produced substantial yawing moments, and these yawing moments generally decreased with angle of attack. (See fig. 26(a).) However, uniform deflection of the rudders (as directional controls) produced rather large and adverse rolling moments; the rolling moments also generally decreased with angle of attack. (See fig. 26(b).)

Differential deflection of the rudders of ±10° (with trailing edges of rudders deflected outward) had essentially no effect on the angle-of-attack range in which the configuration was directionally stable at Mach numbers of 0.90 and above, but reduced this range by 2° to 5° at Mach numbers of 0.50 and 0.70. The magnitude of the derivative C_{n_β} was usually increased at low angles of attack and particularly at the subsonic Mach numbers. (See figs. 36(a) and 40.)

Differential deflection of either the upper or the lower flaps or differential deflection of both the upper and the lower flaps on the canopy-off configuration (configuration 2) usually had rather small effect on the extent of the angle-of-attack range in which the configuration was directionally stable; differential deflection of the lower flaps increased this range, however, by about 5° at a Mach number of 1.20. (See figs. 37(a) and 41.)

At $\beta \approx 0.4°$, the roll effectiveness of the upper flaps when differentially deflected was greater than that of the lower flaps at the lower angles of attack but generally much less at the higher angles of attack. (See fig. 32(b).) At $\beta \approx -6.5°$, the levels of the rolling moments indicate that the upper flaps, in addition to being more effective at the lower angles of attack, were also generally somewhat more effective at the higher angles of attack. The magnitudes of the rolling moments produced by differential deflection of the flaps, it should be pointed out, were considerably less than those produced by uniform deflection of the rudders (as directional controls) at all angles of attack except the highest. (Compare figs. 26(b) and 32(b).)

In general, the magnitude of the effective-dihedral derivative C_{l_β} was usually increased at all Mach numbers by differential deflection of the lower flaps or, to a lesser extent, by differential deflection of the upper flaps, and was increased at the low Mach numbers at low angles of attack by differential deflection of the rudders. (See figs. 36(b) and 37(b).)

CONCLUSIONS

An investigation was made in the Langley 8-foot transonic pressure tunnel of the static longitudinal and lateral stability and control characteristics of a 1/10-scale model of the SV-5 lifting-body reentry vehicle having a 77° swept delta planform, a blunt nose, a flat bottom, and extensive boattailing. The investigation was made at Mach numbers from 0.50 to 1.20 and through an angle-of-attack range from approximately -2° to 24° at fixed angles of sideslip of approximately 0.4°, -3.4°, and -6.5°. The results include the effect on the aerodynamic characteristics of deflection of upper and lower trailing-edge flaps, of deflection of rudders on outboard vertical tails, and of model components. The combination of flap deflection of -30° on the upper flaps and 20° on the lower flaps was taken to be the basic flap setting in the present investigation, and most of the tests were made with this flap setting. The following conclusions are indicated:

1. The body-canopy configuration was longitudinally stable at the higher angles of attack and directionally unstable at all angles of attack.

2. Addition of the basic outboard vertical tails to the body-canopy configuration shifted the pitching-moment curves in a negative direction and generally made the configuration longitudinally stable. Addition of these vertical tails made the configuration directionally stable at angles of attack up to about 18° at a Mach number of 0.50, up to only about 1°, however, at a Mach number of 0.95, and up to about 9° at Mach numbers of 1.00 and 1.20.

3. Addition of the basic central vertical tail to the configuration consisting of body, canopy, and basic outboard vertical tails extended the angle-of-attack range in which the configuration was directionally stable by about 2° to 8°, the amount depending on Mach number, and increased the magnitude of the directional-stability derivative.

4. Replacement of the basic outboard and central vertical tails on the canopy-off configuration by the modified outboard and central vertical tails generally increased the magnitude of the directional-stability derivative and had a variable and, at most, small effect on the angle-of-attack range wherein the configuration was directionally stable. The modified vertical tails generally increased the magnitude of the effective-dihedral derivative at all angles of attack and Mach numbers.

5. Addition of the canopy to the configuration consisting of body, basic outboard vertical tails, and basic central vertical tail increased the trim angle of attack by a small amount at most Mach numbers but aggravated a loss in longitudinal stability already evident at high angles of attack at the high subsonic Mach numbers. Addition of the canopy generally decreased the magnitude of the directional-stability derivative and generally reduced the angle-of-attack range wherein the configuration was directionally stable by 2° to 5°.

6. Deflection of the upper and lower flaps to large values on the configurations which included the outboard vertical tails substantially improved the

longitudinal-stability characteristics. The upper and lower flaps were effective in changing the trim angle of attack, with the lower flaps being more effective at high angles of attack at all Mach numbers except the lowest.

7. Differential deflection of the rudders so that the trailing edges of the rudders were deflected outward resulted in substantial decreases in the trim angle of attack and some decreases in longitudinal stability. Uniform deflection of the rudders (as directional controls) produced substantial yawing moments but rather large adverse rolling moments.

8. The effective-dihedral derivative of all configurations was usually negative in sign (that is, positive dihedral effect) except in some cases at the highest angles of attack at some of the subsonic Mach numbers.

Langley Research Center,
National Aeronautics and Space Administration,
Langley Station, Hampton, Va., December 4, 1964.

REFERENCES

1. Dennis, David H.; and Edwards, George G.: The Aerodynamic Characteristics of Some Lifting Bodies. NASA TM X-376, 1960.

2. Rainey, Robert W., compiler: Summary of Aerodynamic Characteristics of Low-Lift-Drag-Ratio Reentry Vehicles From Subsonic to Hypersonic Speeds. NASA TM X-588, 1961.

3. Ware, George M.: Investigation of the Low-Subsonic Aerodynamic Characteristics of a Model of a Modified Lenticular Reentry Configuration. NASA TM X-756, 1962.

4. Spencer, Bernard, Jr.; and Phillips, W. Pelham: Low-Speed Aerodynamic Characteristics of a Modified Blunt 13° Half-Cone Lifting-Body Configuration Having Deployable Horizontal Tails With or Without Variable-Sweep Wings. NASA TM X-847, 1963.

5. Ware, George M.: Aerodynamic Characteristics of Models of Two Thick 74° Delta Manned Lifting Entry Vehicles at Low-Subsonic Speeds. NASA TM X-914, 1964.

6. Ladson, Charles L.: Aerodynamic Characteristics of a Manned Lifting Entry Vehicle at a Mach Number of 6.8. NASA TM X-915, 1964.

7. Rainey, Robert W.; and Ladson, Charles L.: Aerodynamic Characteristics of a Manned Lifting Entry Vehicle at Mach Numbers From 0.2 to 1.2. NASA TM X-1015, 1964.

8. Silvers, H. Norman; and Lowery, Jerry L.: Stability and Control Characteristics of a Flat-Bottom Lifting Reentry Configuration at a Mach Number of 1.61. NASA TM X-981, 1964.

TABLE I.- GEOMETRIC CHARACTERISTICS OF 1/10-SCALE MODEL

OF LIFTING-BODY REENTRY VEHICLE

Body (without vertical tails):	
Length (to trailing edge of undeflected flaps), in.	28.8
Maximum width (reference length, b), in.	12.0
Maximum height, in.	6.6
Planform area, sq ft	1.705
Maximum cross-sectional area, sq ft	0.401
Equivalent fineness ratio	3.36
Upper flap:	
Area (single flap, true), sq ft	0.098
Chord, in.	3.42
Span (true), in.	4.98
Hinge-line sweep, deg	0
Lower flap:	
Area (single flap, true), sq ft	0.1224
Chord, in.	4.04
Span, in.	4.75
Hinge-line sweep, deg	0
Basic outboard vertical tail:	
Area (true), sq ft	0.23
Span (true), in.	4.66
Chord:	
Tip, in.	4.30
Root (theoretical), in.	9.88
Thickness ratio:	
Tip, percent	18.4
Root, percent	8.9
Taper ratio	0.436
Aspect ratio	0.66
Leading-edge sweep, deg	55
Incidence (leading edge toed in), deg	4
Dihedral, deg	16
Rudder:	
Area (true), sq ft	0.109
Chord (perpendicular to hinge line), in.	3.00
Span (along trailing edge), in.	5.625
Hinge-line sweep, deg	10
Basic central vertical tail:	
Area, sq ft	0.156
Tip chord, in.	4.30
Thickness (constant), in.	0.312
Leading-edge sweep, deg	55

TABLE II.- CONTROL DEFLECTIONS INVESTIGATED

Configuration	$\delta_{u,L}$, deg	$\delta_{u,R}$, deg	$\delta_{l,L}$, deg	$\delta_{l,R}$, deg	$\delta_{r,L}$, deg	$\delta_{r,R}$, deg
1	-30	-30	20	20	---	---
2	-30	-30	20	20	0	0
3	-30	-30	20	20	0	0
3	-20	-20	20	20	0	0
3	-40	-40	20	20	0	0
3	-30	-30	10	10	0	0
3	-30	-30	30	30	0	0
3	-30	-30	20	20	10	-10
3	-30	-30	20	20	20	-20
4	-30	-30	20	20	0	0
4	-30	-30	20	20	10	10
4	-30	-30	20	20	-10	-10
4	-10	-10	0	0	-10	10
4	-40	-20	20	20	0	0
4	-30	-30	10	30	0	0
4	-40	-30	20	30	0	0

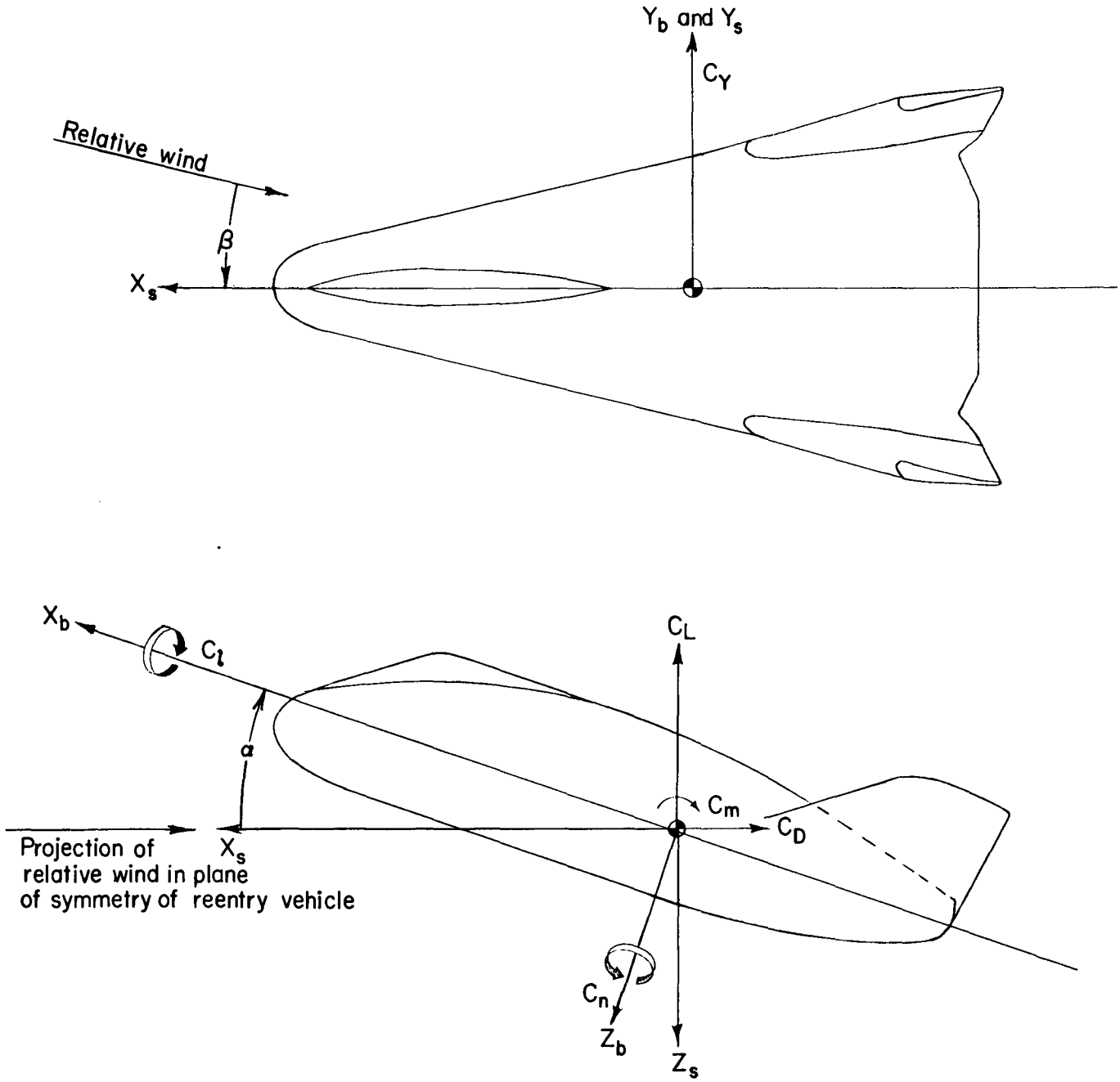

Figure 1.- Stability and body axes. Arrows indicate positive direction of forces, moments, and angles. (Subscripts b and s denote body and stability axes, respectively.)

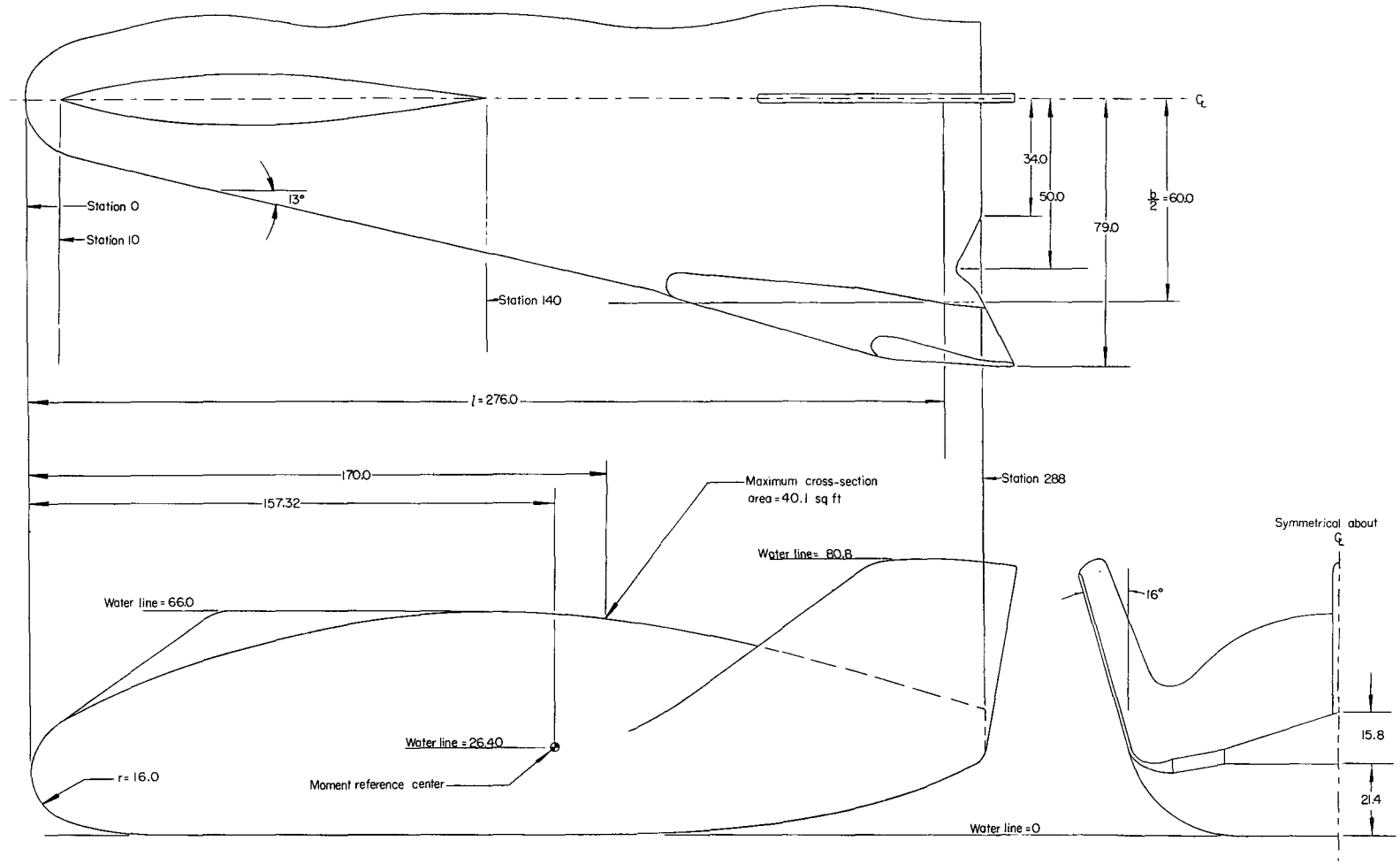

Figure 2.- General arrangement of SV-5 configuration. All dimensions are full-scale and in inches unless otherwise noted.

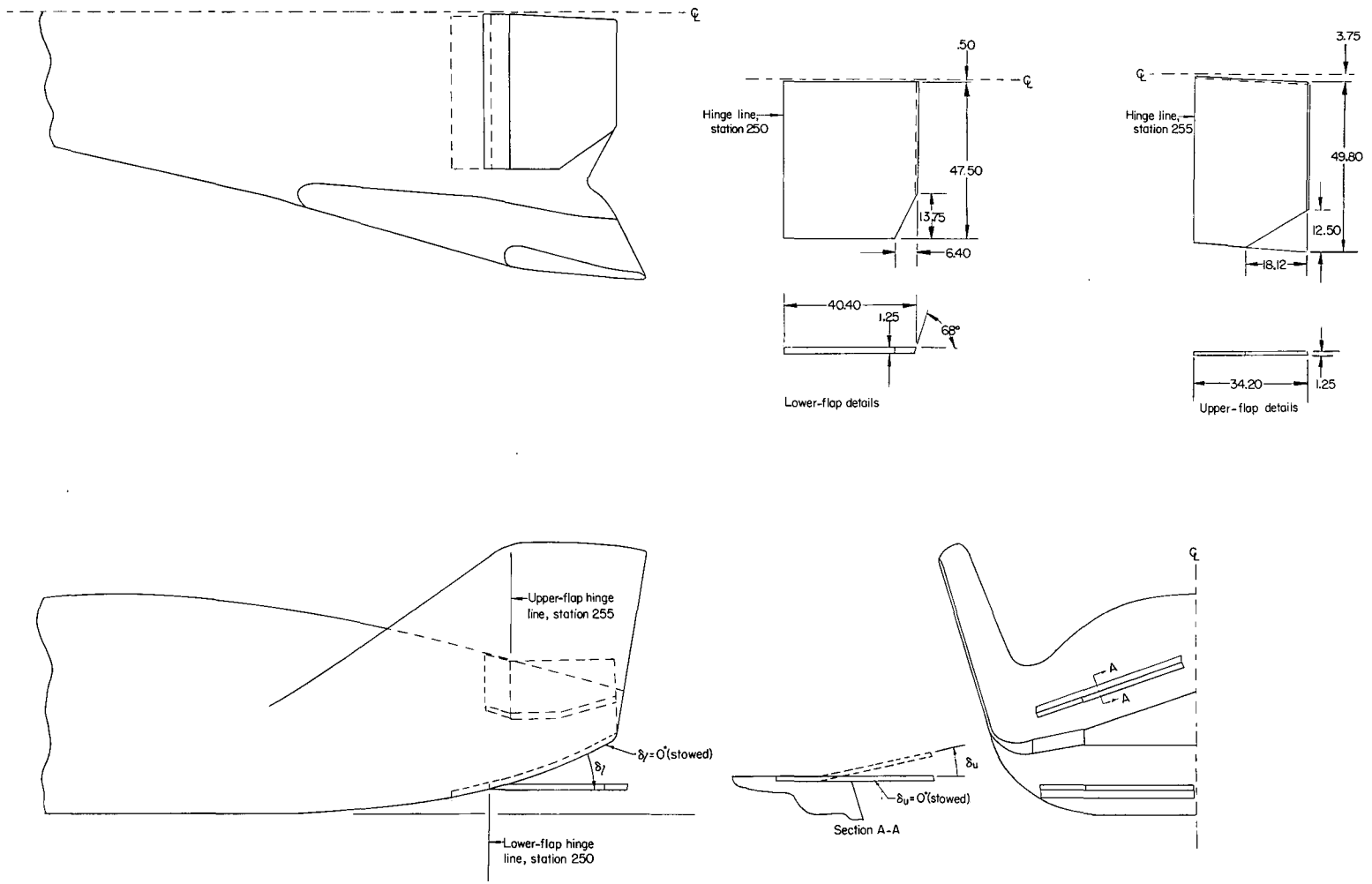

Figure 3.- Upper and lower flaps of model. All dimensions are full-scale and in inches unless otherwise noted. Arrows indicate positive direction of δ_l and negative direction of δ_u.

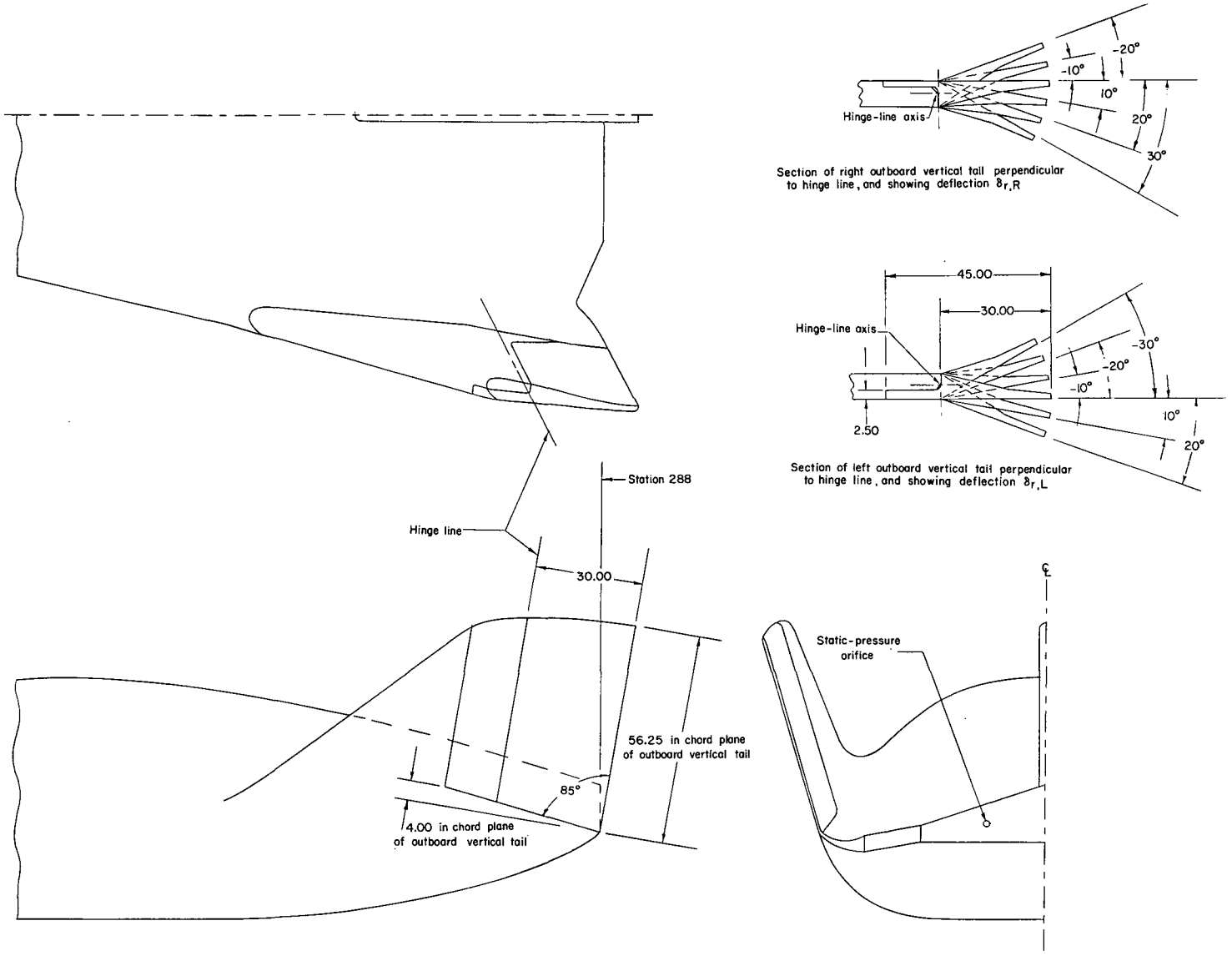

(a) Basic outboard and central vertical tails.

Figure 4.- Vertical tails of model. All dimensions are full-scale and in inches unless otherwise noted.

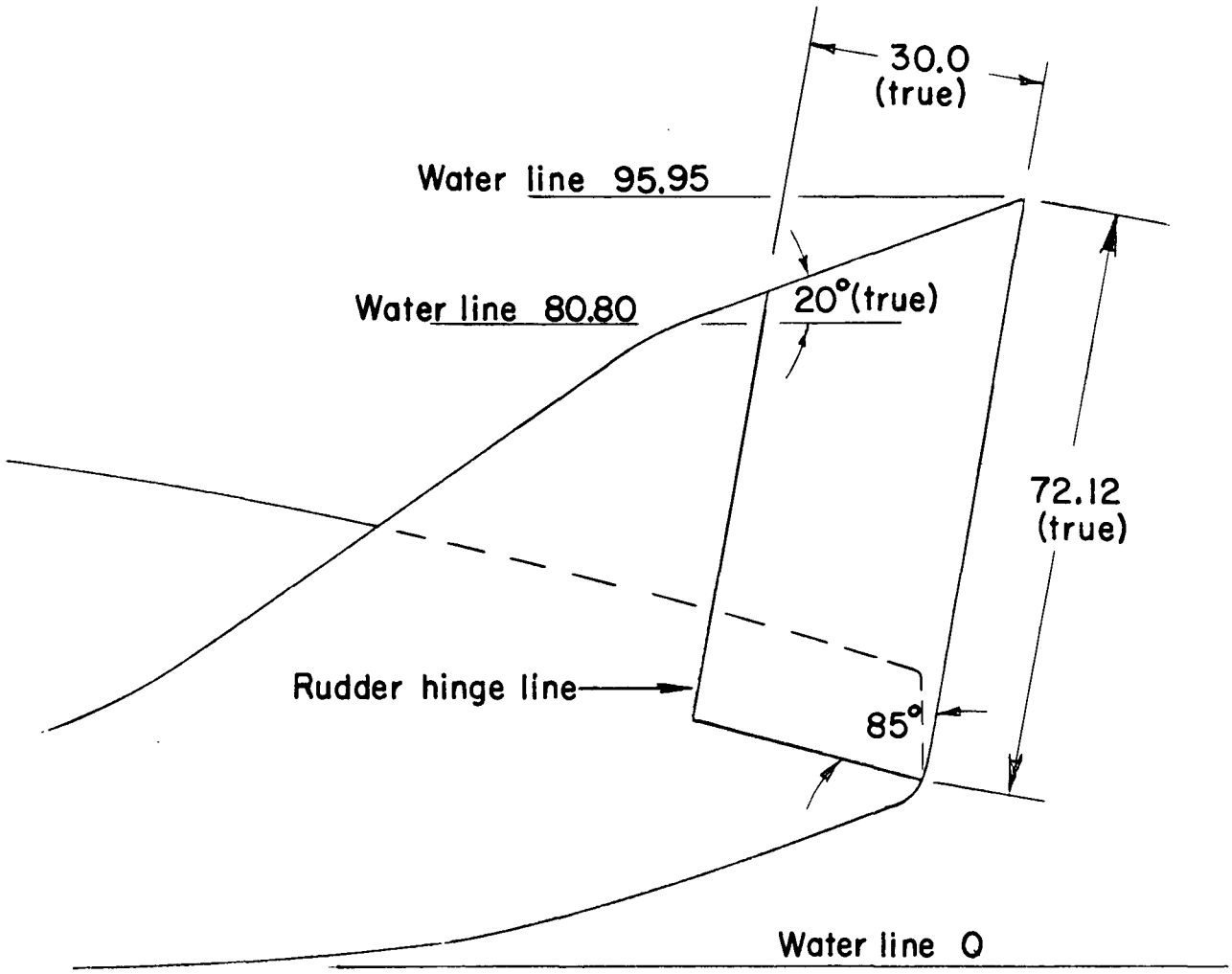

(b) Modified outboard and central vertical tails.

Figure 4.- Concluded.

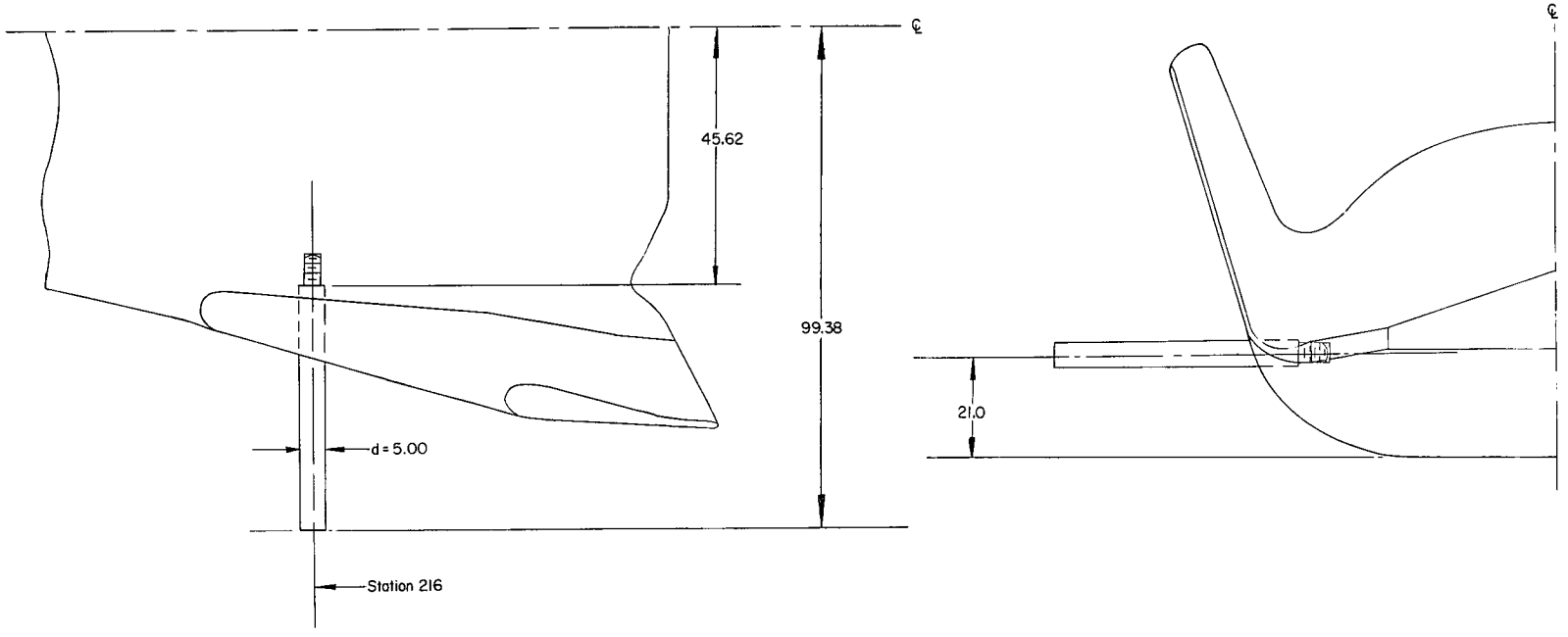

Figure 5.- External dummy support rods of model. All dimensions are full-scale and in inches unless otherwise noted.

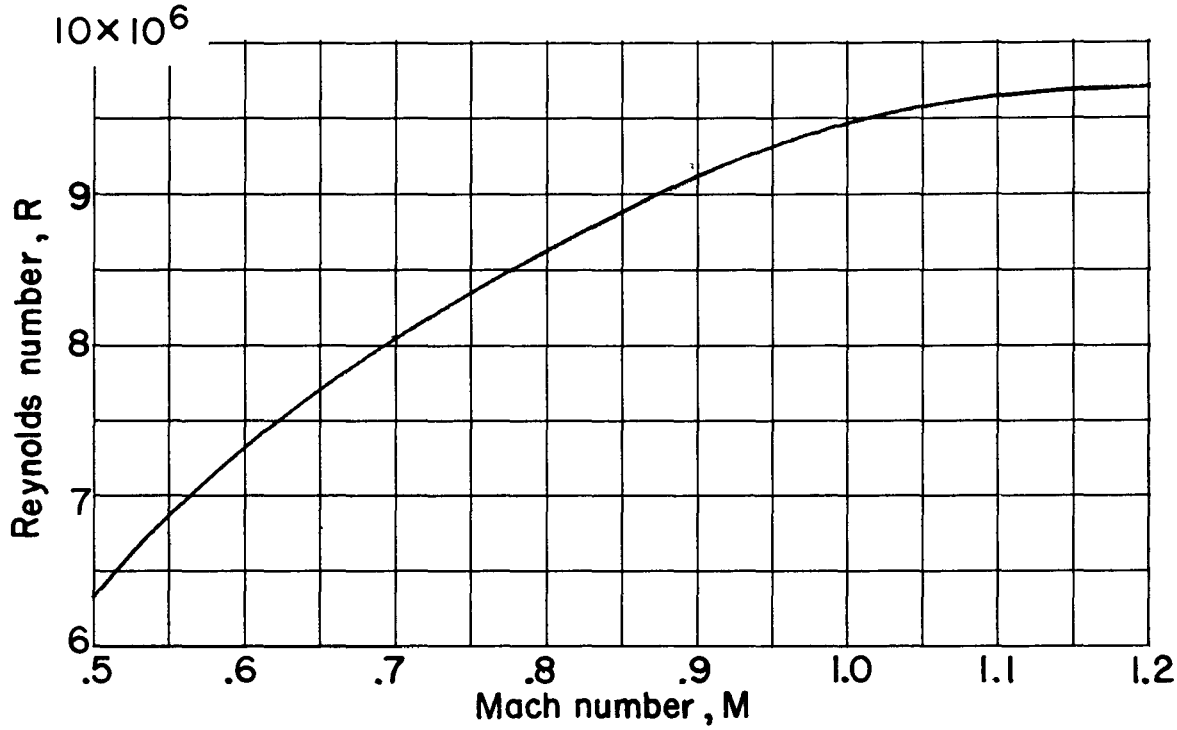

Figure 6.- Variation with Mach number of test Reynolds number based on reference body length l (27.60 in.).

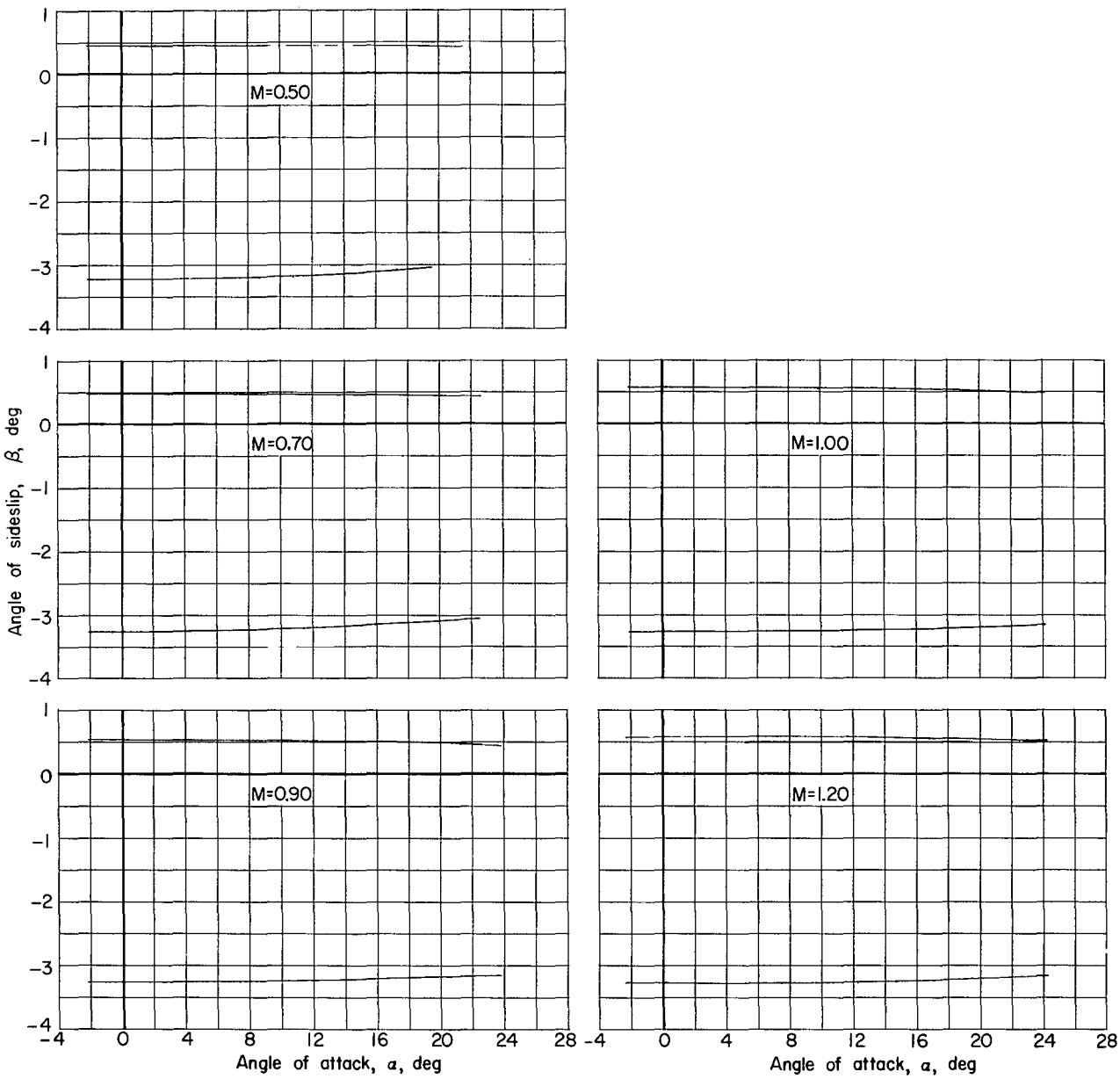

(a) Configuration 4 (basic outboard and central vertical tails on, canopy off); $\delta_u = -30^\circ$; $\delta_l = 20^\circ$; $\delta_r = 10^\circ$.

Figure 7.- Actual values of angle of sideslip for various configurations.

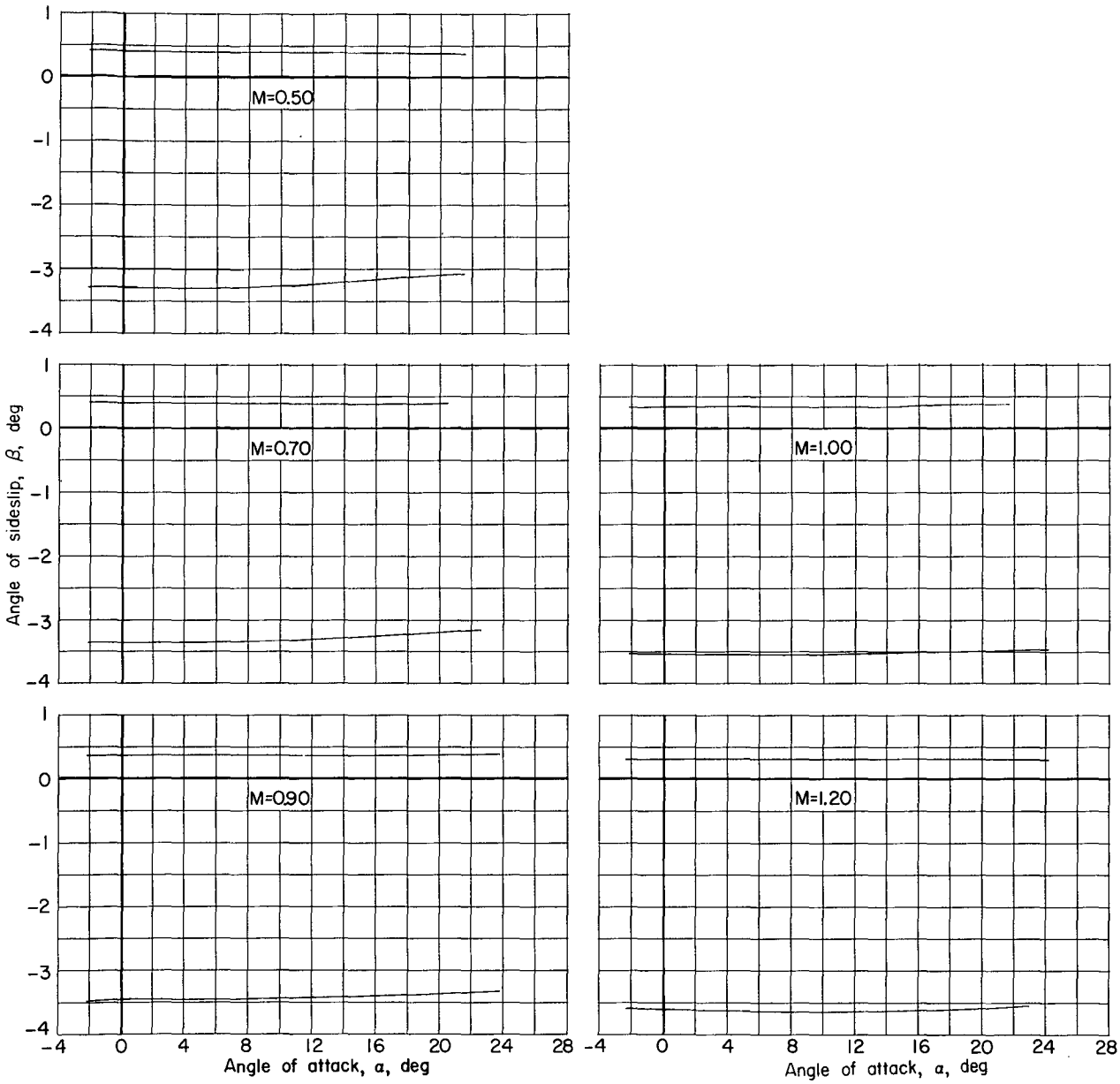

(b) Configuration 4 (basic outboard and central vertical tails on, canopy off); $\delta_u = -30^\circ$; $\delta_l = 20^\circ$; $\delta_r = -10^\circ$.

Figure 7.- Continued.

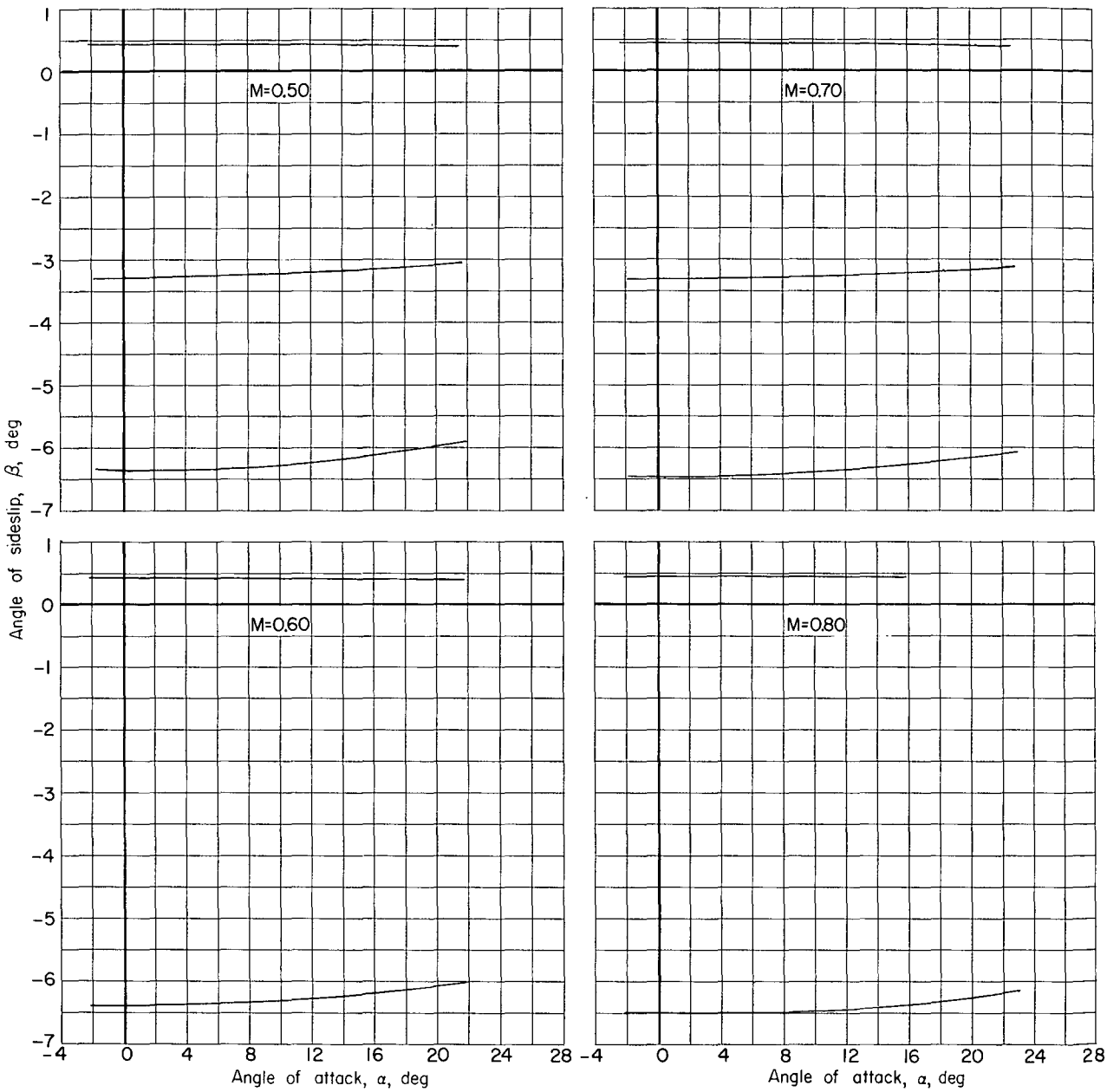

(c) Configurations 1 to 6 except configuration 4 at control deflections noted in figures 7(a) and 7(b).

Figure 7.- Continued.

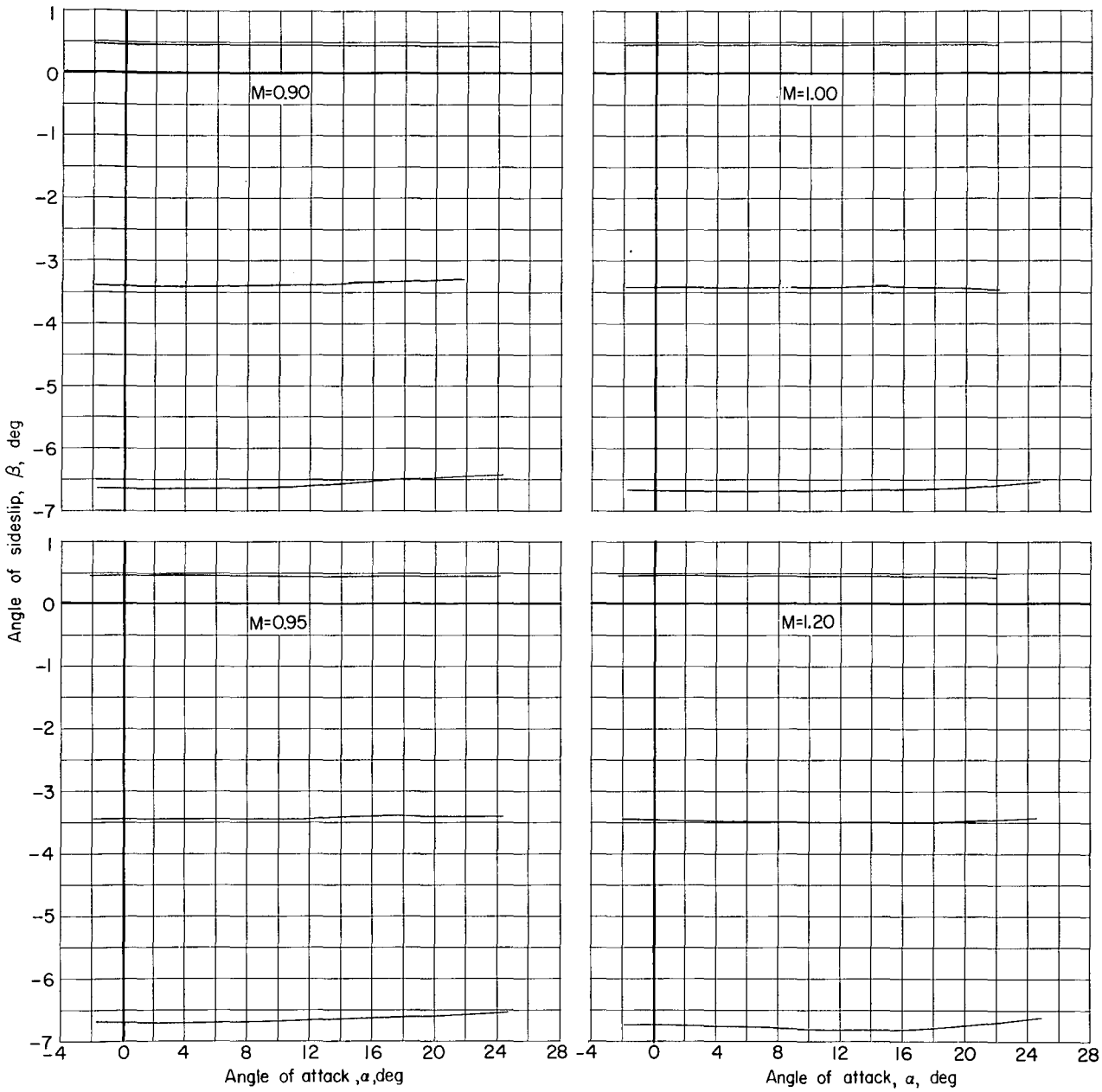

(c) Concluded.

Figure 7.- Concluded.

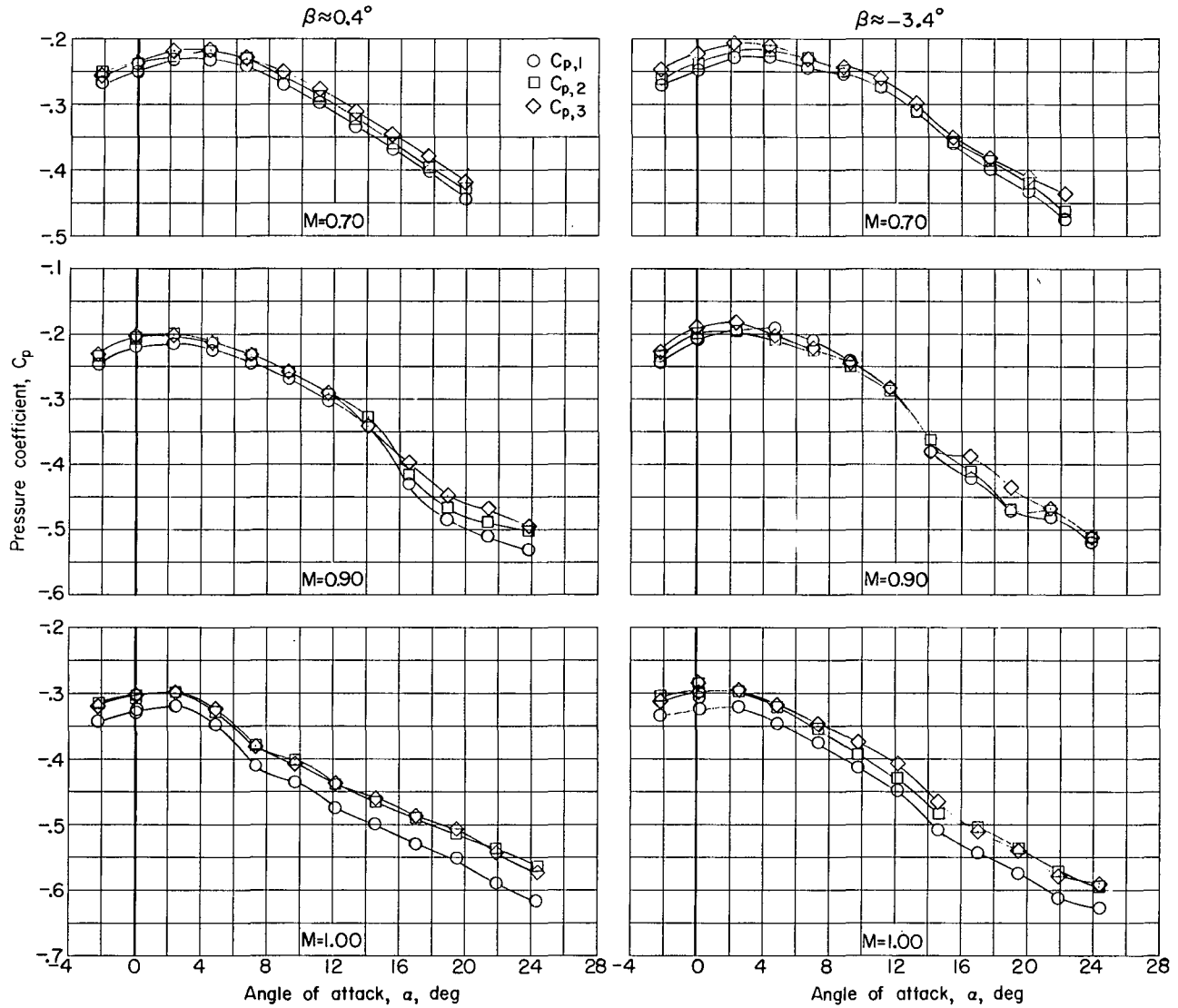

Figure 8.- Base pressure coefficient against angle of attack. Configuration 1 (canopy on, outboard and central vertical tails off); $\delta_u = -30^o$; $\delta_l = 20^o$.

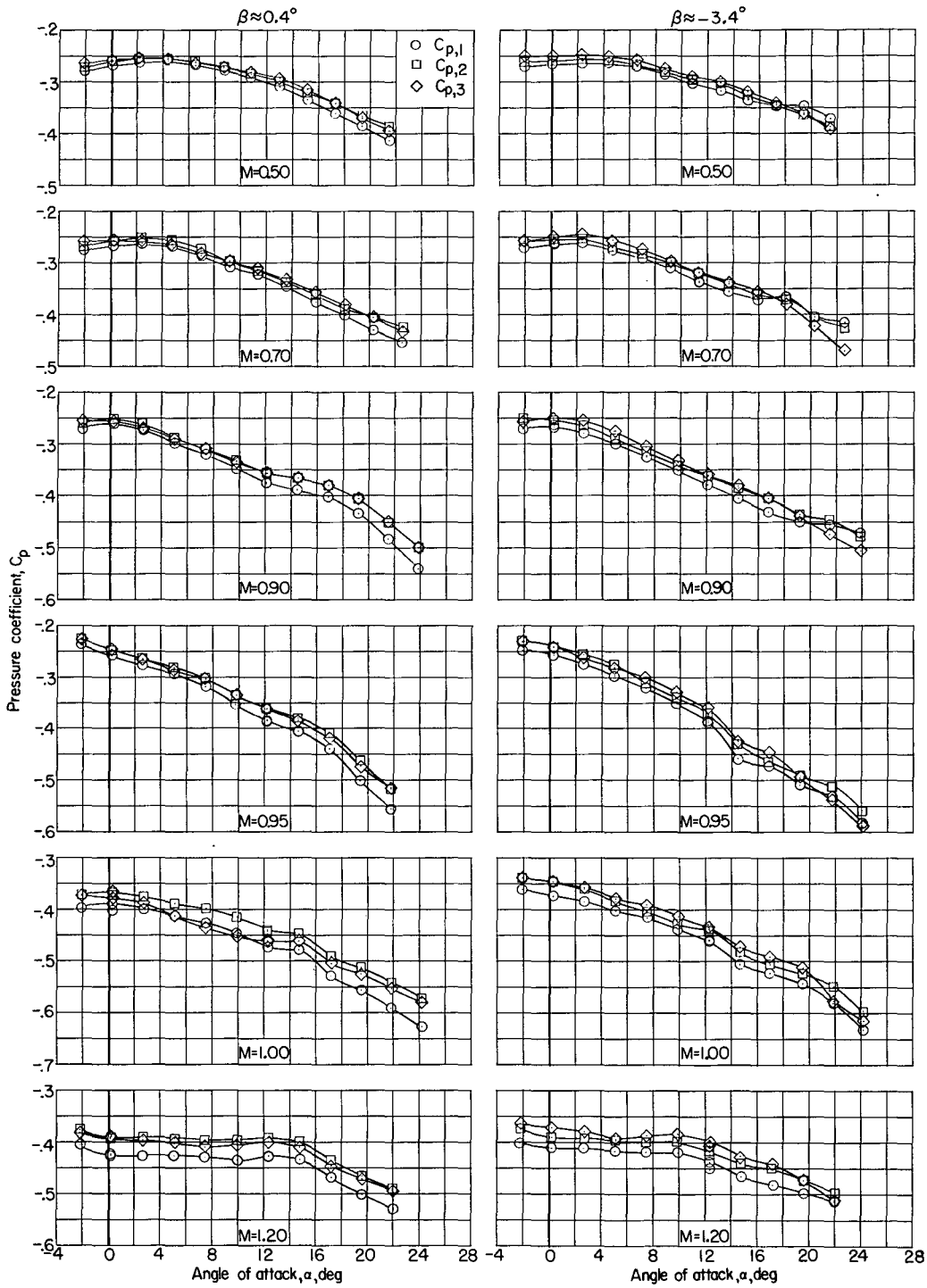

Figure 9.- Base pressure coefficient against angle of attack. Configuration 2 (canopy on, basic outboard vertical tails on, central vertical tail off); $\delta_u = -30^\circ$; $\delta_l = 20^\circ$; $\delta_r = 0^\circ$.

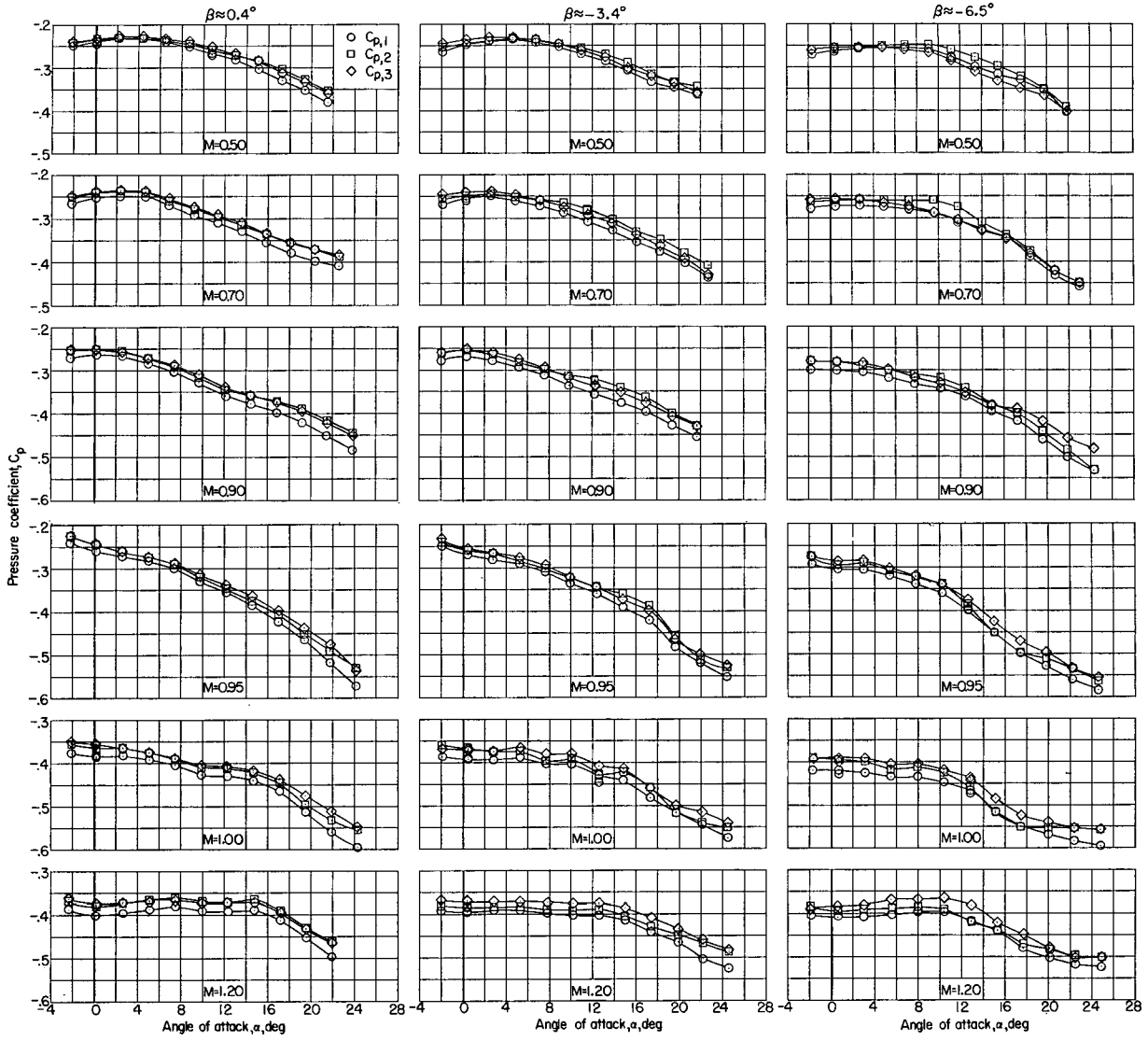

(a) $\delta_u = -30^\circ$; $\delta_l = 20^\circ$; $\delta_r = 0^\circ$.

Figure 10.- Base pressure coefficient against angle of attack. Configuration 3 (basic outboard and central vertical tails on, canopy on).

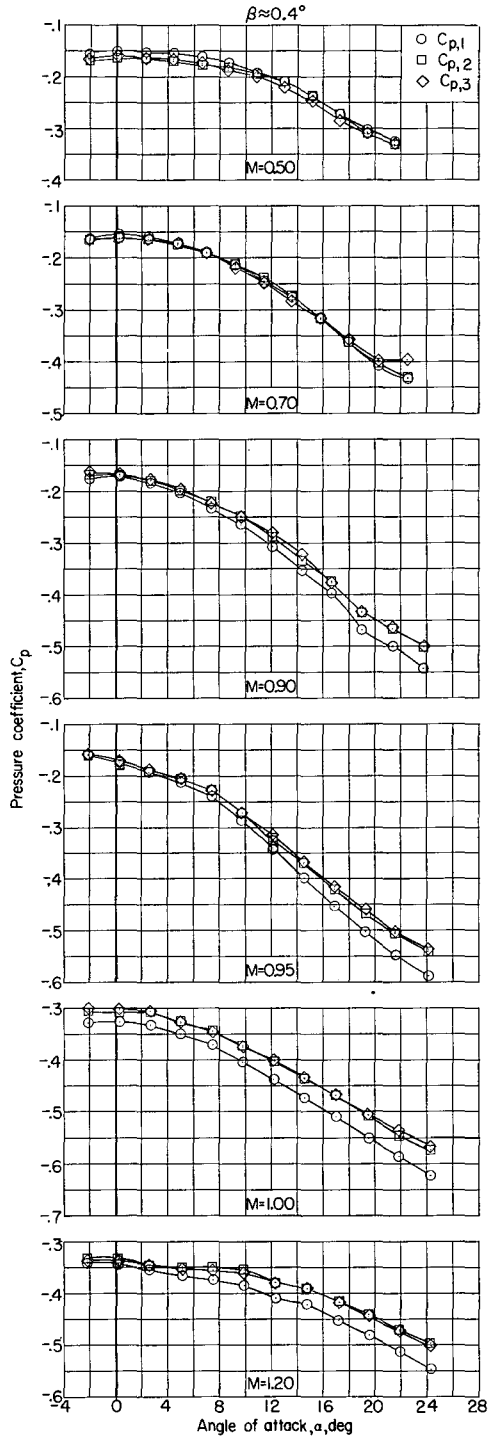

(b) $\delta_u = -20^\circ$; $\delta_l = 20^\circ$; $\delta_r = 0^\circ$.

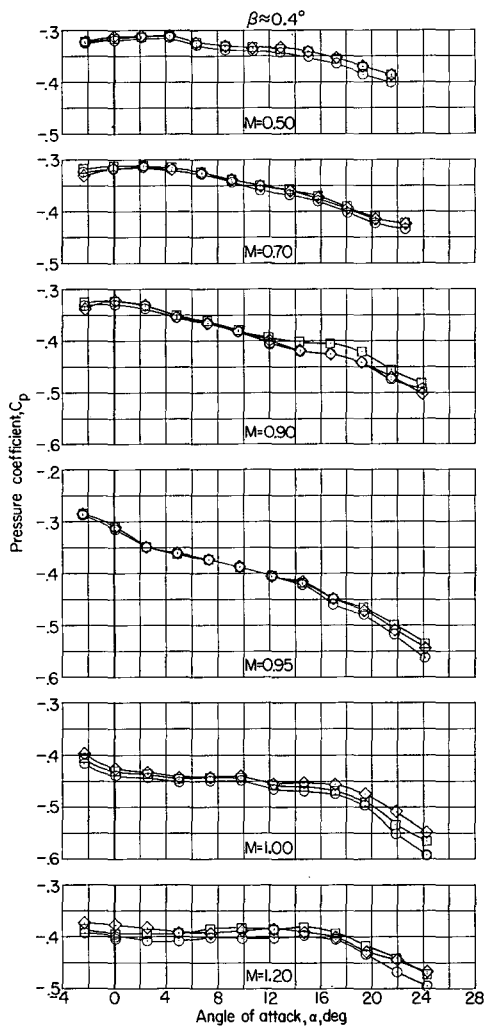

(c) $\delta_u = -40^\circ$; $\delta_l = 20^\circ$; $\delta_r = 0^\circ$.

Figure 10.- Continued.

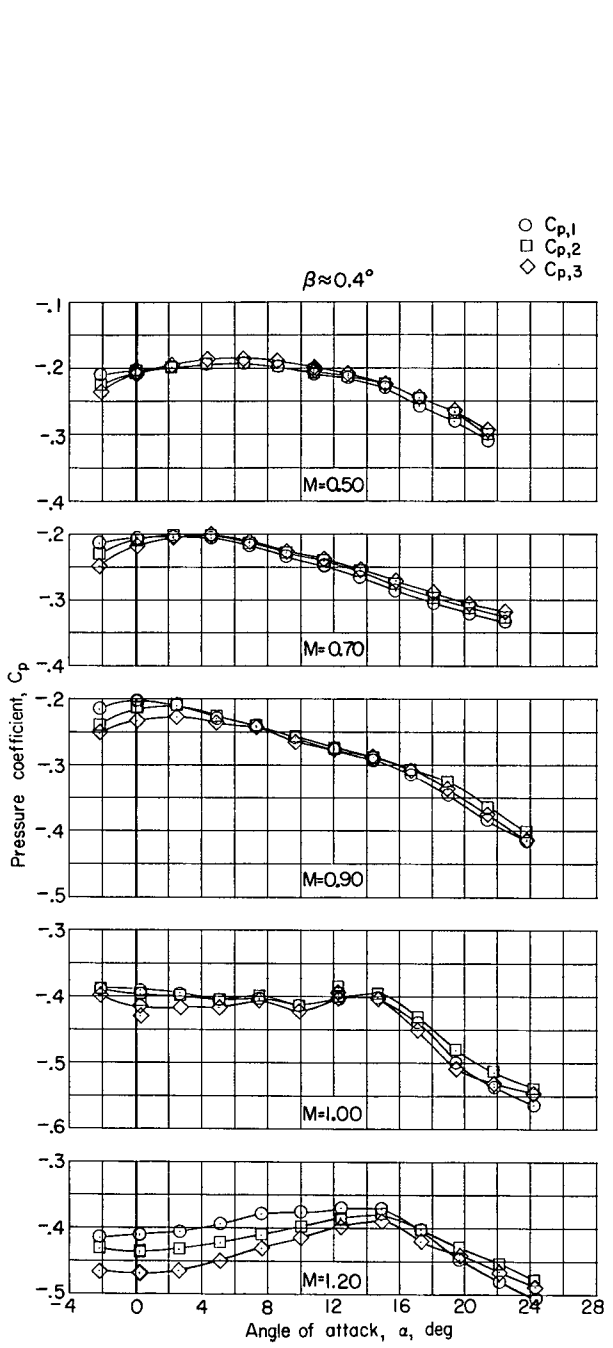

(d) $\delta_u = -30^\circ$; $\delta_l = 10^\circ$; $\delta_r = 0^\circ$.

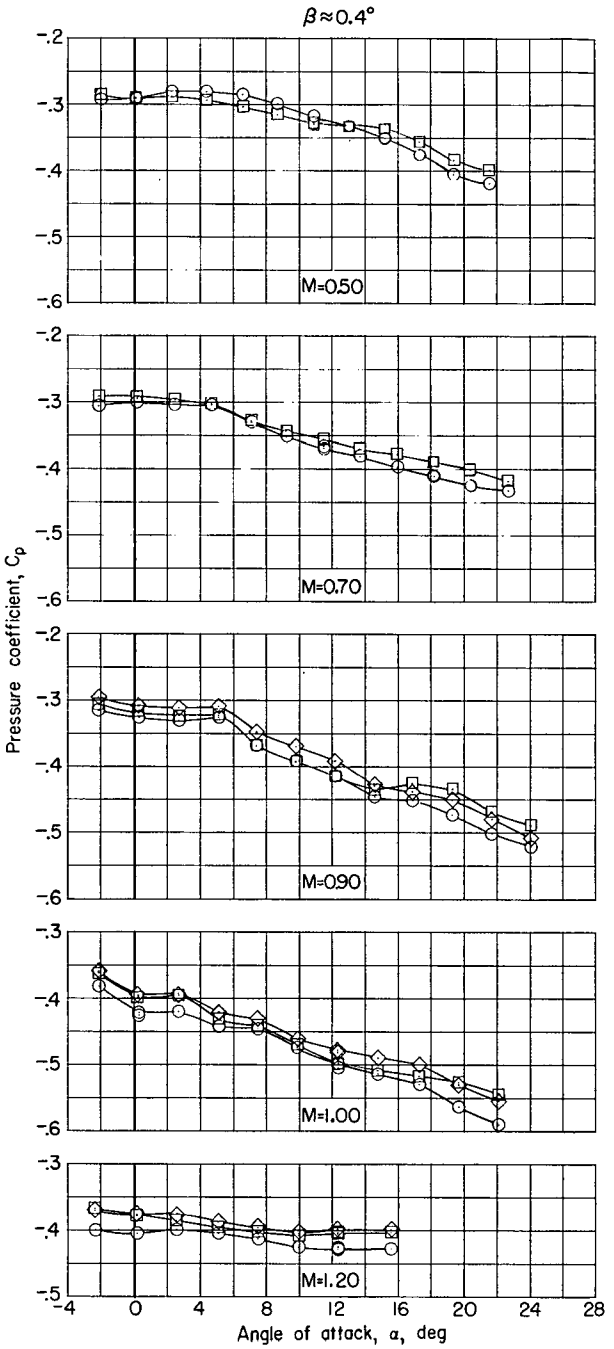

(e) $\delta_u = -30^\circ$; $\delta_l = 30^\circ$; $\delta_r = 0^\circ$.

Figure 10.- Continued.

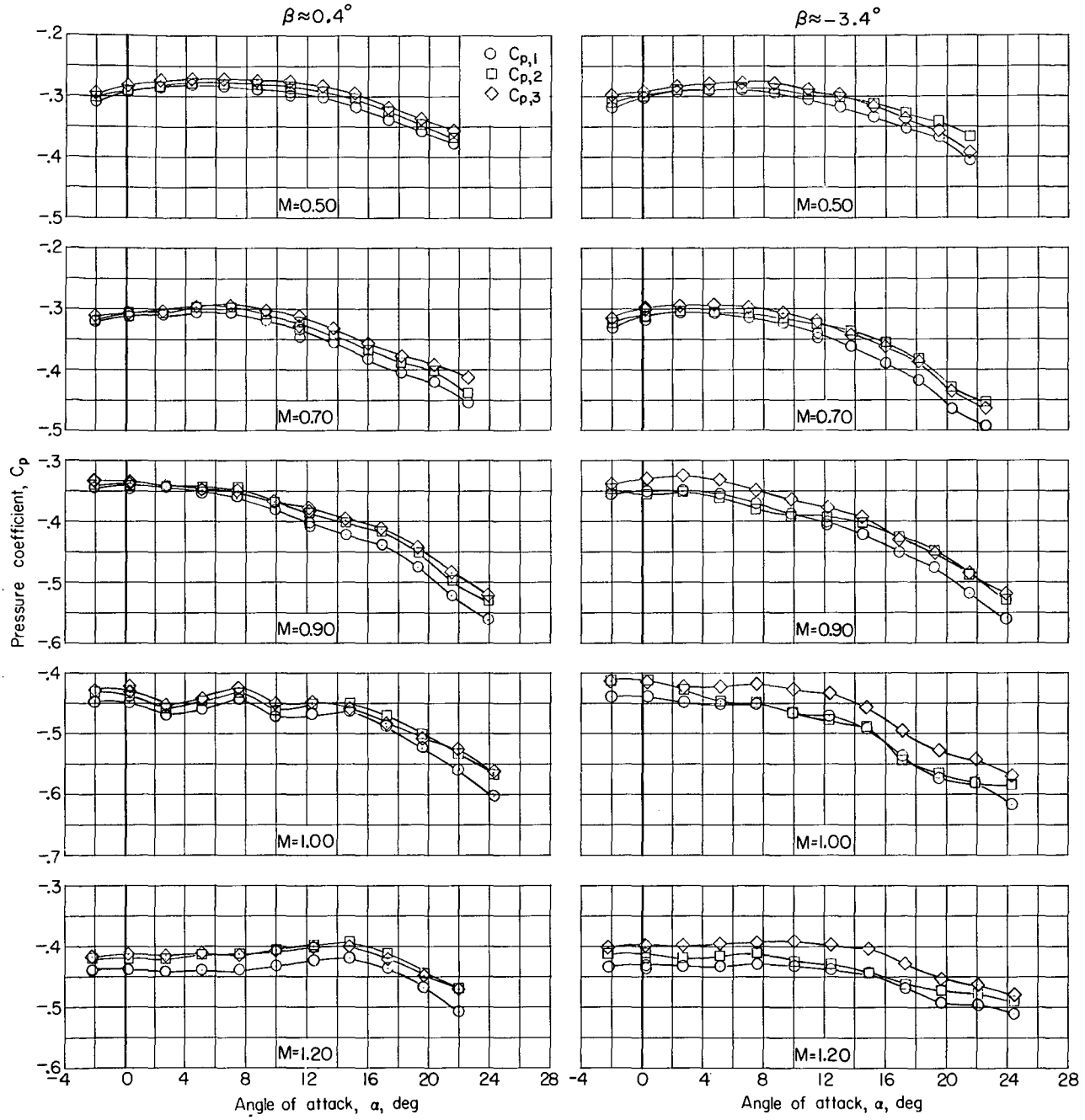

(f) $\delta_u = -30^\circ$; $\delta_l = 20^\circ$; $\delta_{r,L} = 10^\circ$; $\delta_{r,R} = -10^\circ$.

Figure 10.- Continued.

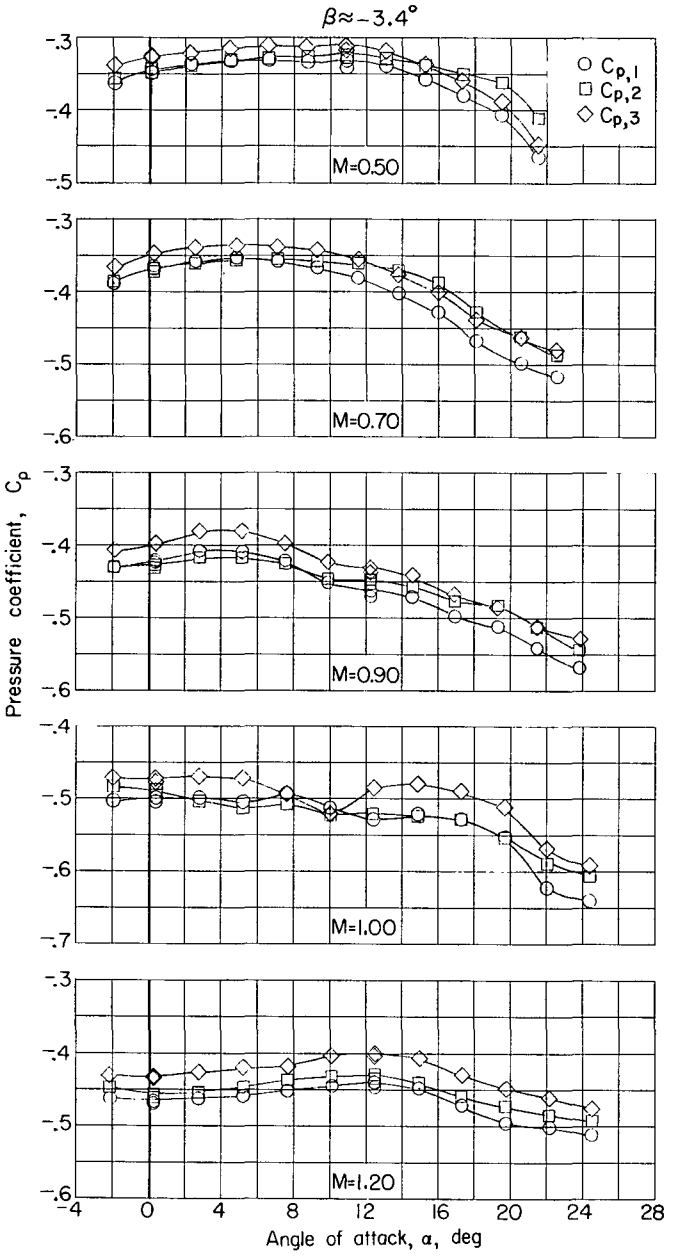

(g) $\delta_u = -30^\circ$; $\delta_l = 20^\circ$; $\delta_{r,L} = 20^\circ$; $\delta_{r,R} = -20^\circ$.

Figure 10.- Concluded.

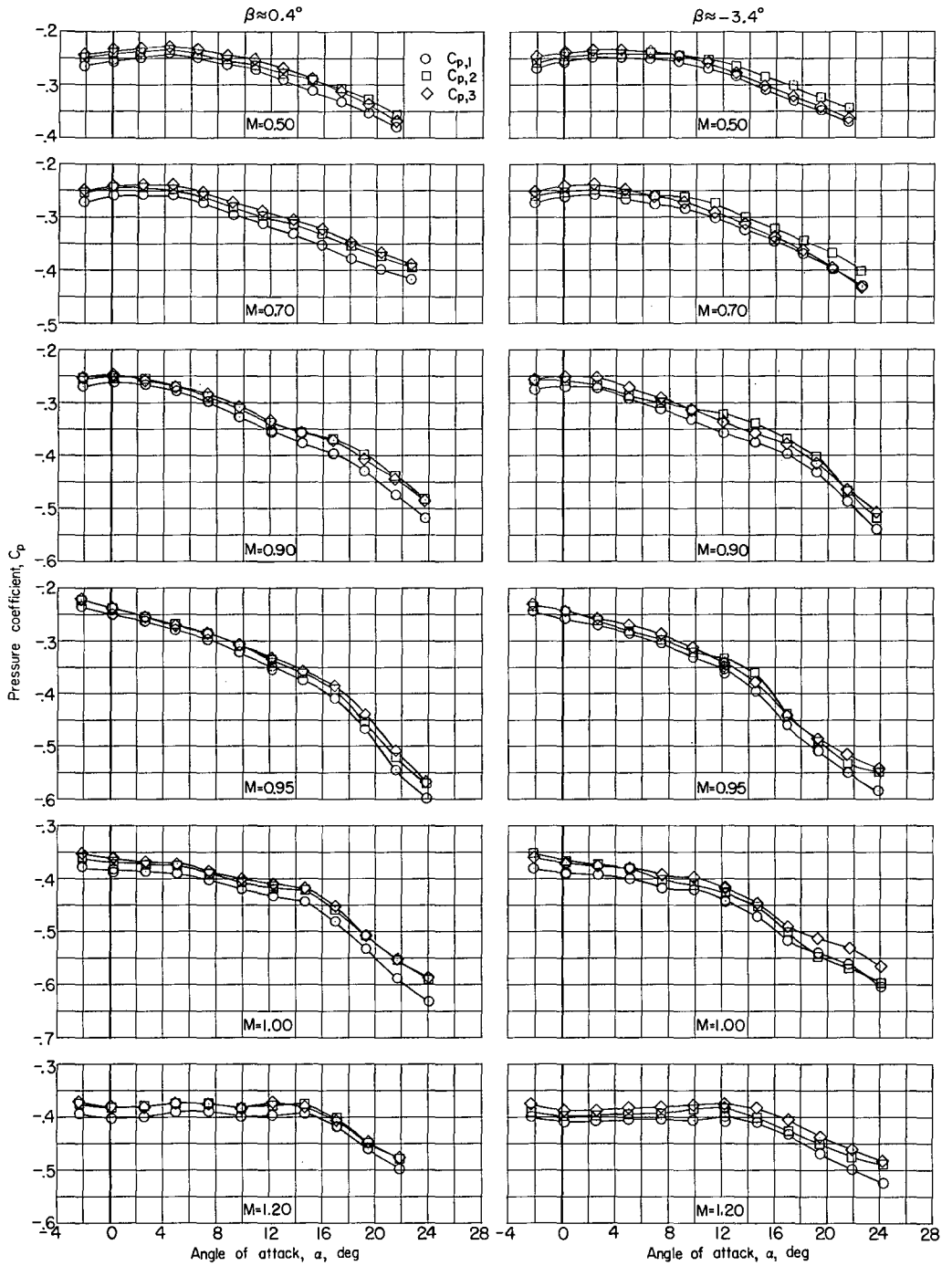

(a) $\delta_u = -30^\circ$; $\delta_l = 20^\circ$; $\delta_r = 0^\circ$.

Figure 11.- Base pressure coefficient against angle of attack. Configuration 4 (basic central and outboard vertical tails on, canopy off).

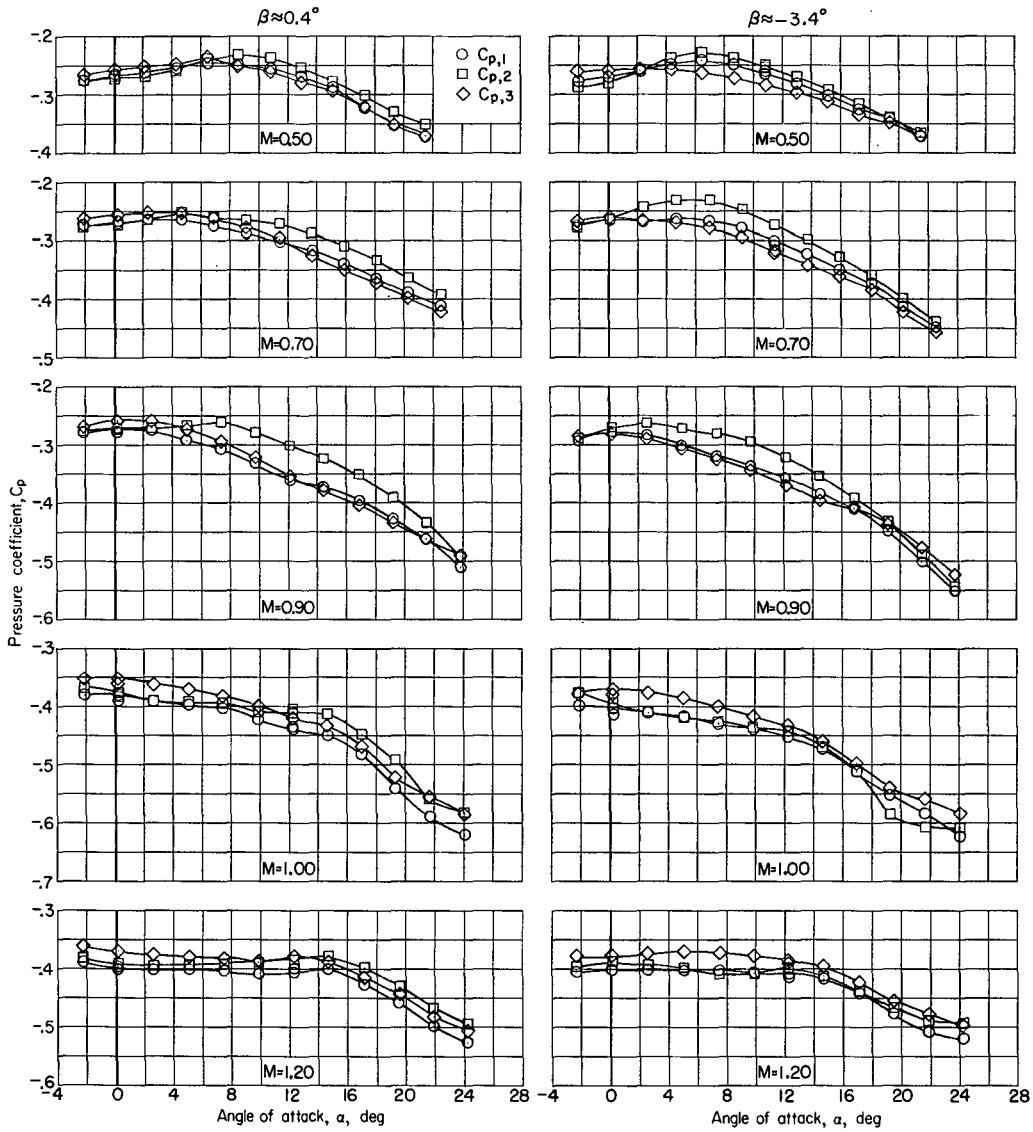

(b) $\delta_u = -30^\circ$; $\delta_l = 20^\circ$; $\delta_r = 10^\circ$.

Figure 11.- Continued.

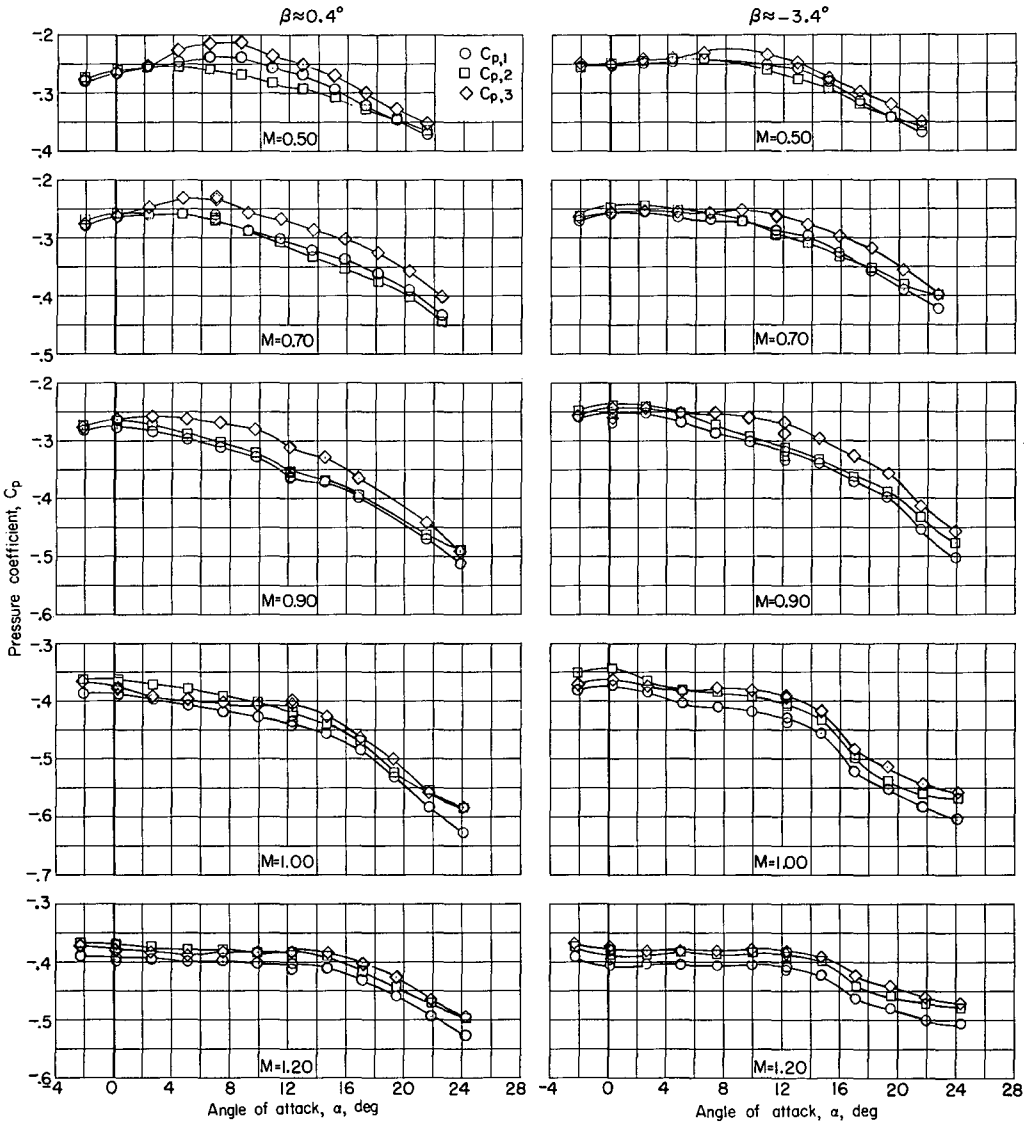

(c) $\delta_u = -30^\circ$; $\delta_l = 20^\circ$; $\delta_r = -10^\circ$.

Figure 11.- Continued.

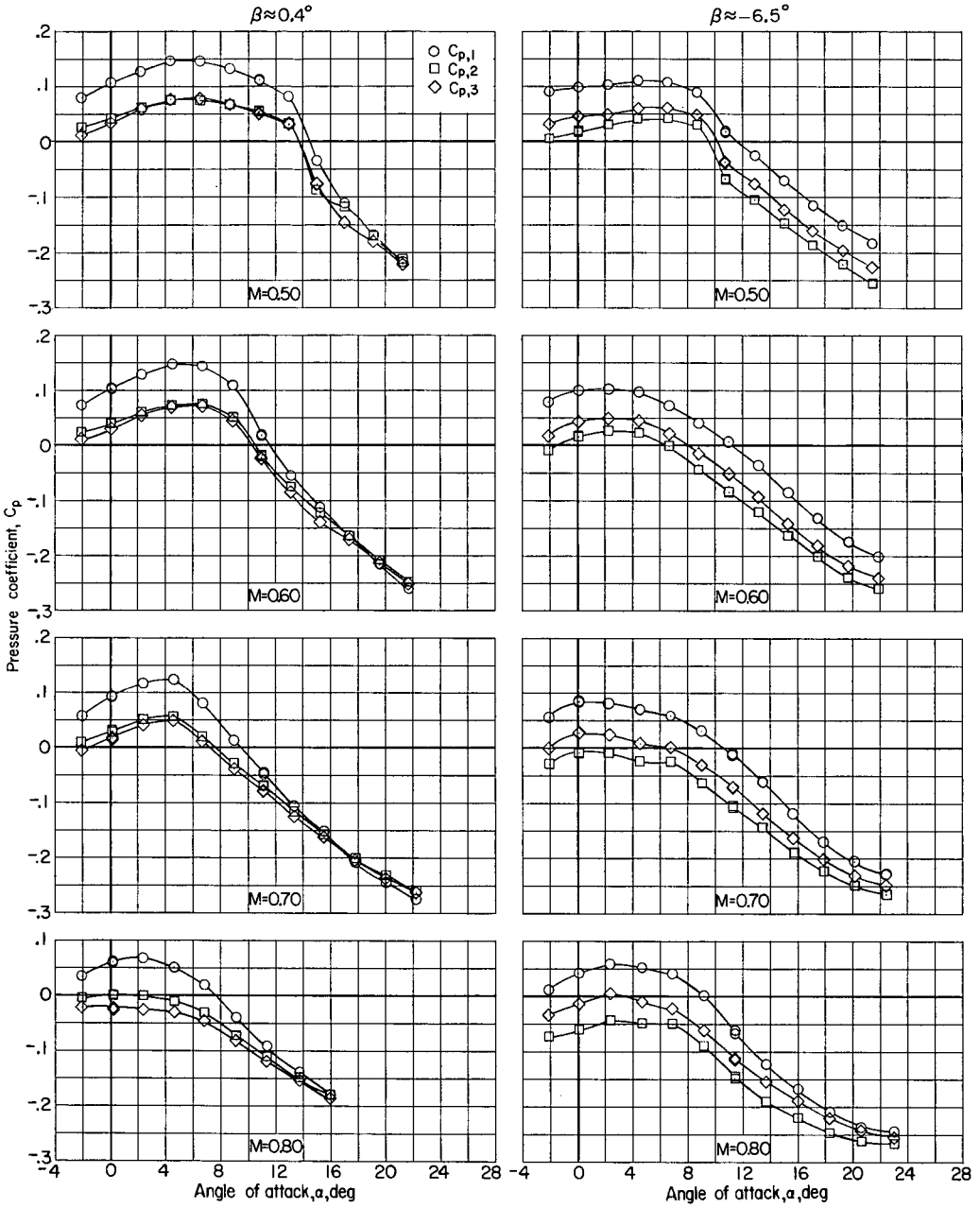

(d) $\delta_u = -10^\circ$; $\delta_l = 0^\circ$; $\delta_{r,L} = -10^\circ$; $\delta_{r,R} = 10^\circ$.

Figure 11.- Continued.

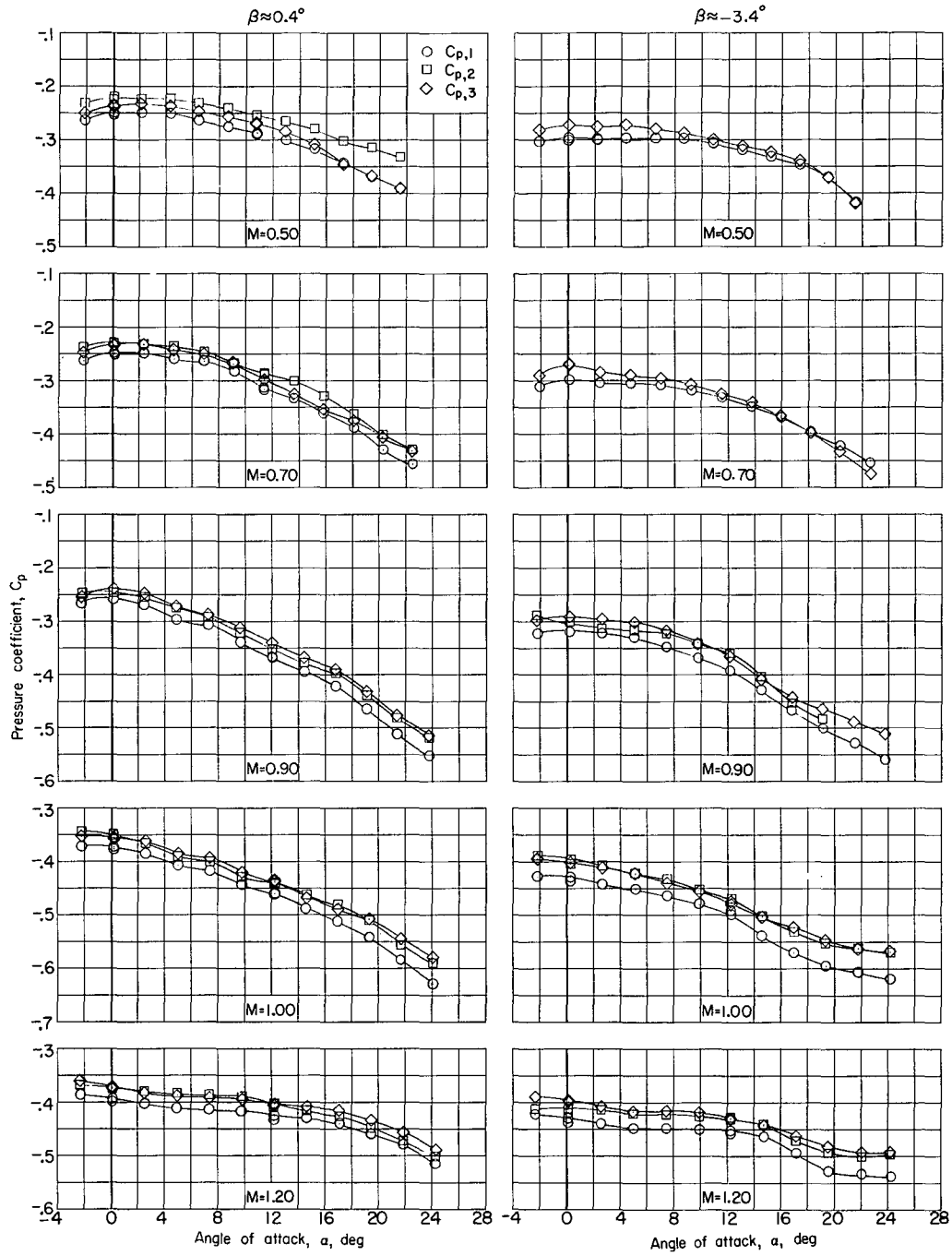

(e) $\delta_{u,L} = -40°$; $\delta_{u,R} = -20°$; $\delta_l = 20°$; $\delta_r = 0°$.

Figure 11.- Continued.

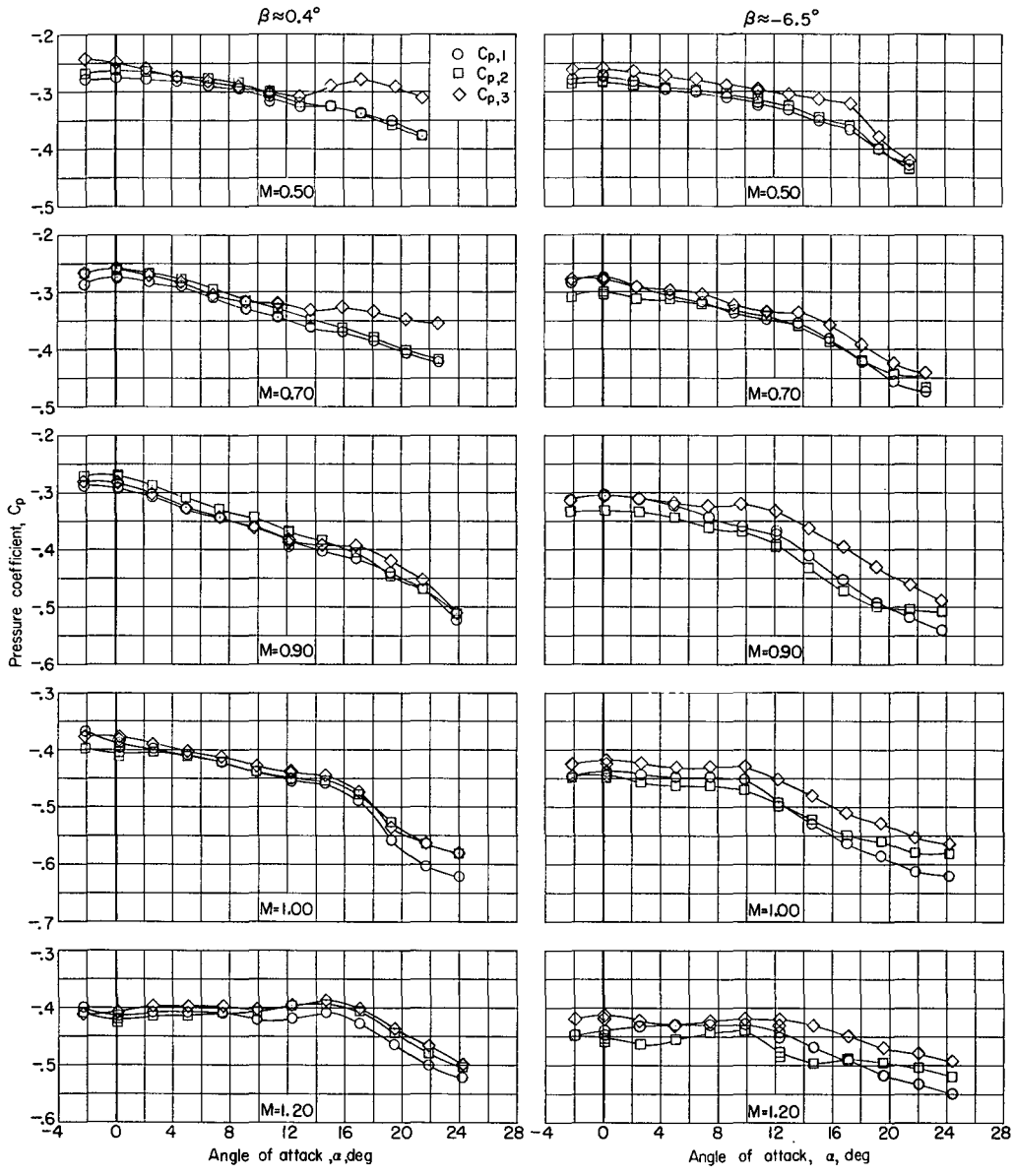

(f) $\delta_u = -30^\circ$; $\delta_{l,L} = 10^\circ$; $\delta_{l,R} = 30^\circ$; $\delta_r = 0^\circ$.

Figure 11.- Continued.

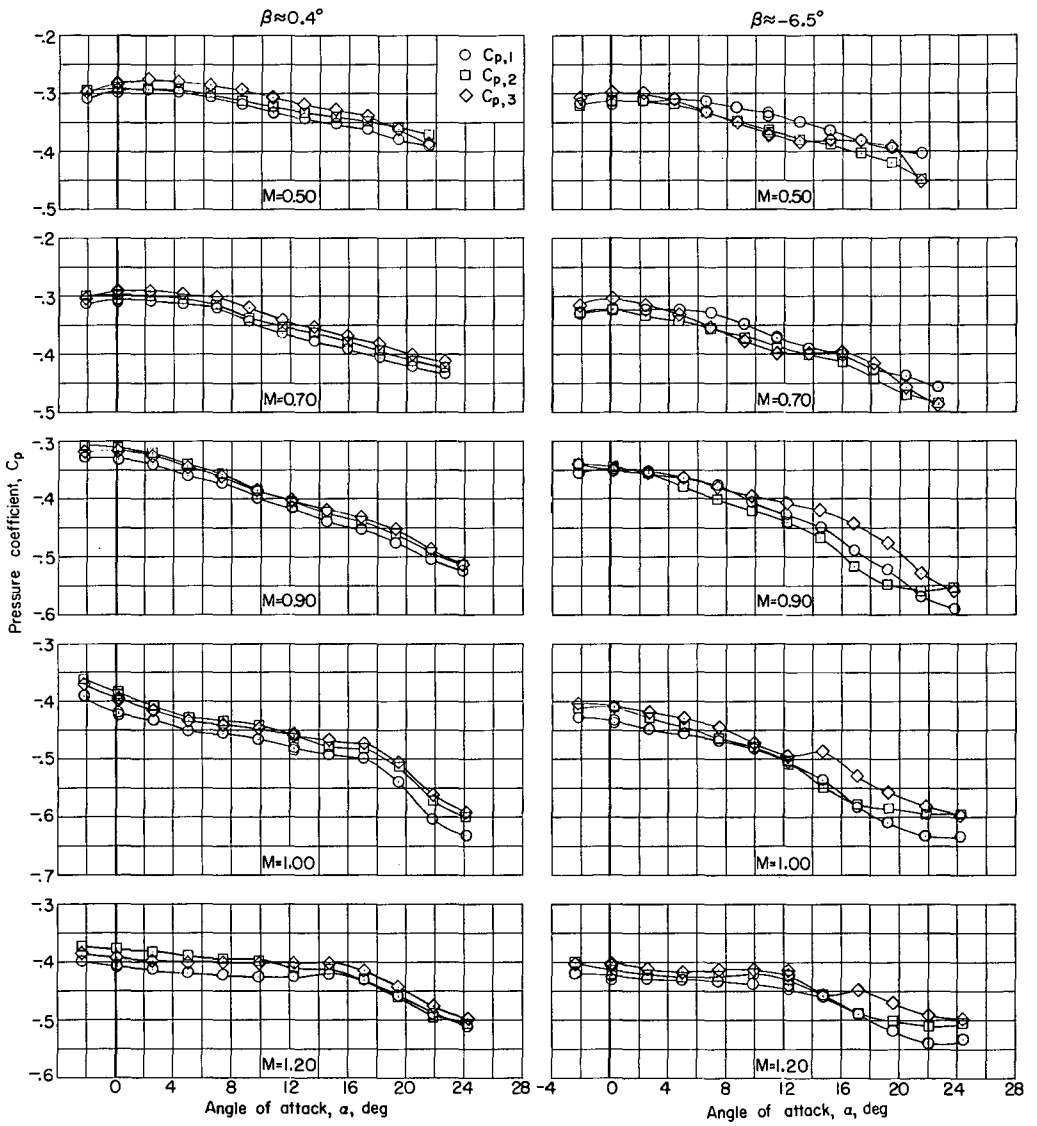

(g) $\delta_{u,L} = -40^{\circ}$; $\delta_{u,R} = -30^{\circ}$; $\delta_{l,L} = 20^{\circ}$; $\delta_{l,R} = 30^{\circ}$; $\delta_r = 0^{\circ}$.

Figure 11.- Concluded.

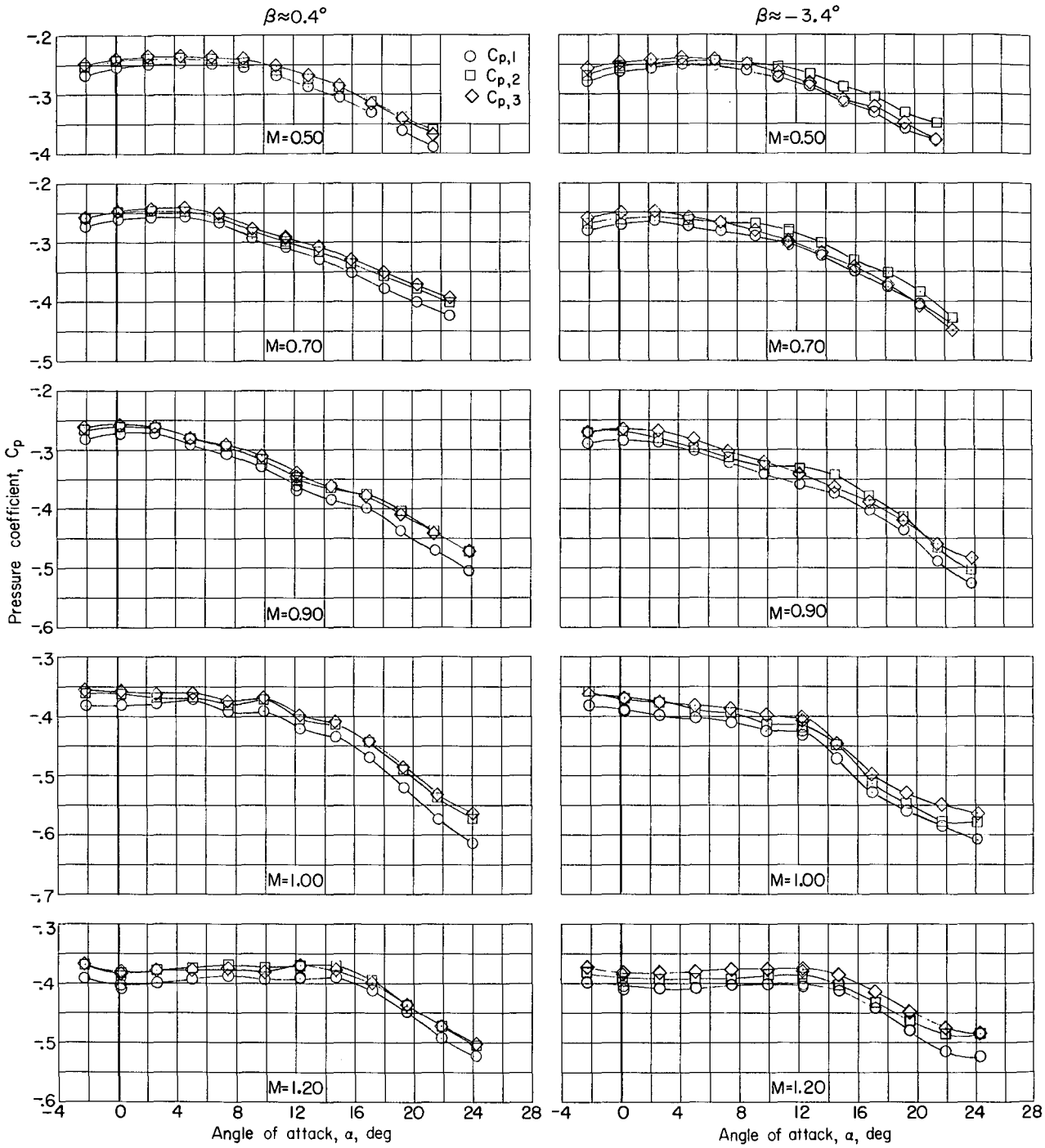

Figure 12.- Base pressure coefficient against angle of attack. Configuration 5 (modified outboard and central vertical tails on, canopy off); $\delta_u = -30^\circ$; $\delta_l = 20^\circ$; $\delta_r = 0^\circ$.

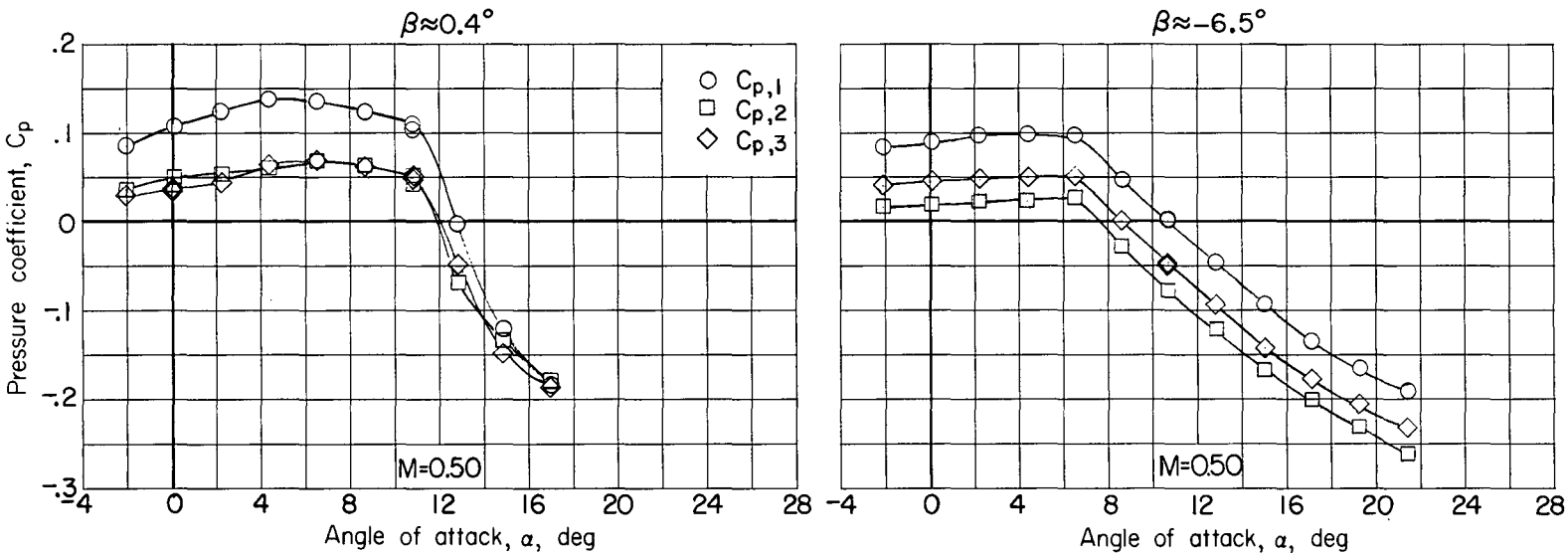

Figure 13.- Base pressure coefficient against angle of attack. Configuration 6 (basic outboard and central vertical tails on, canopy off, dummy support rods on); $\delta_u = -10^\circ$; $\delta_l = 0^\circ$; $\delta_{r,L} = -10^\circ$; $\delta_{r,R} = 10^\circ$.

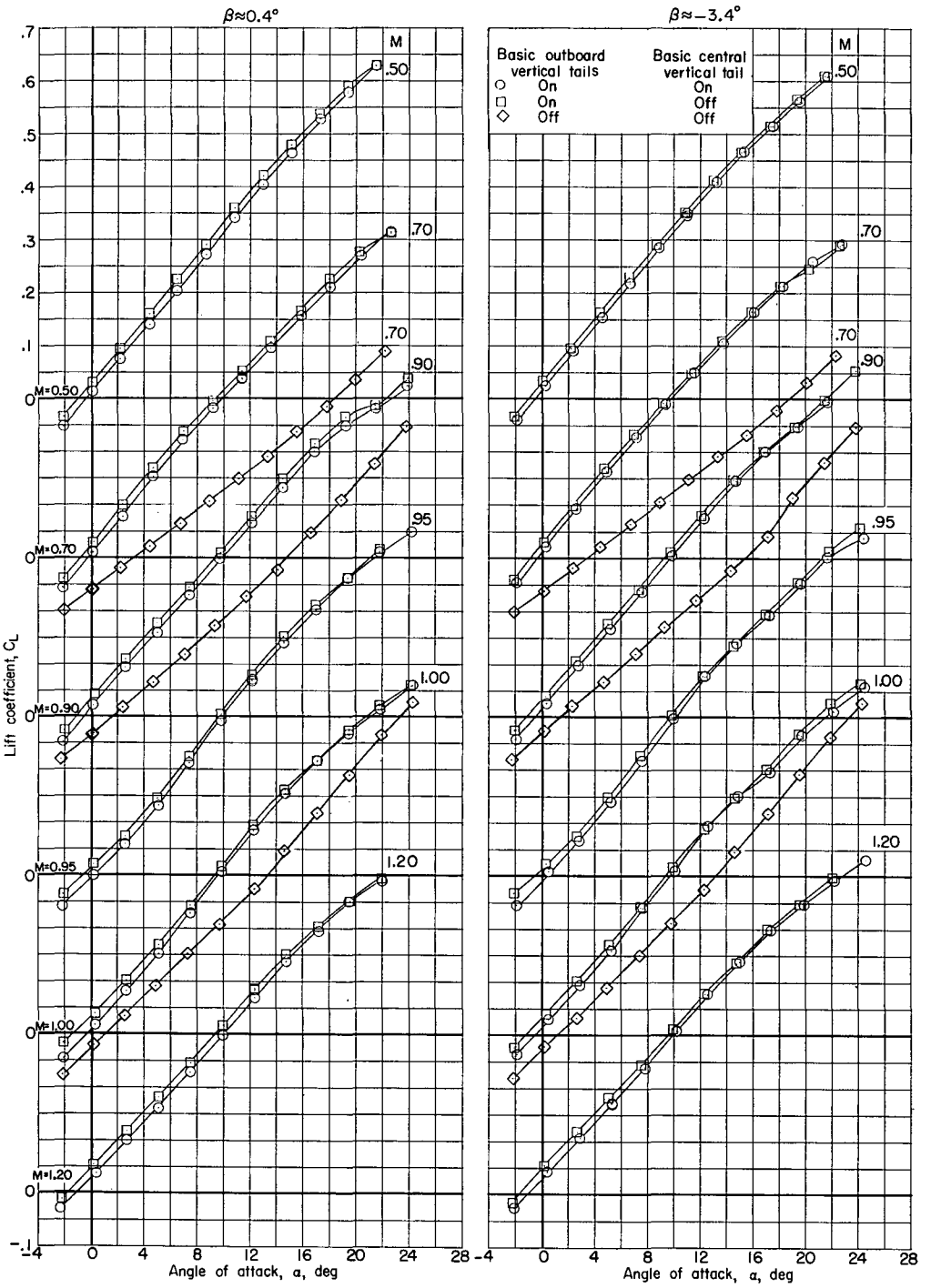

(a) C_L against α.

Figure 14.- Effect of basic outboard and central vertical tails on longitudinal aerodynamic characteristics. Configurations 1, 2, and 3 (canopy on); $\delta_u = -30^\circ$; $\delta_l = 20^\circ$; $\delta_r = 0^\circ$

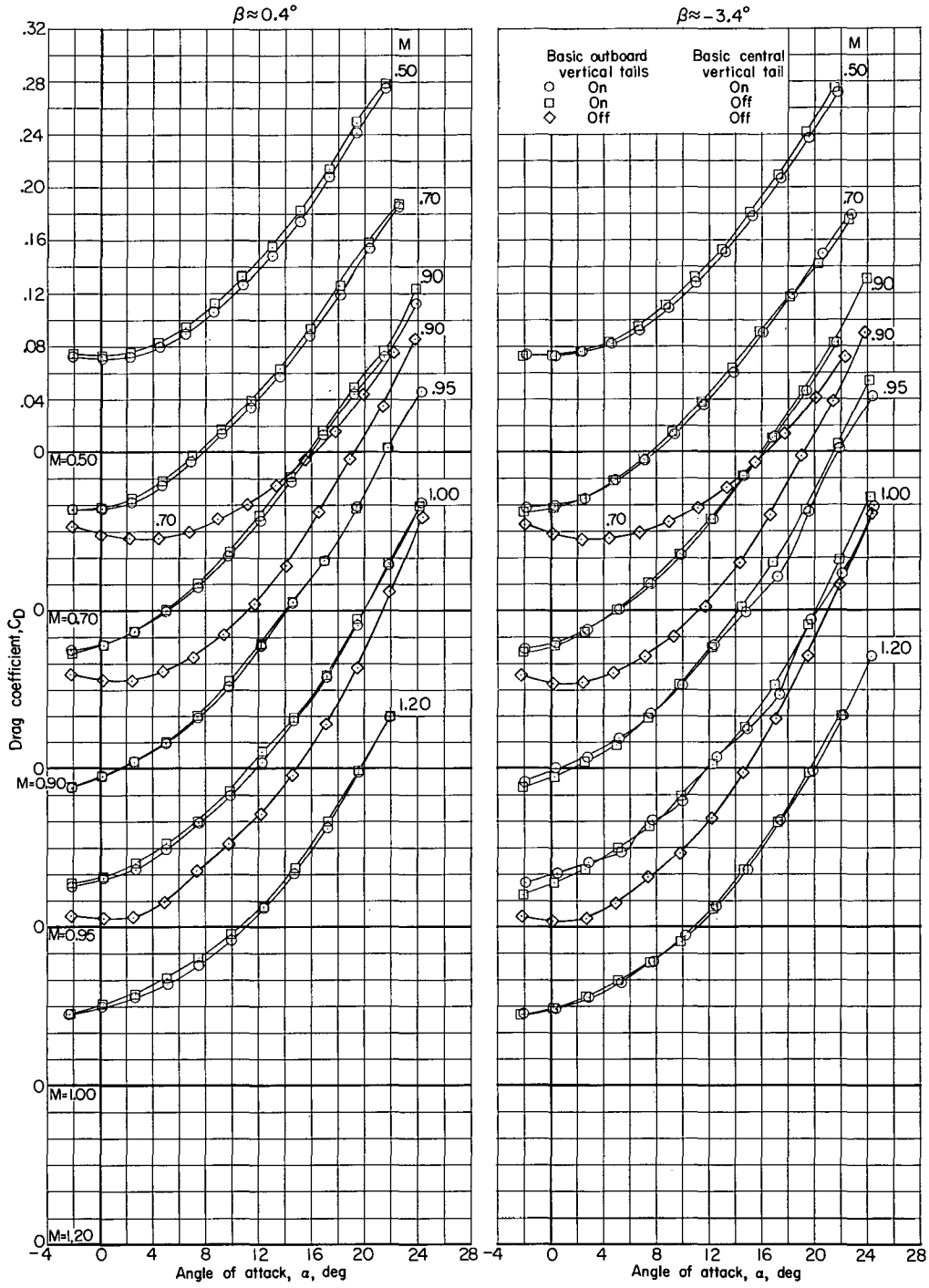

(b) C_D against α.

Figure 14.- Continued.

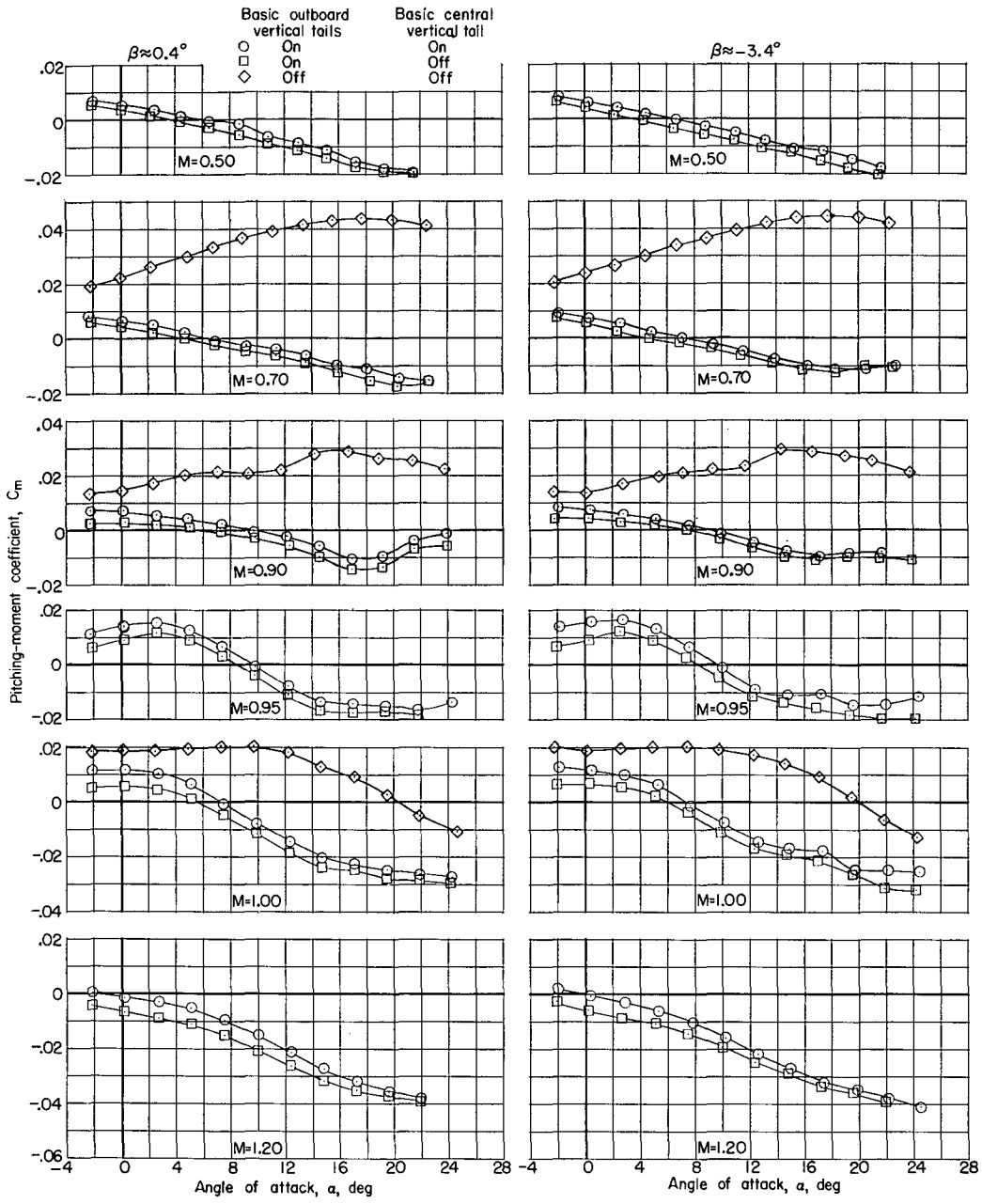

(c) C_m against α.

Figure 14.- Continued.

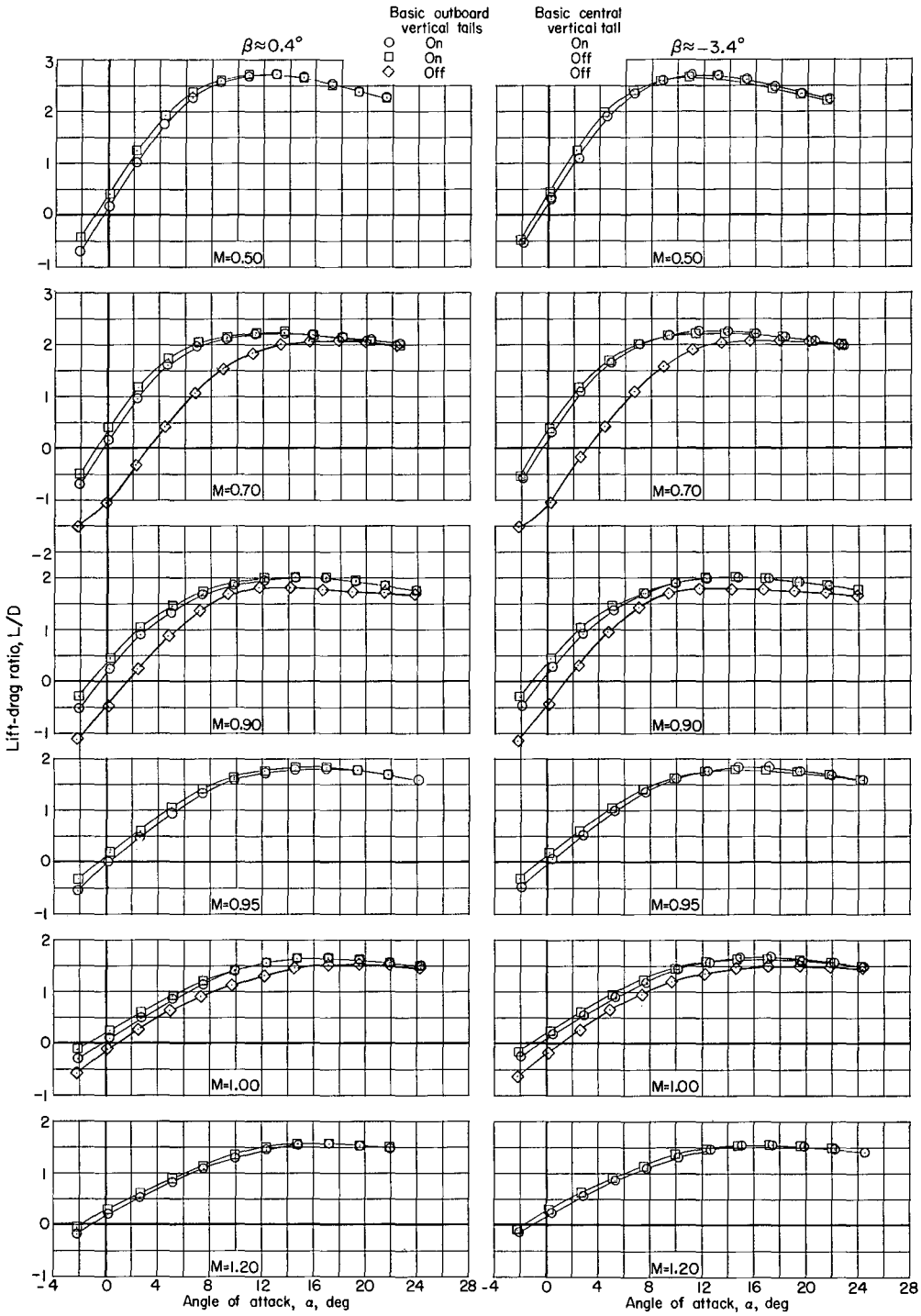

(d) L/D against α.

Figure 14.- Concluded.

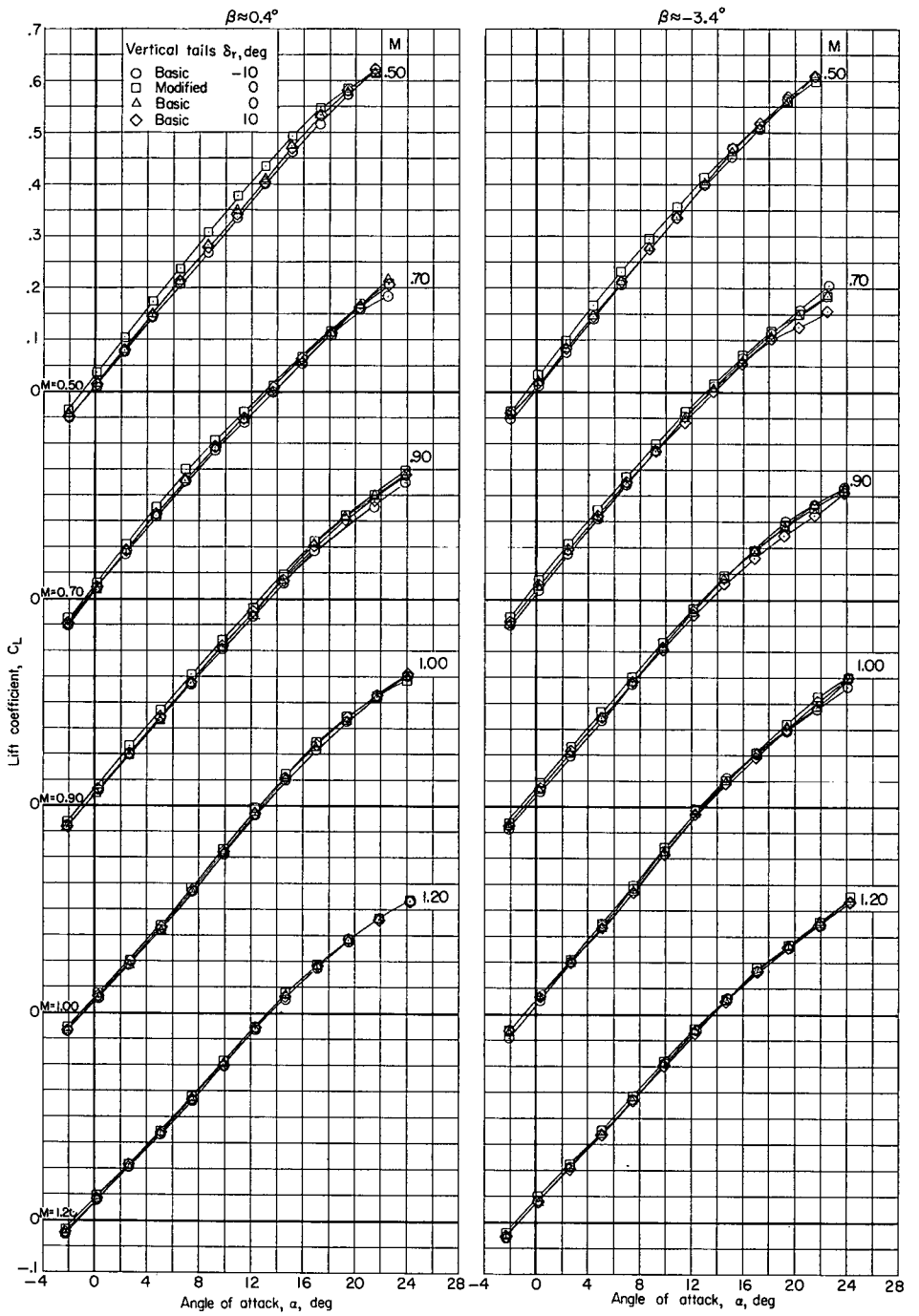

(a) C_L against α.

Figure 15.- Effect of modified outboard and central vertical tails and rudder deflection on longitudinal aerodynamic characteristics. Configurations 4 and 5 (canopy off); $\delta_u = -30^\circ$; $\delta_l = 20^\circ$.

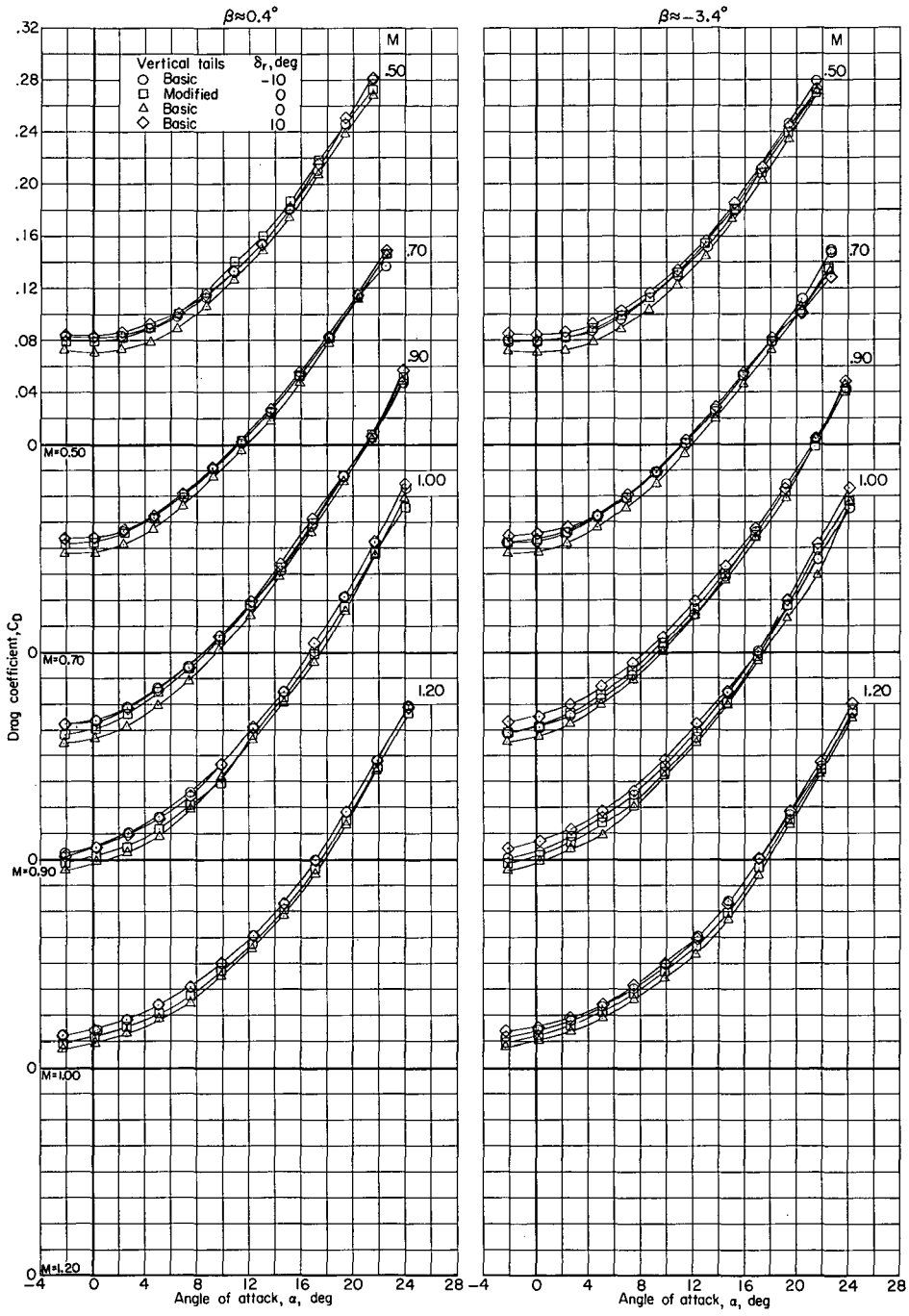

(b) C_D against α.

Figure 15.- Continued.

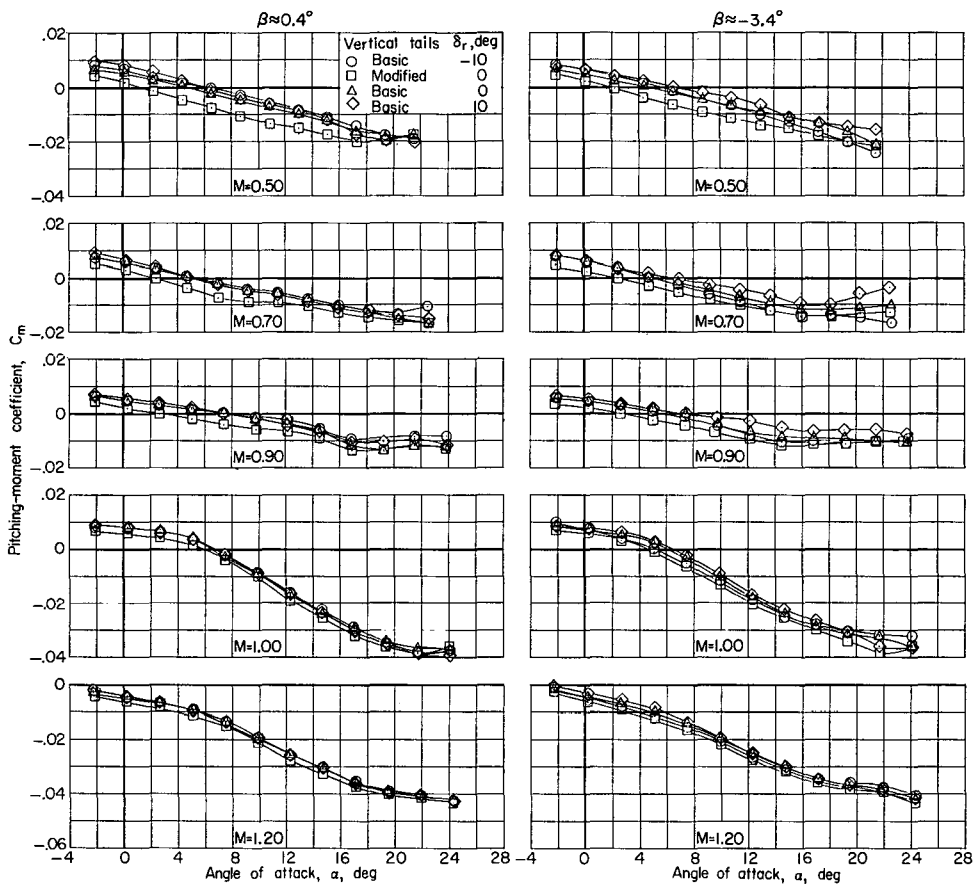

(c) C_m against α.

Figure 15.- Continued.

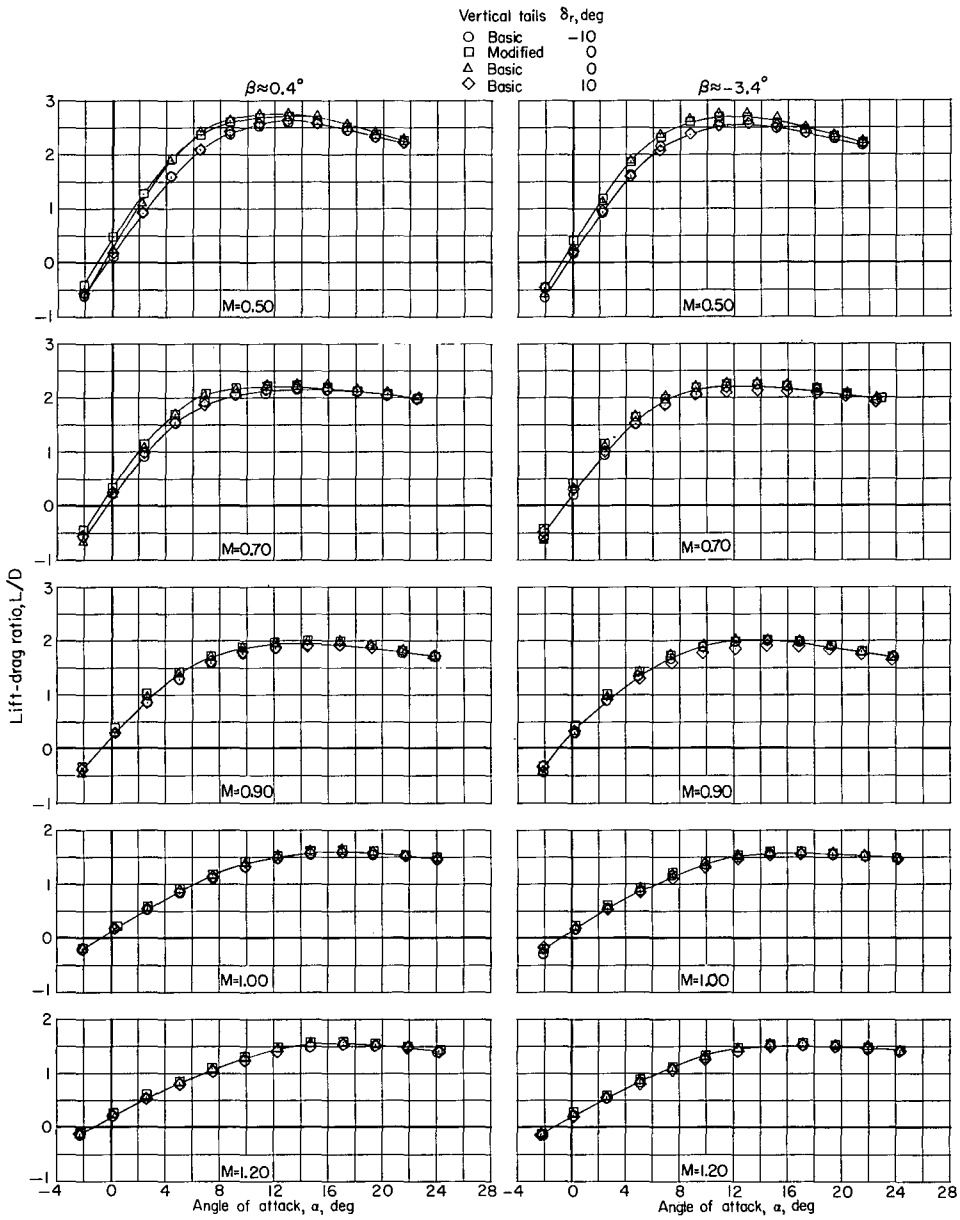

(d) L/D against α.

Figure 15.- Concluded.

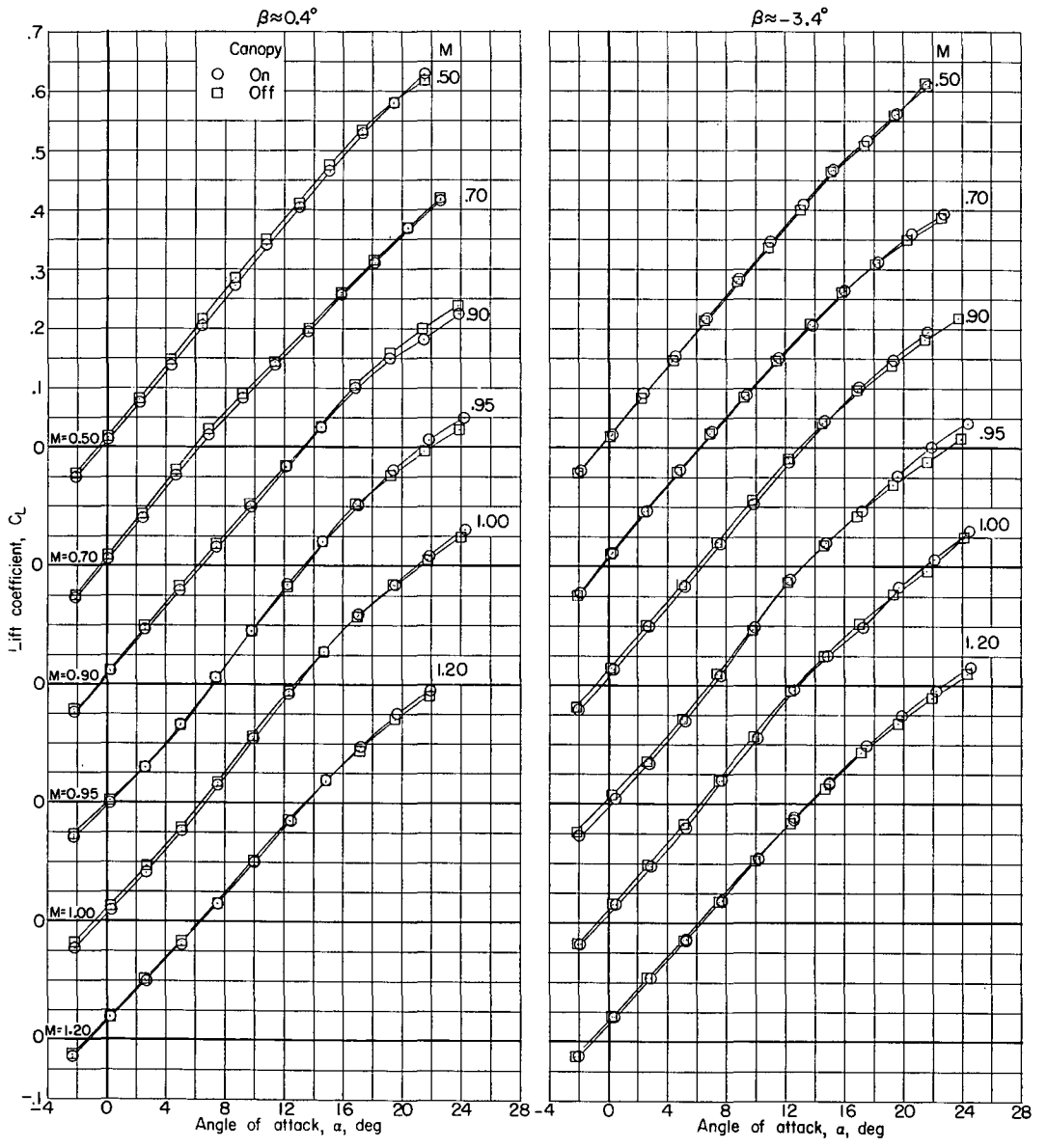

(a) C_L against α.

Figure 16.- Effect of canopy on longitudinal aerodynamic characteristics. Configurations 3 and 4 (basic outboard and central vertical tails on); $\delta_u = -30^\circ$; $\delta_l = 20^\circ$; $\delta_r = 0^\circ$.

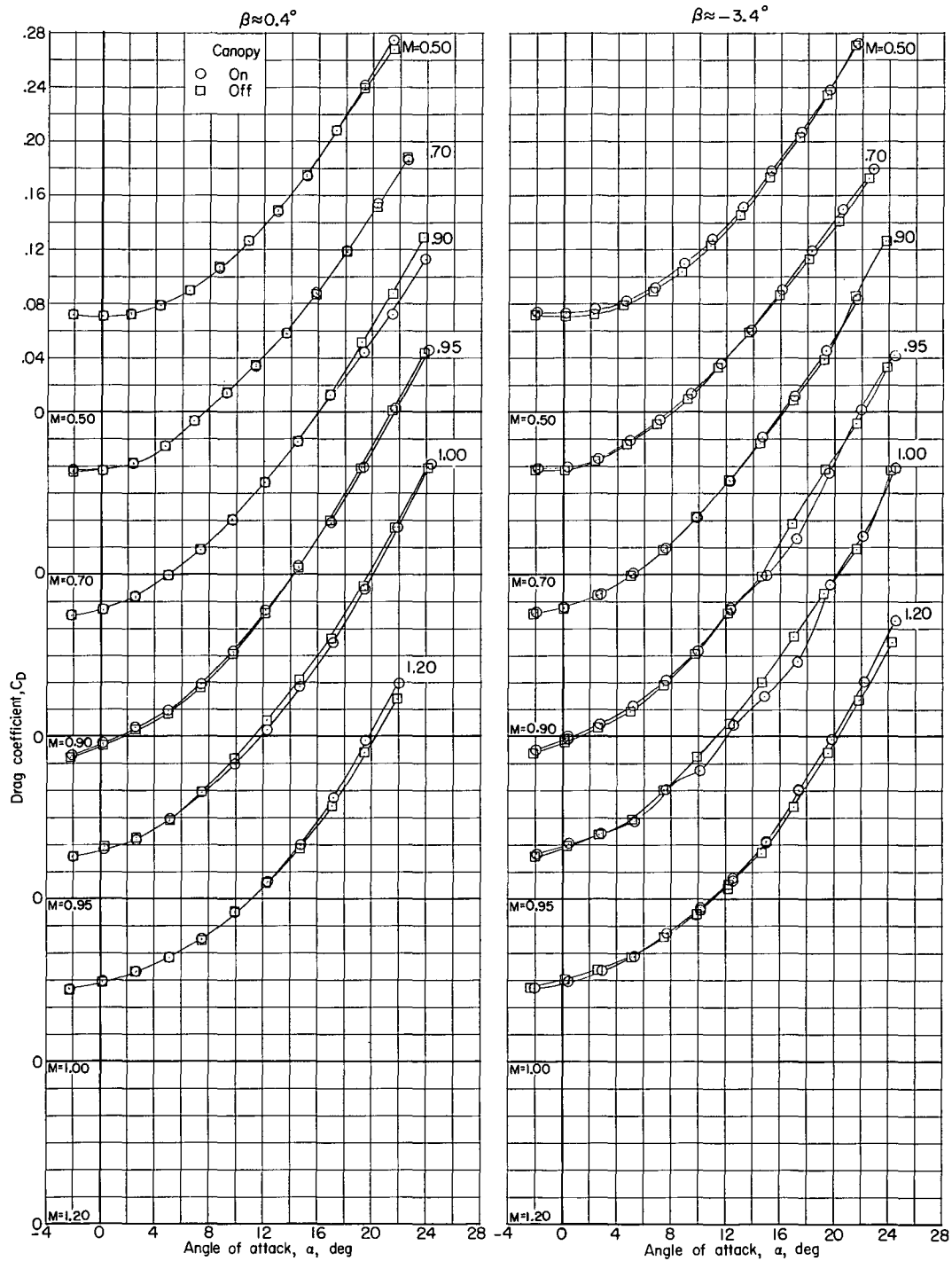

(b) C_D against α.

Figure 16.- Continued.

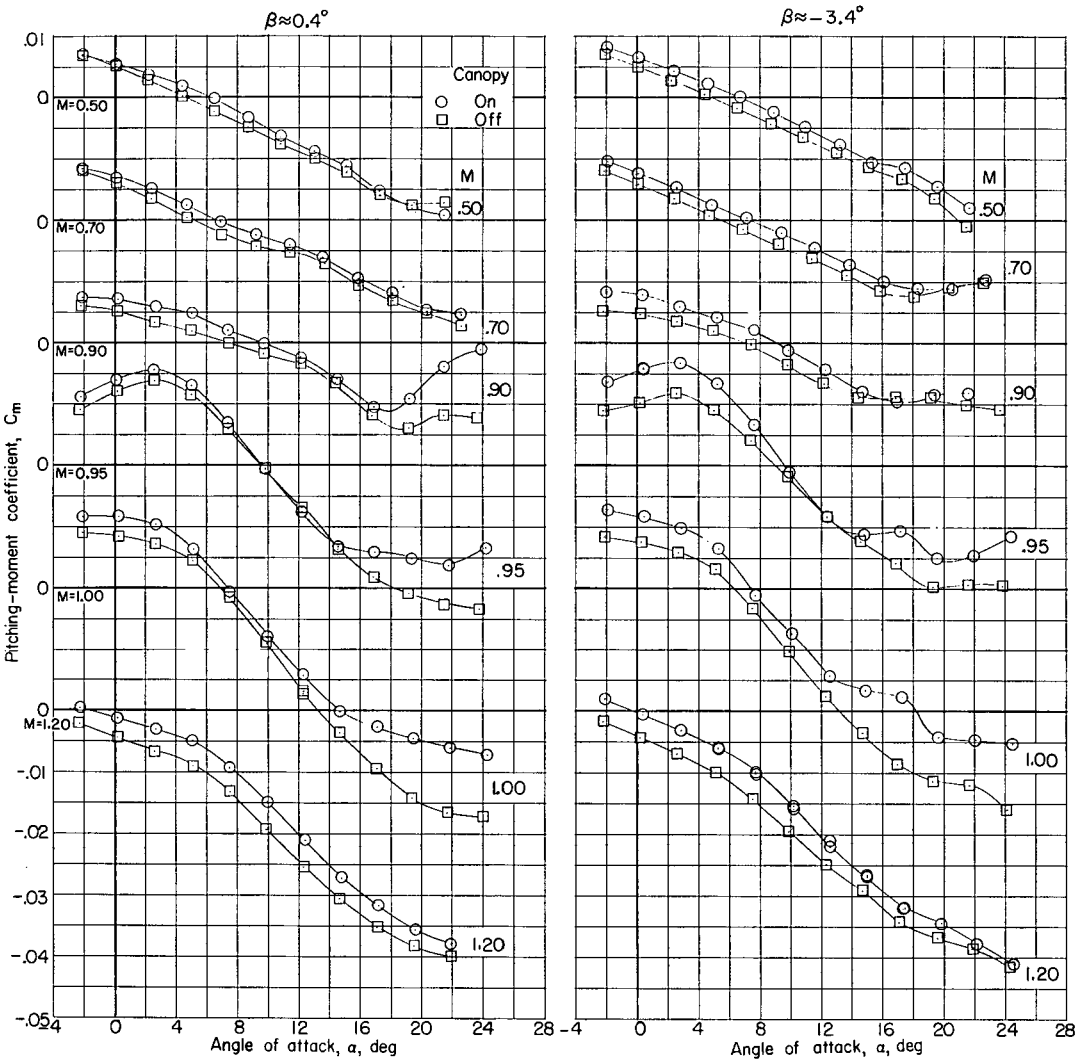

(c) C_m against α.

Figure 16.- Continued.

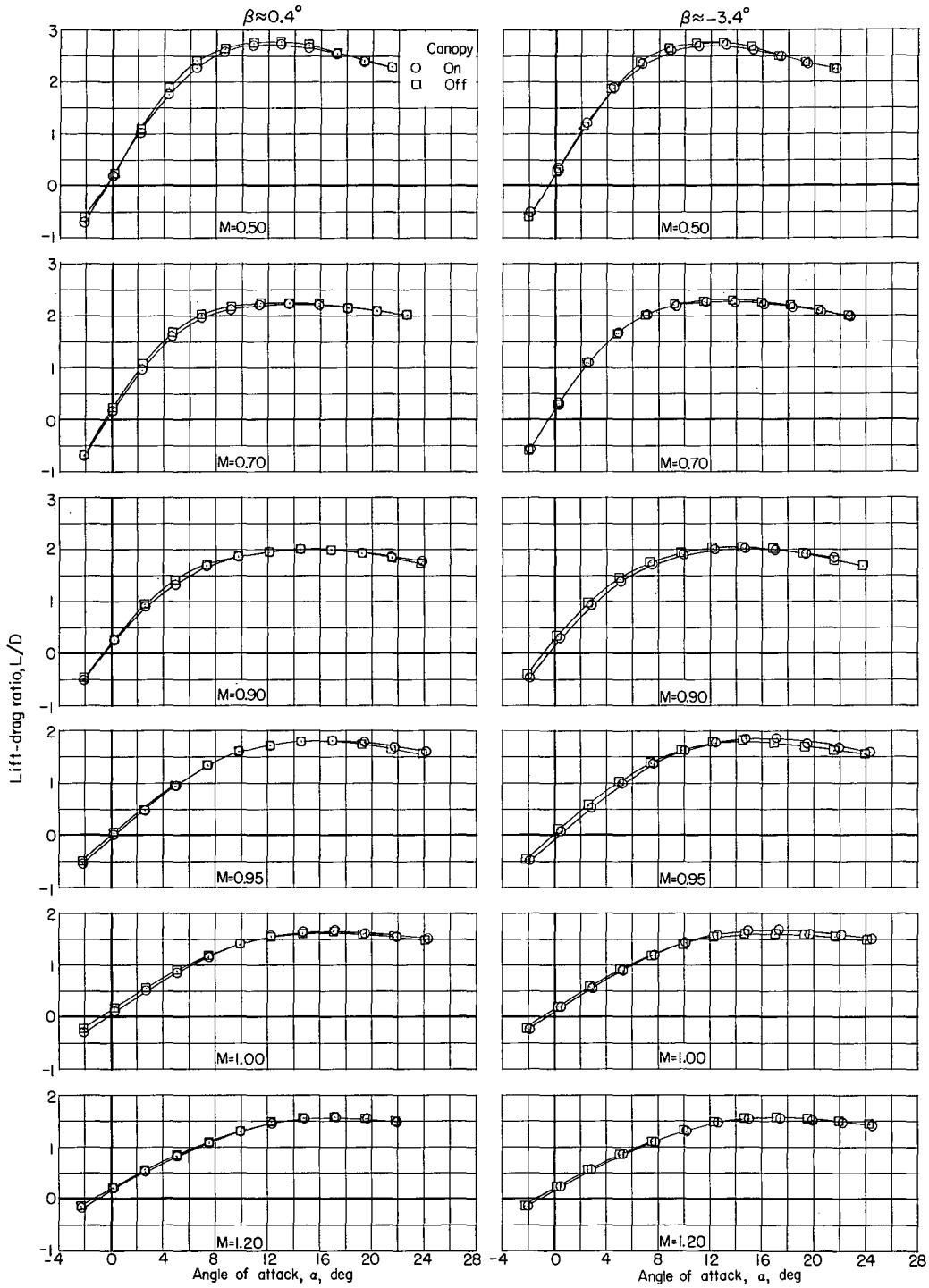

(d) L/D against α.

Figure 16.- Concluded.

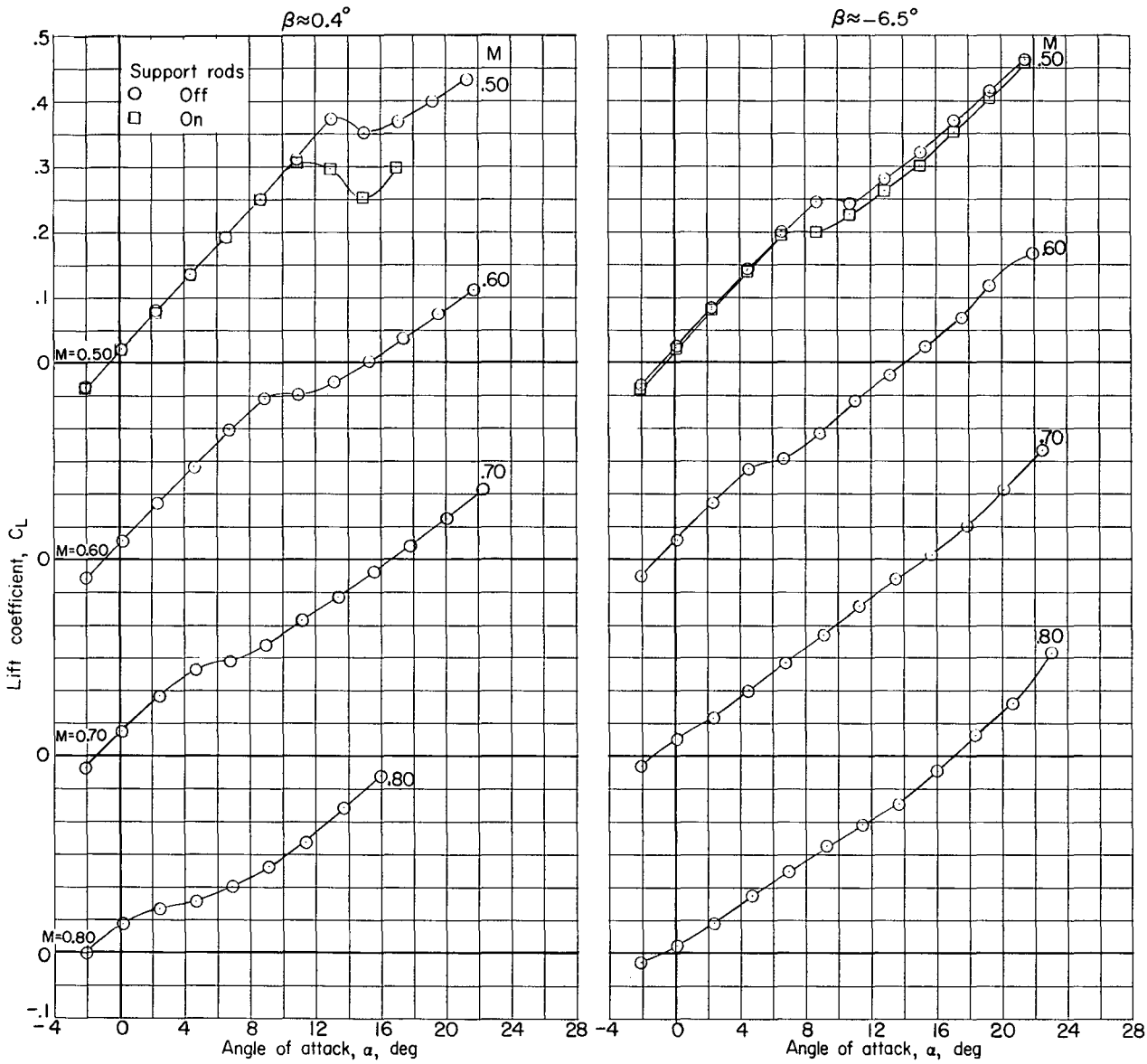

(a) C_L against α.

Figure 17.- Effect of external dummy support rods on longitudinal aerodynamic characteristics. Configurations 4 and 6 (basic outboard and central vertical tails on, canopy off); $\delta_u = -10^\circ$; $\delta_l = 0^\circ$; $\delta_{r,L} = -10^\circ$; $\delta_{r,R} = 10^\circ$.

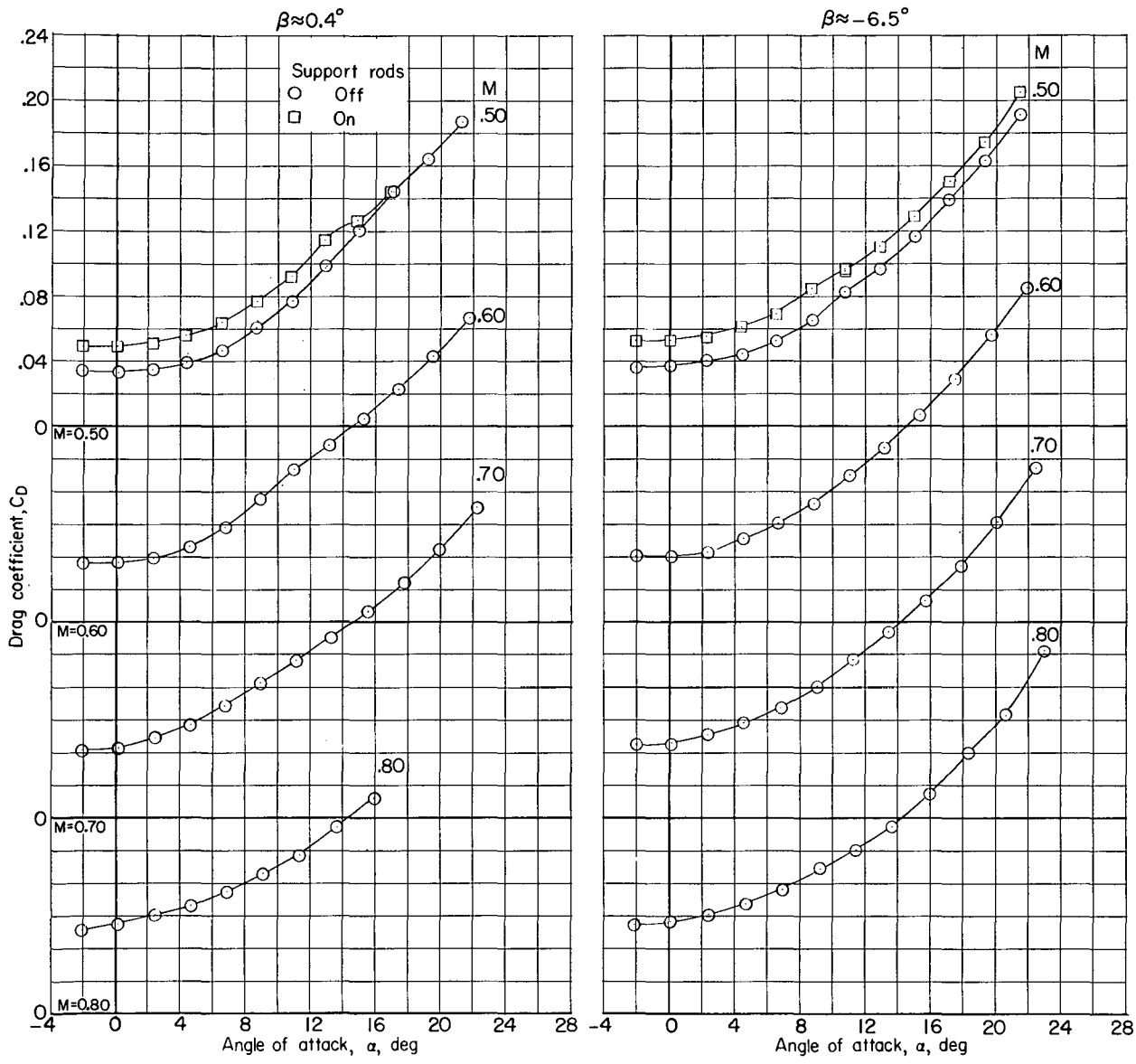

(b) C_D against α.

Figure 17.- Continued.

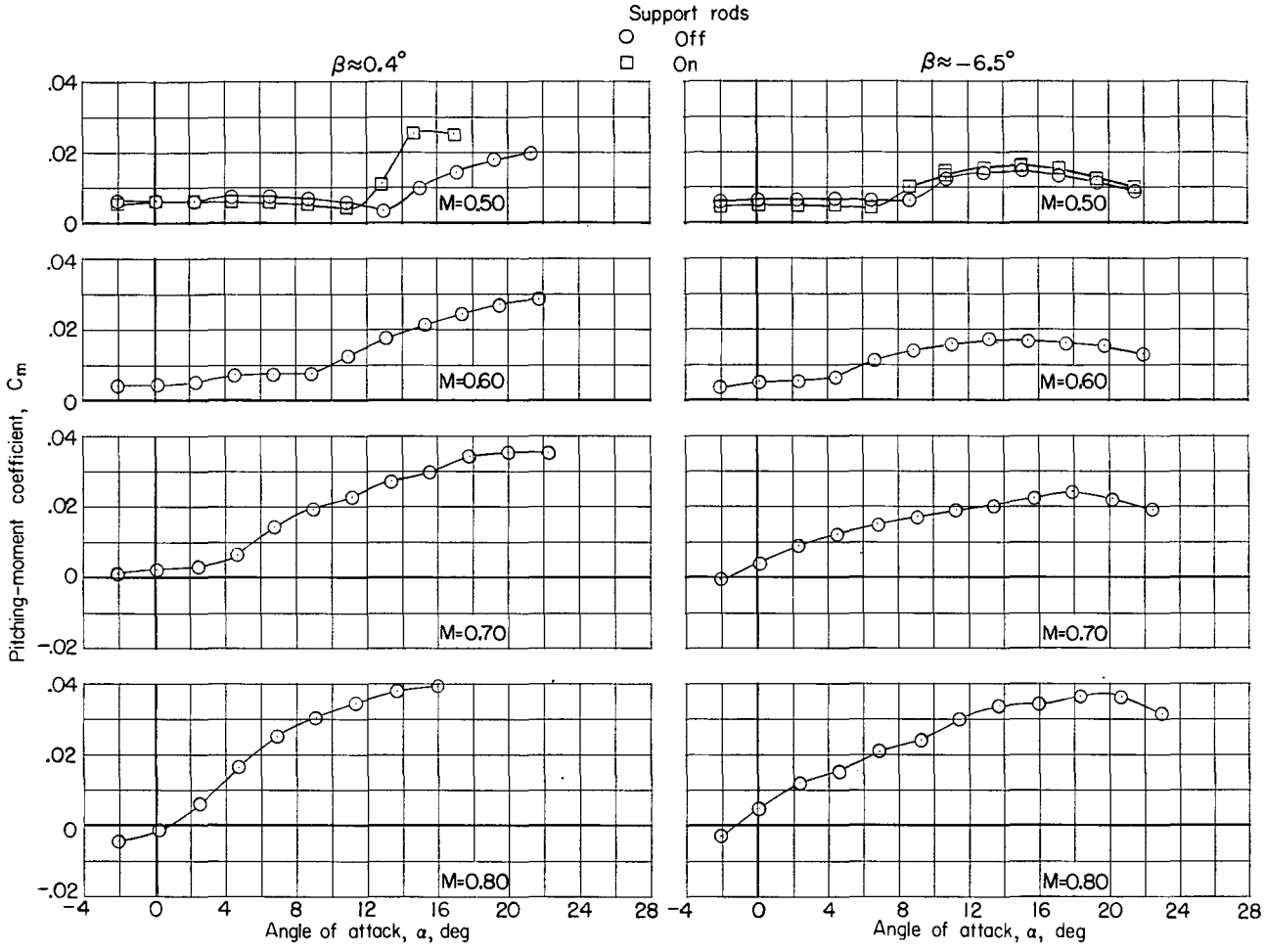

(c) C_m against α.

Figure 17.- Continued.

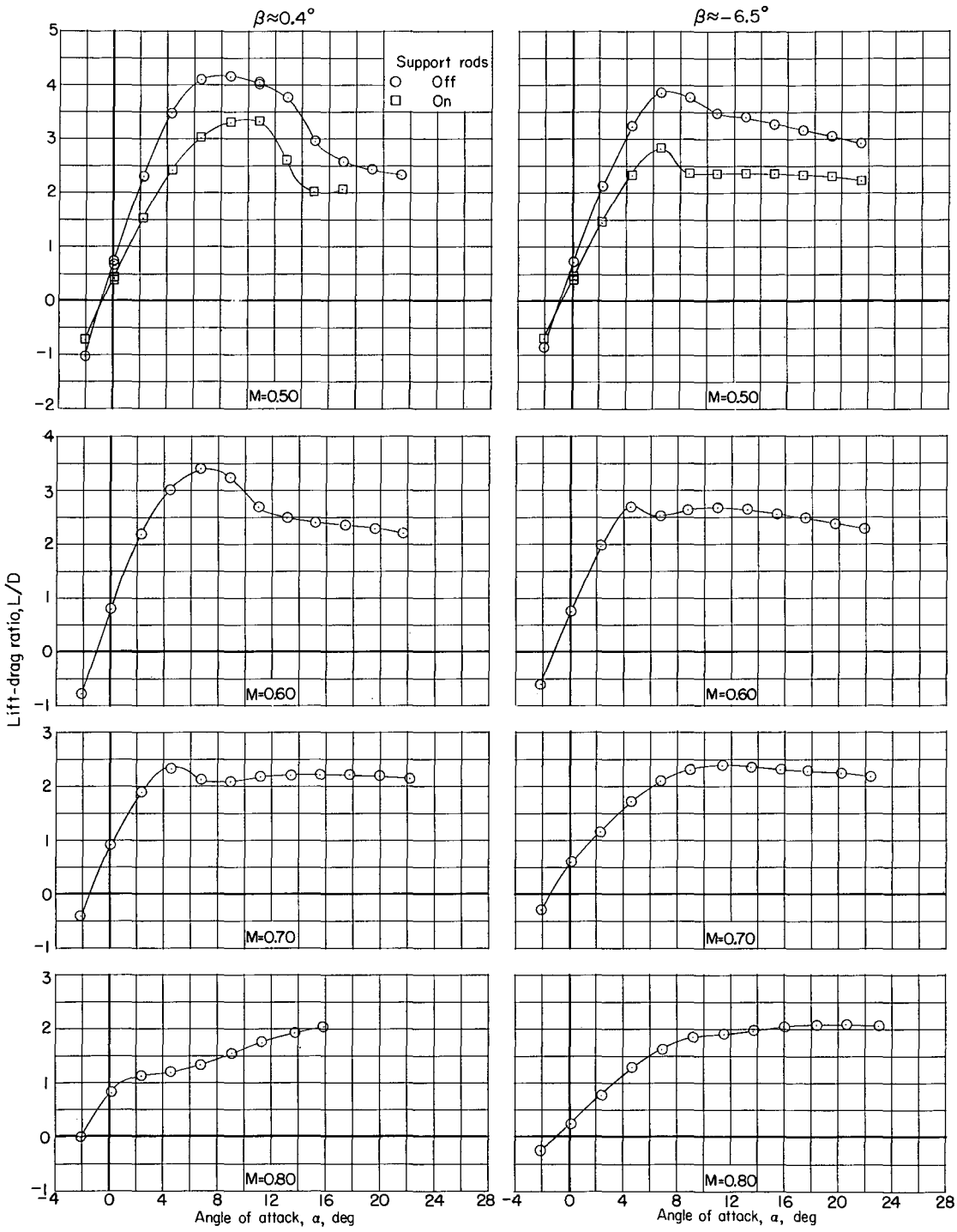

(d) L/D against α.

Figure 17.- Concluded.

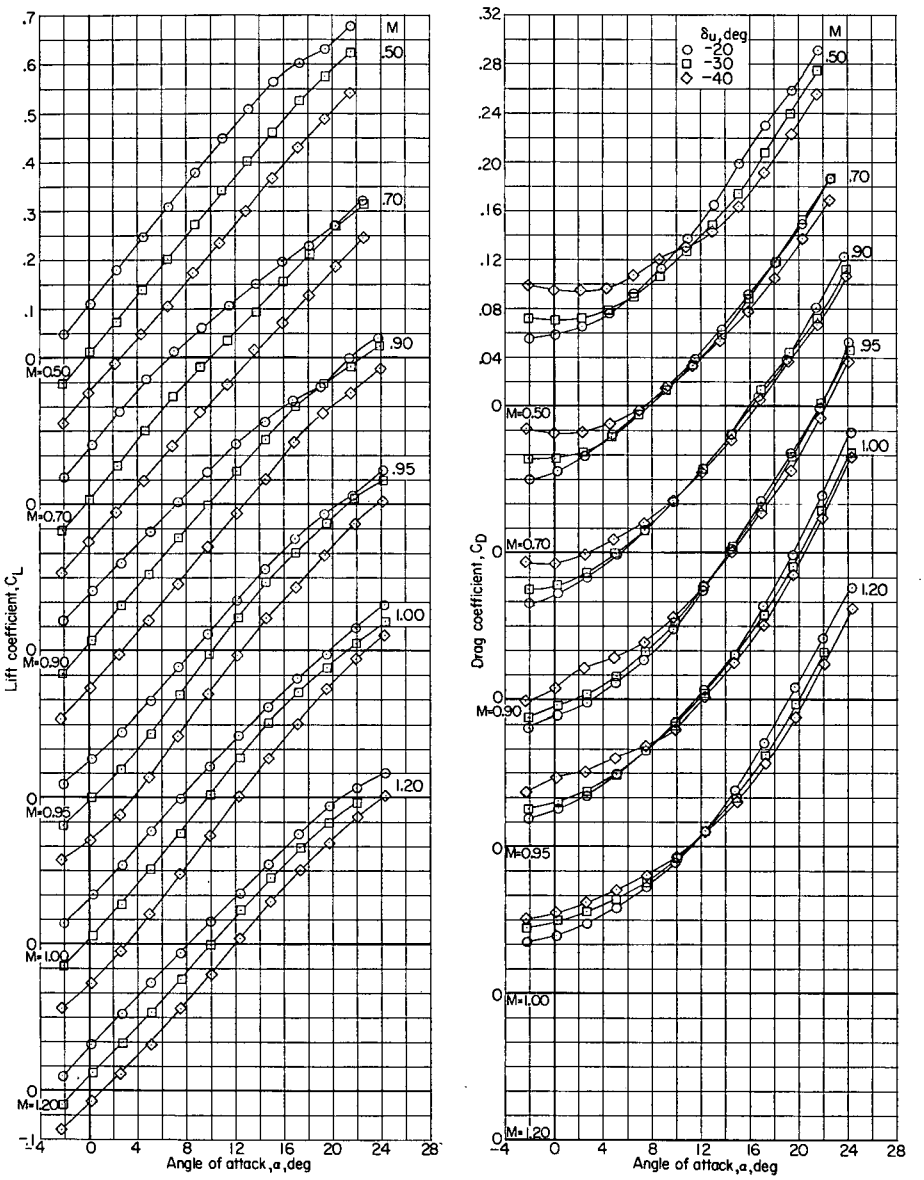

(a) C_L against α.

(b) C_D against α.

Figure 18.- Effect of upper-flap deflection on longitudinal aerodynamic characteristics. Configuration 3 (basic outboard and central vertical tails on, canopy on); $\delta_l = 20^\circ$; $\delta_r = 0^\circ$; $\beta \approx 0.4^\circ$.

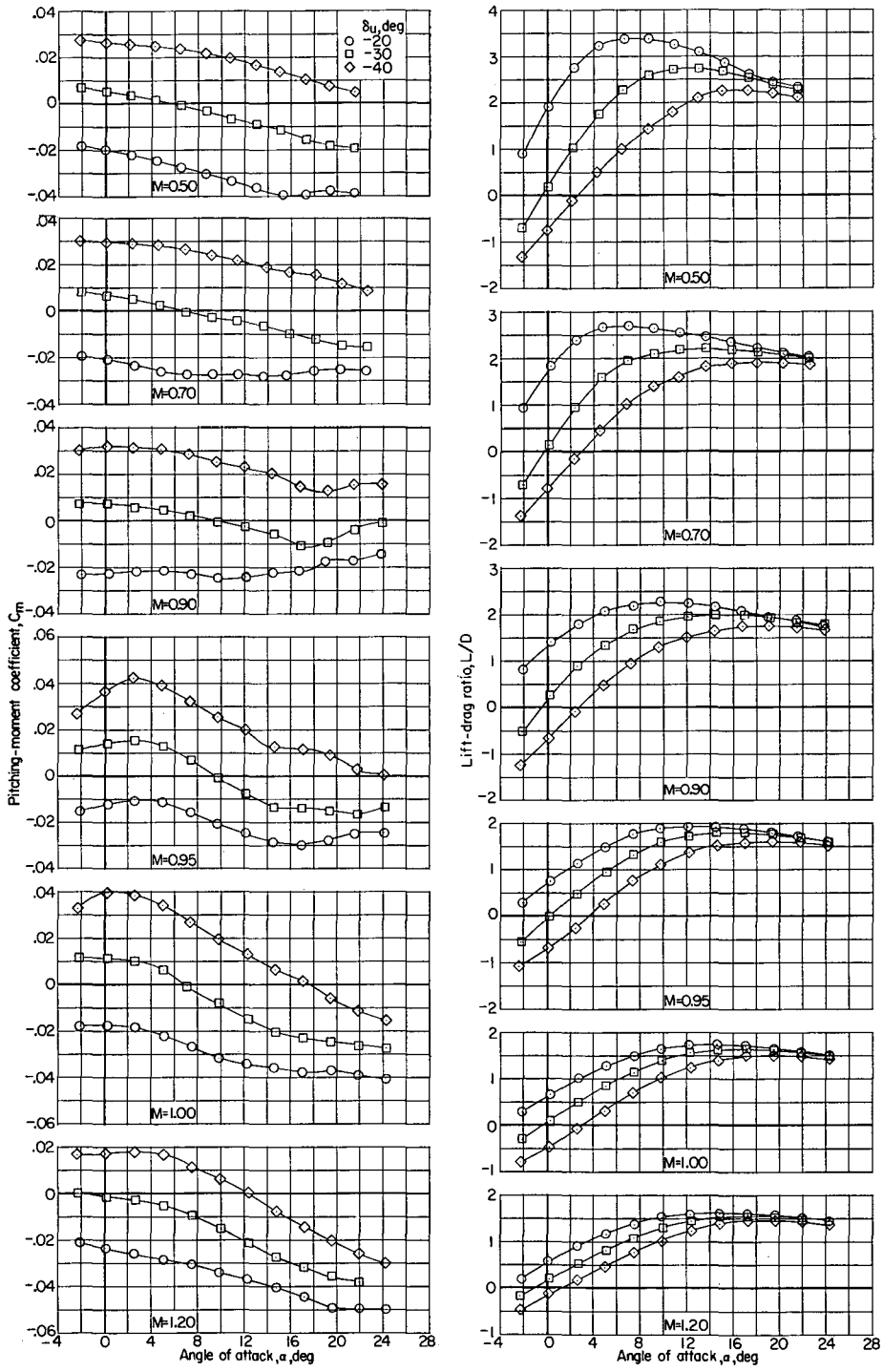

(c) C_m against α.

(d) L/D against α.

Figure 18.- Concluded.

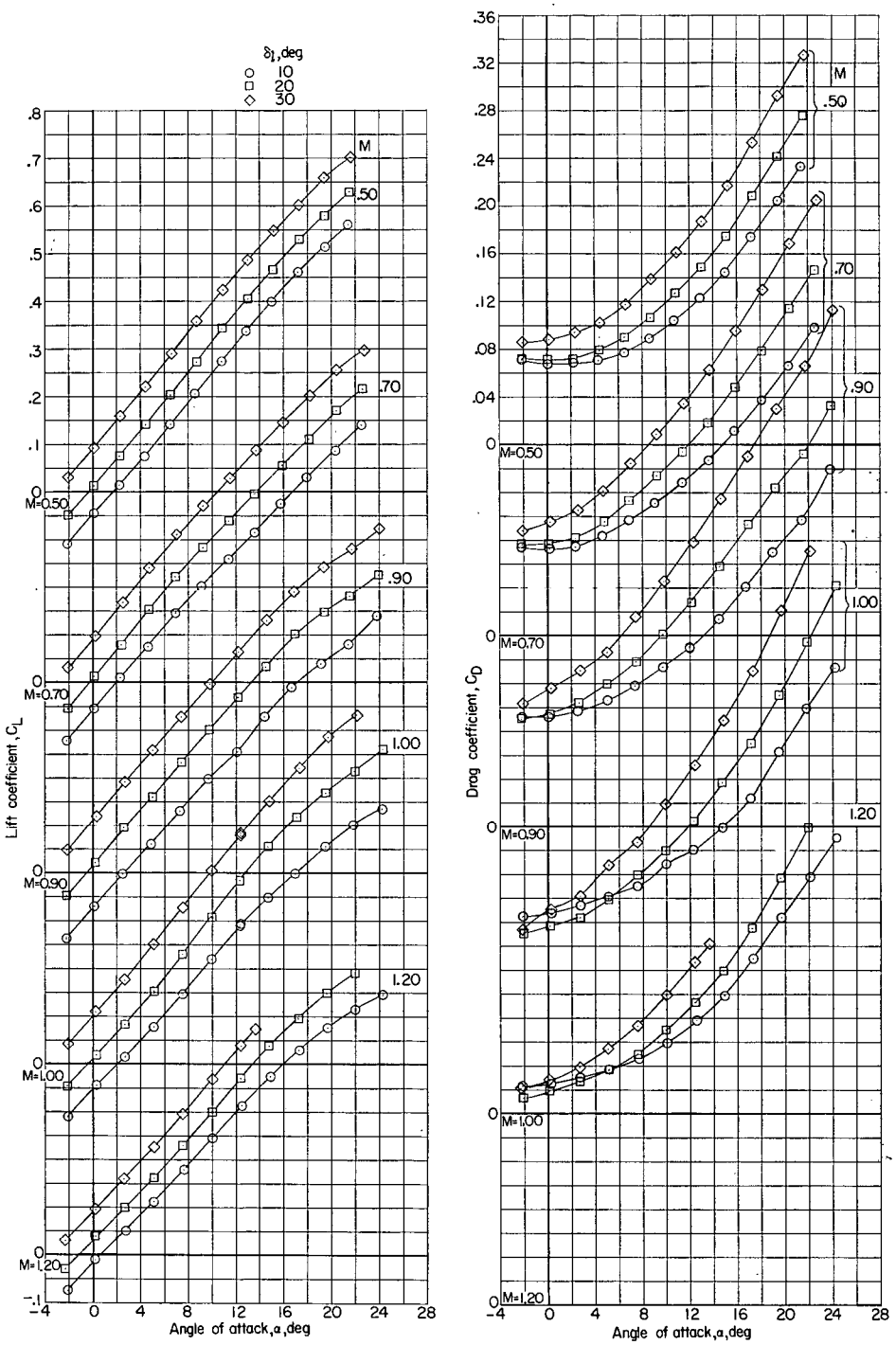

(a) C_L against α.

(b) C_D against α.

Figure 19.- Effect of lower-flap deflection on longitudinal aerodynamic characteristics. Configuration 3 (basic outboard and central vertical tails on, canopy on); $\delta_u = -30^\circ$; $\delta_r = 0^\circ$; $\beta \approx 0.4^\circ$.

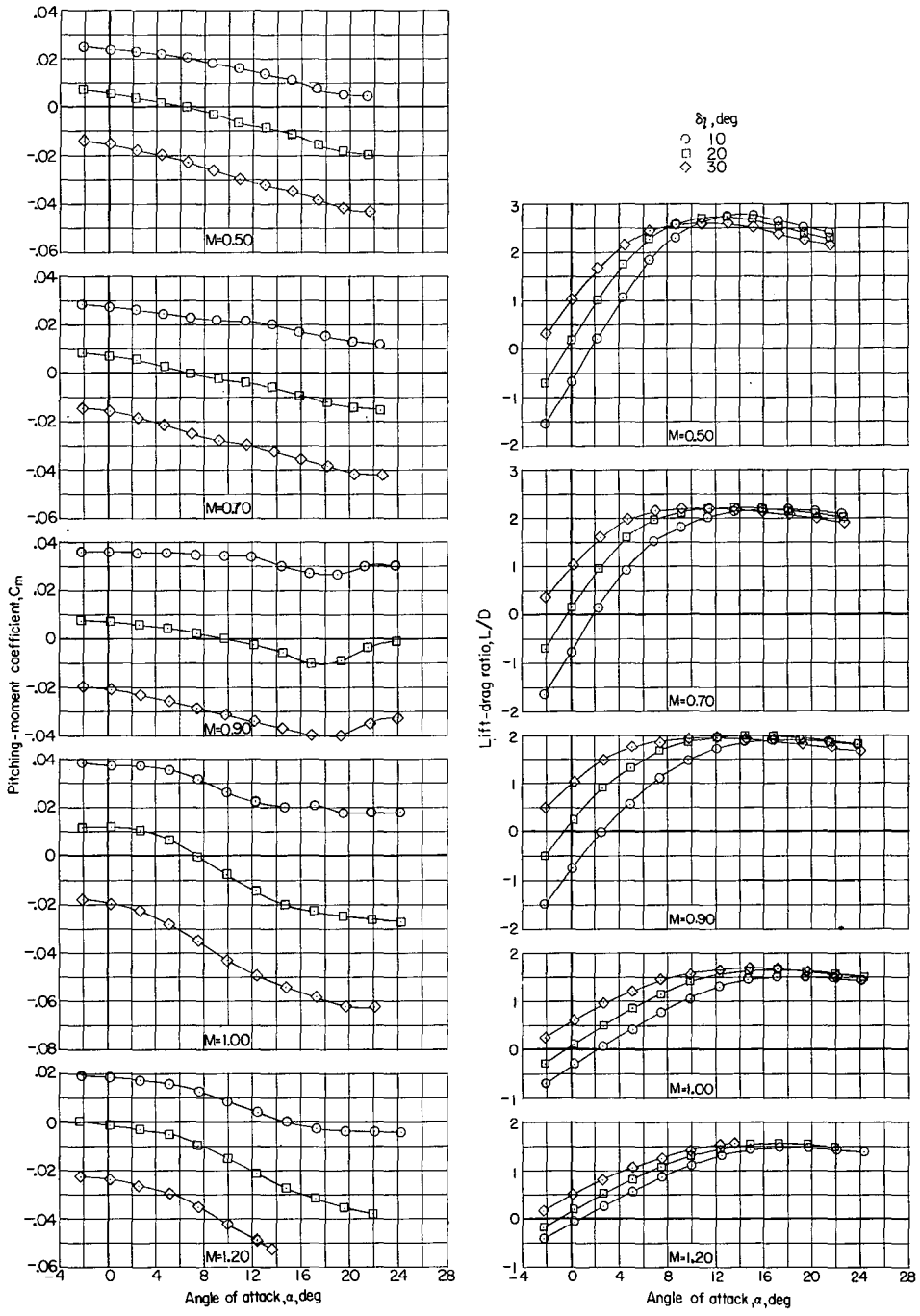

(c) C_m against α.

(d) L/D against α.

Figure 19.- Concluded.

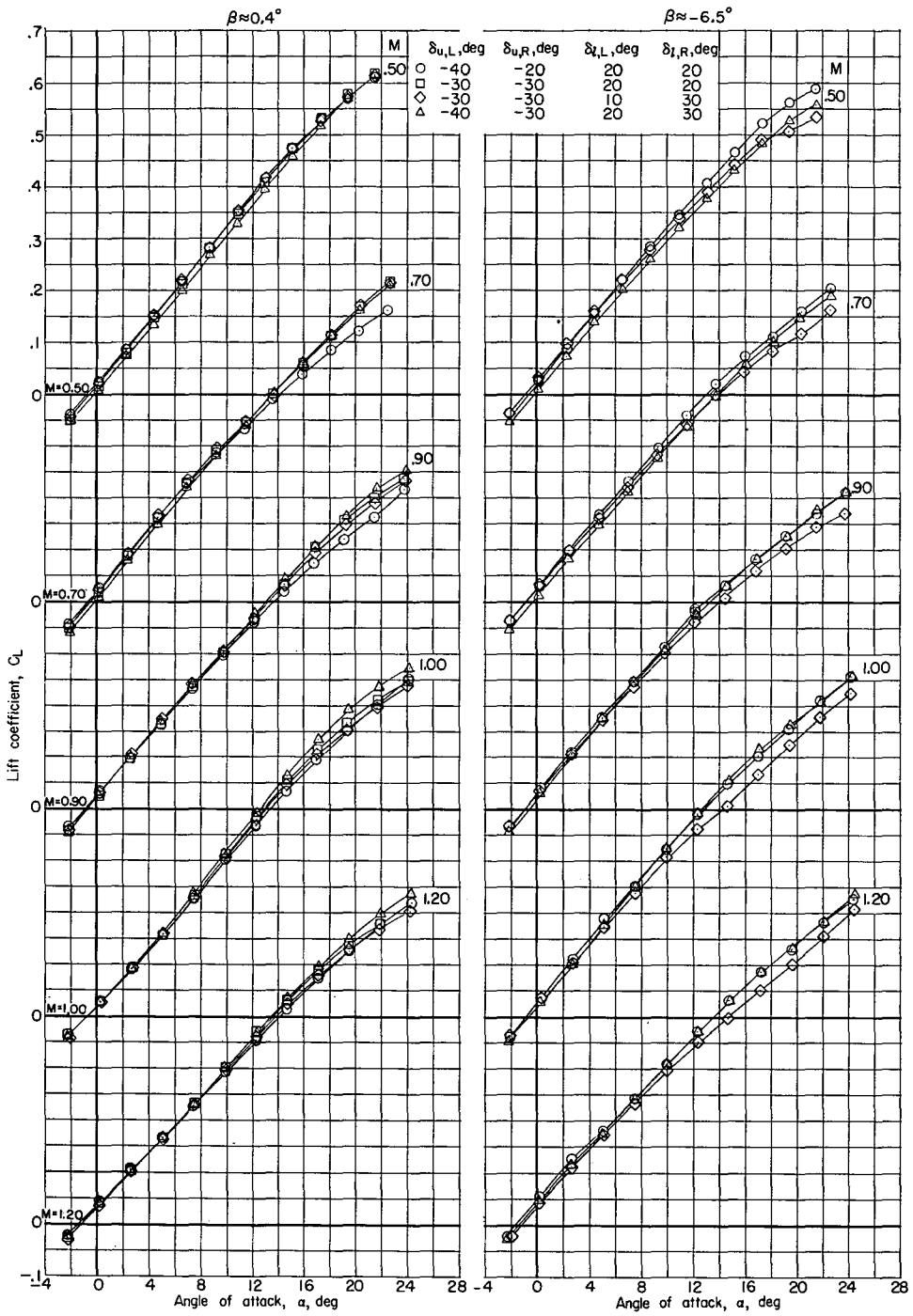

(a) C_L against α.

Figure 20.- Effect of differential flap deflection on longitudinal aerodynamic characteristics. Configuration 4 (basic outboard and central vertical tails on, canopy off); $\delta_r = 0^o$.

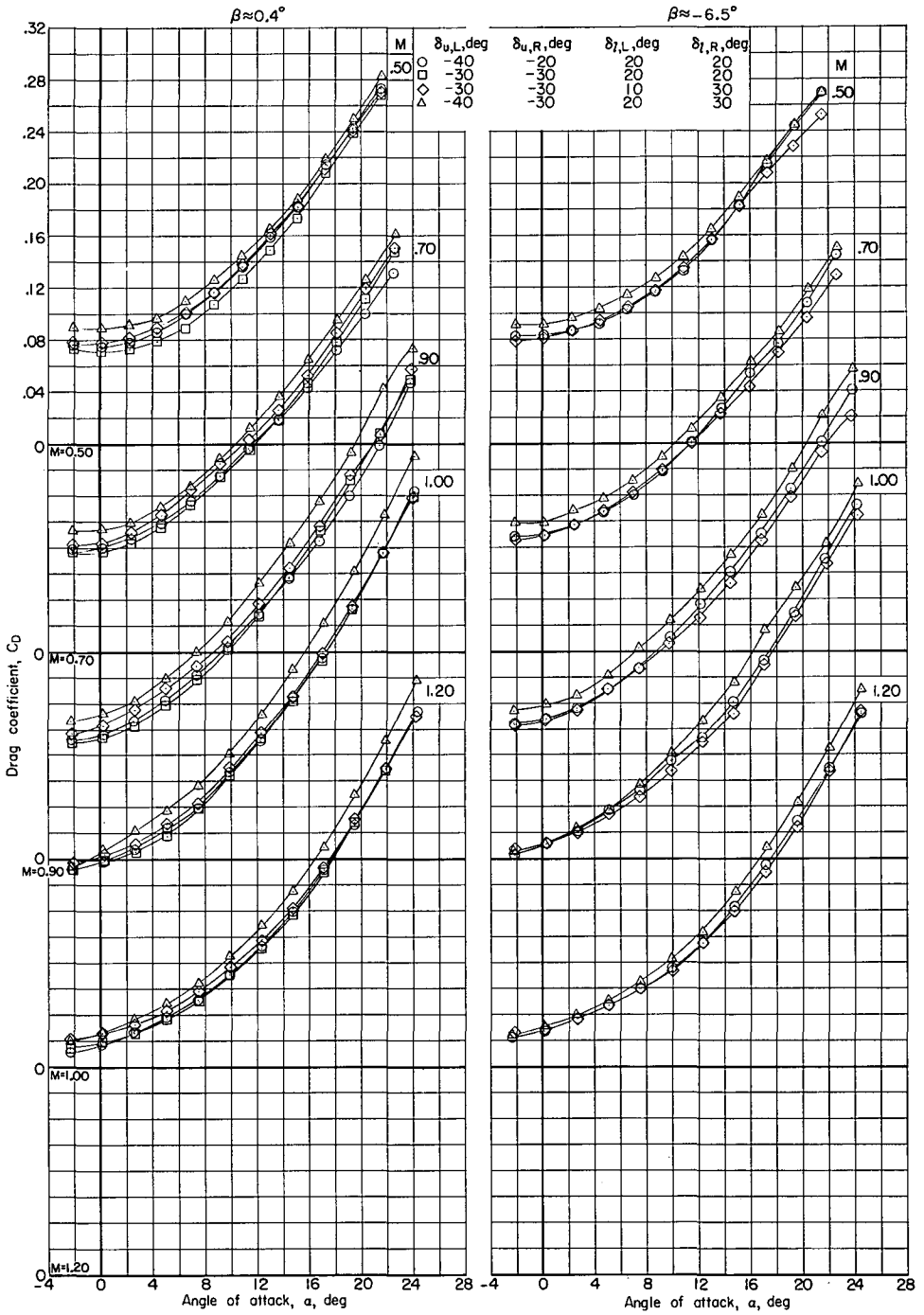

(b) C_D against α.

Figure 20.- Continued.

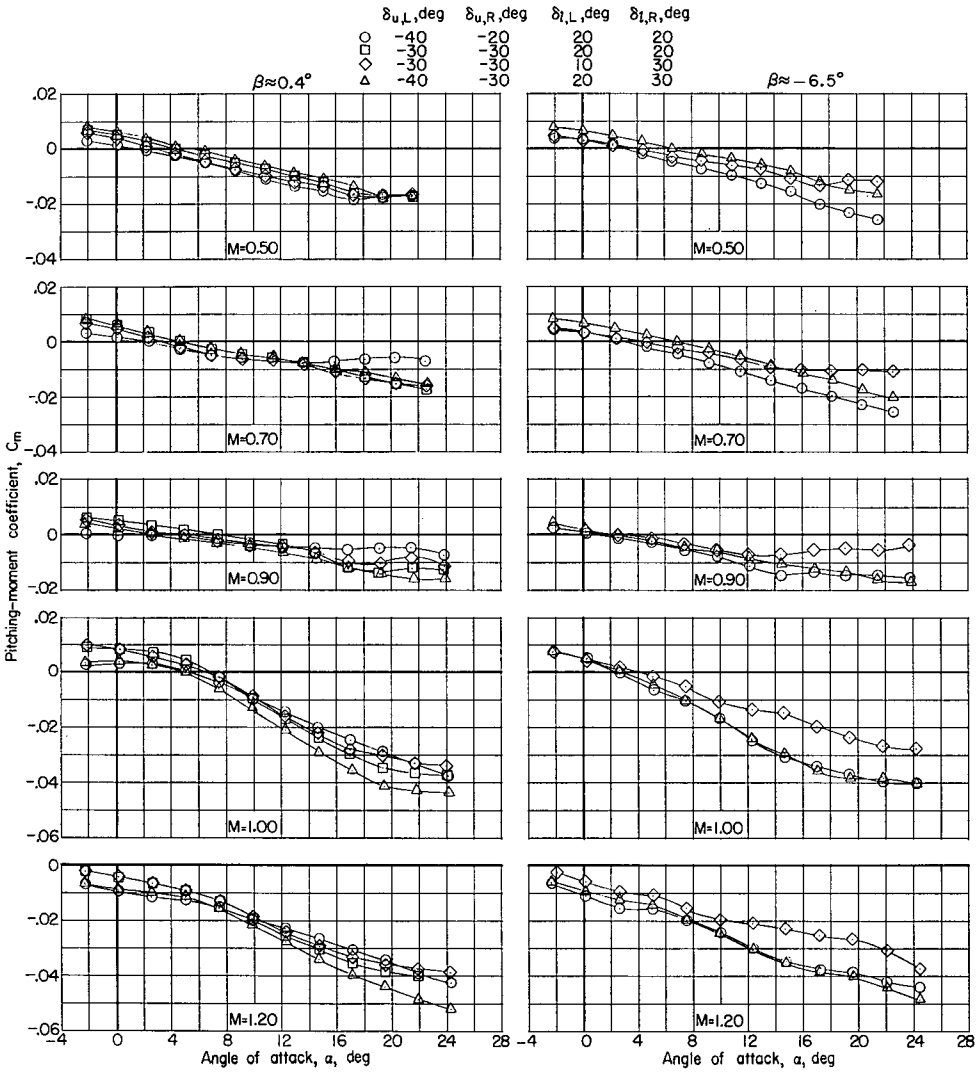

(c) C_m against α.

Figure 20.- Continued.

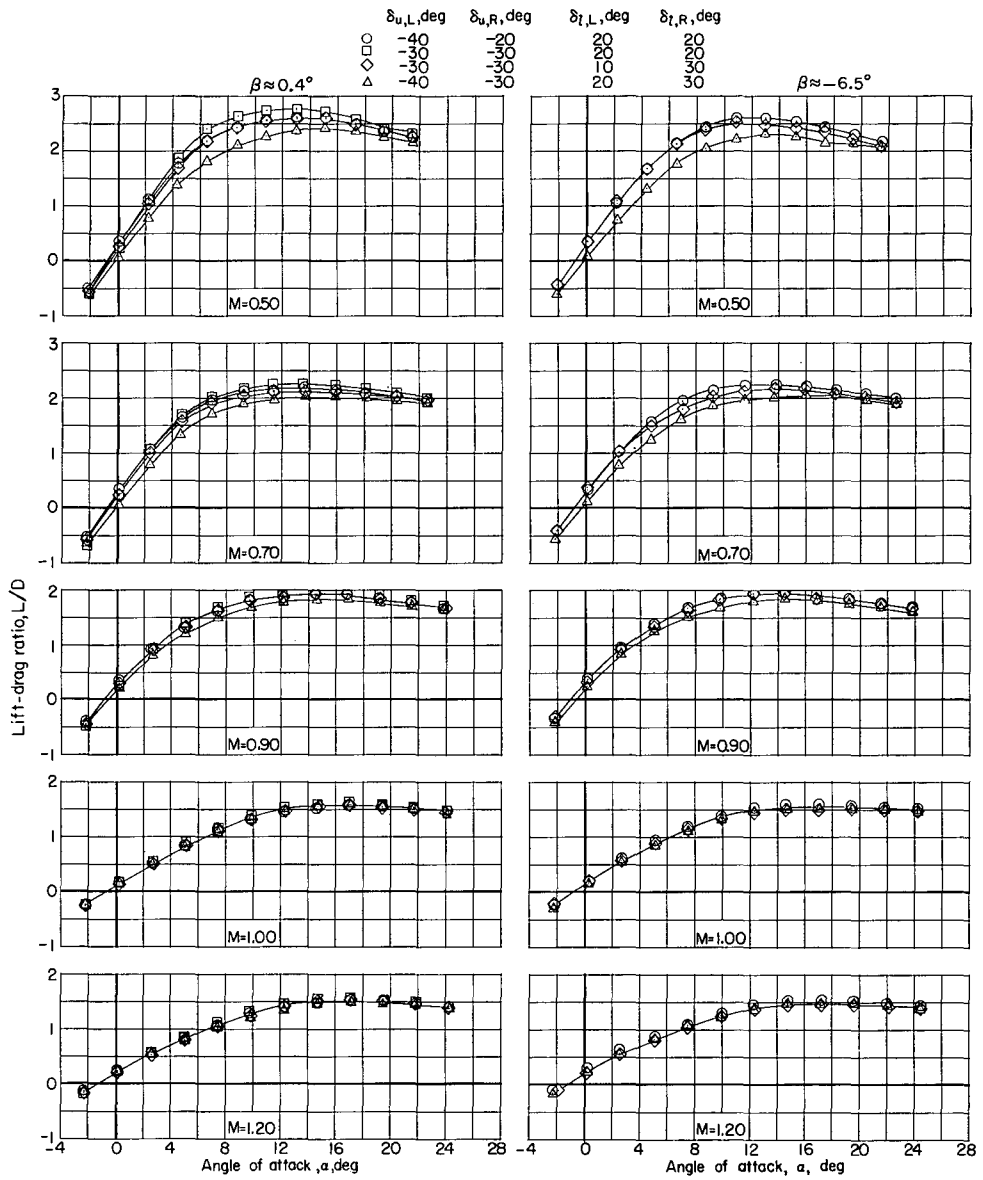

(d) L/D against α.

Figure 20.- Concluded.

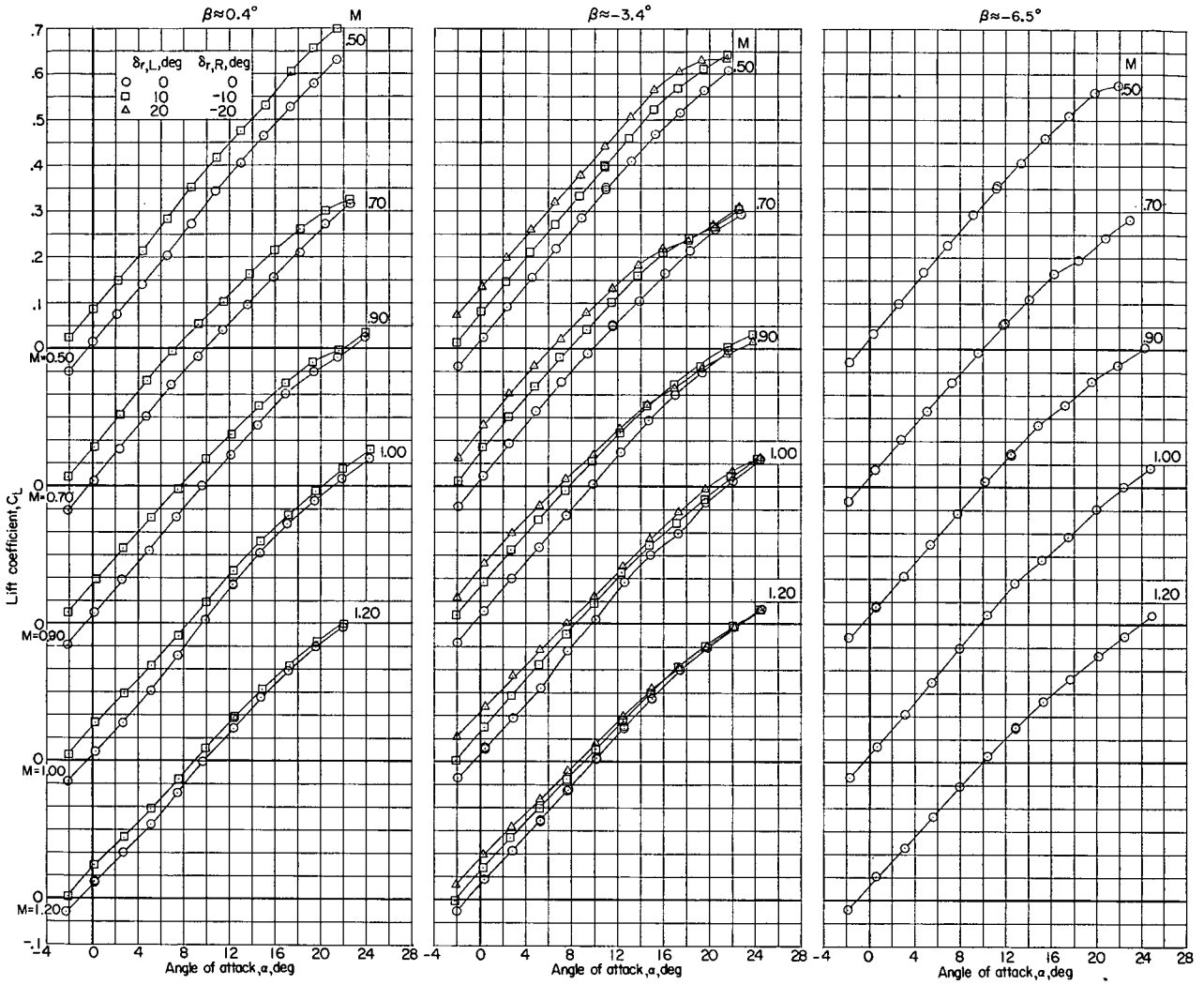

(a) C_L against α.

Figure 21.- Effect of differential rudder deflection on longitudinal aerodynamic characteristics. Configuration 3 (basic outboard and central vertical tails on, canopy on); $\delta_u = -30^\circ$; $\delta_l = 20^\circ$.

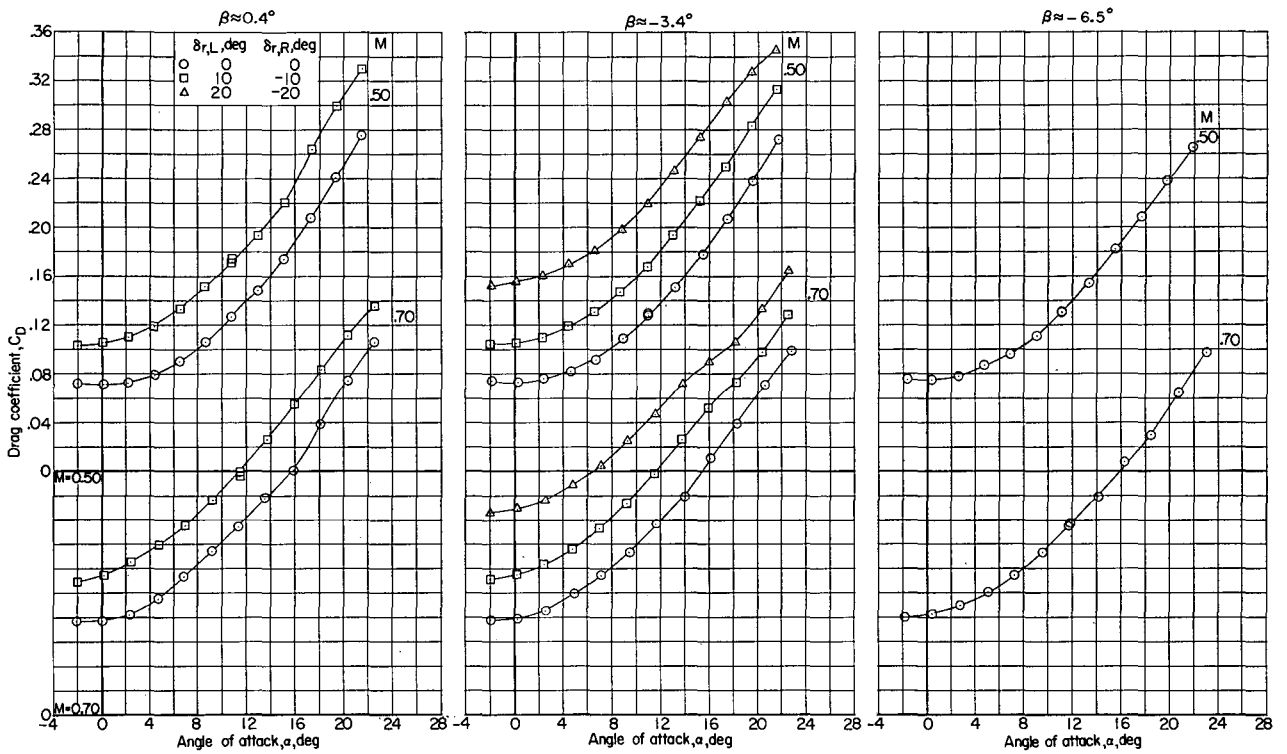

(b) C_D against α.

Figure 21.- Continued.

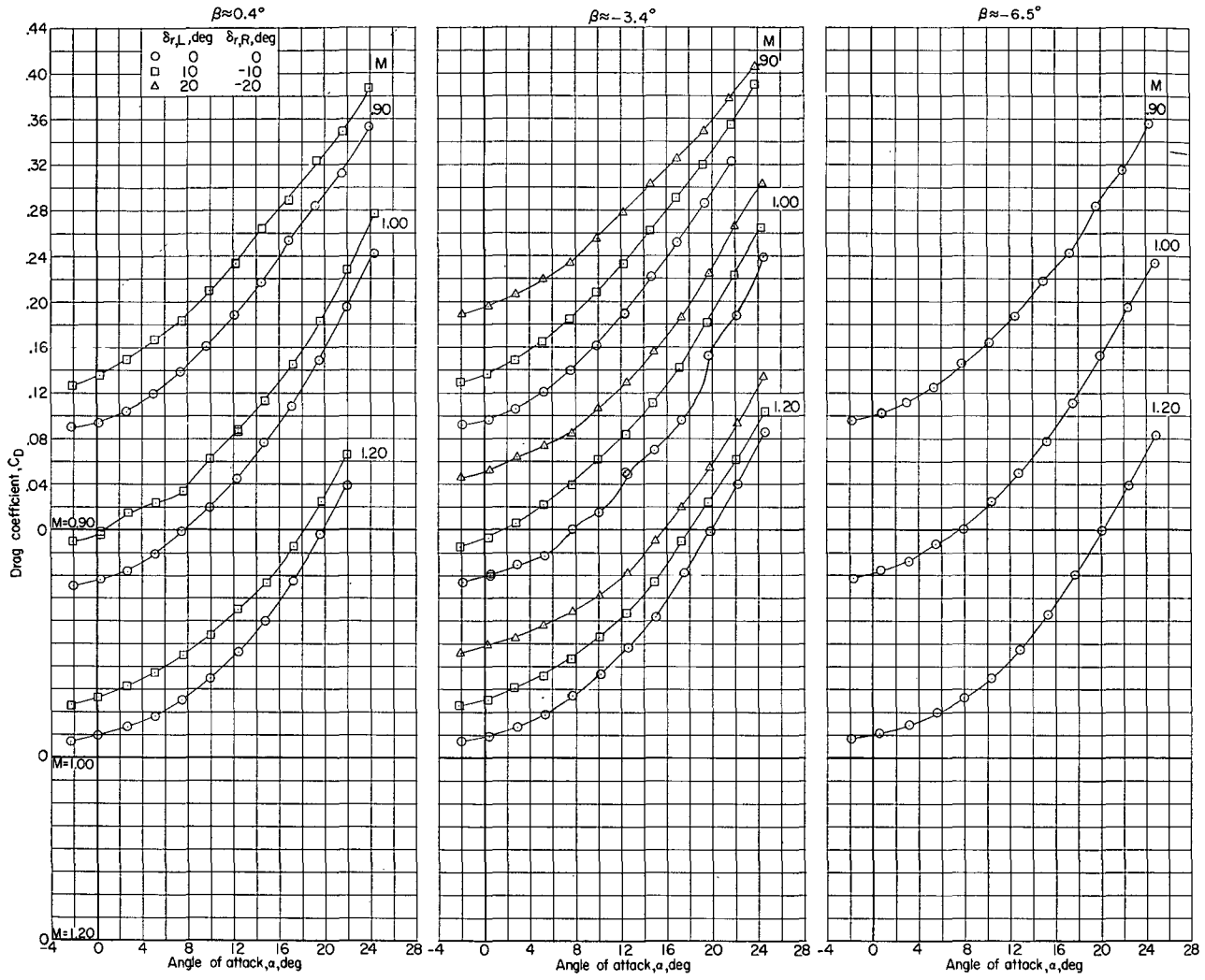

(b) Concluded.

Figure 21.- Continued.

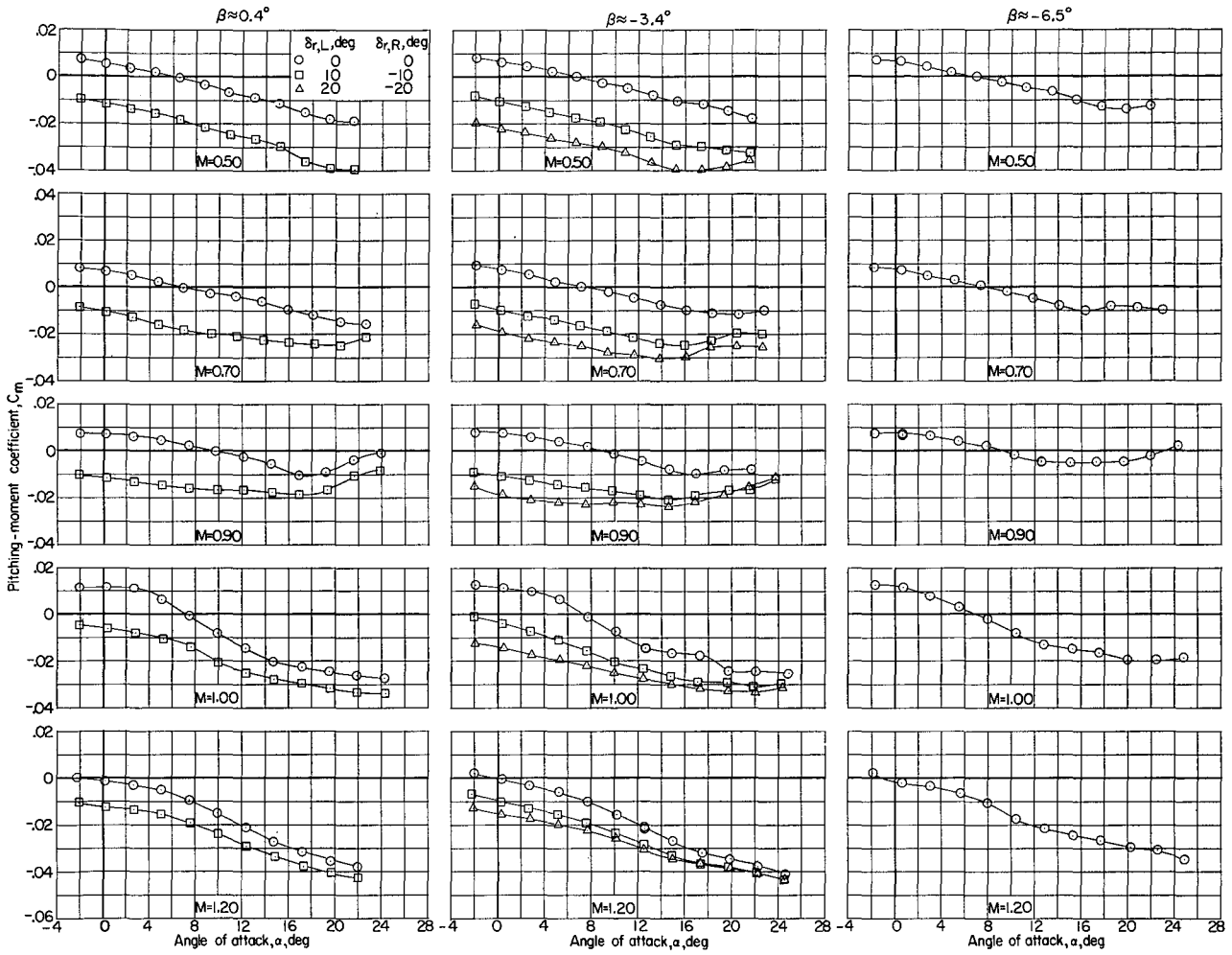

(c) C_m against α.

Figure 21.- Continued.

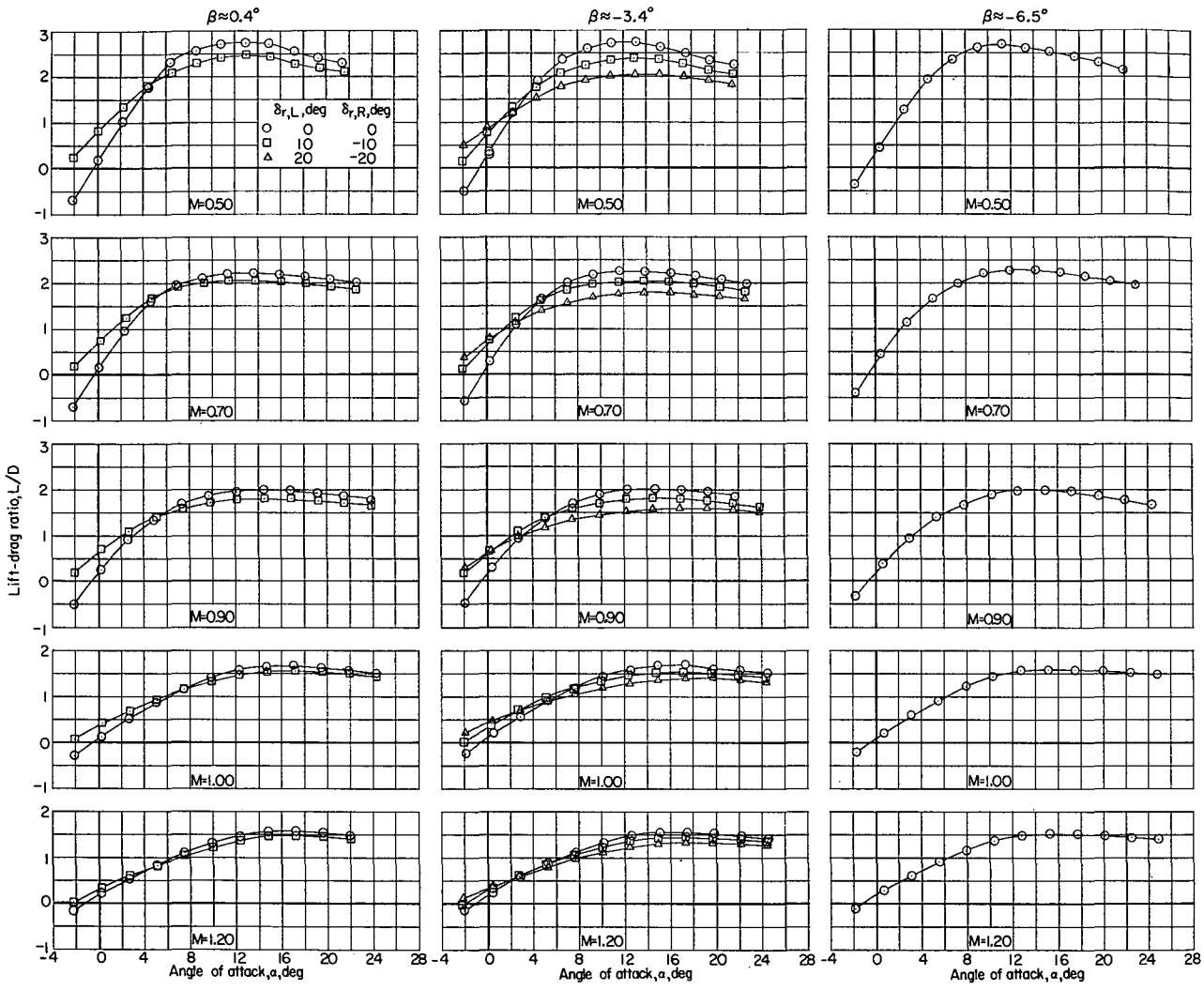

(d) L/D against α.

Figure 21.- Concluded.

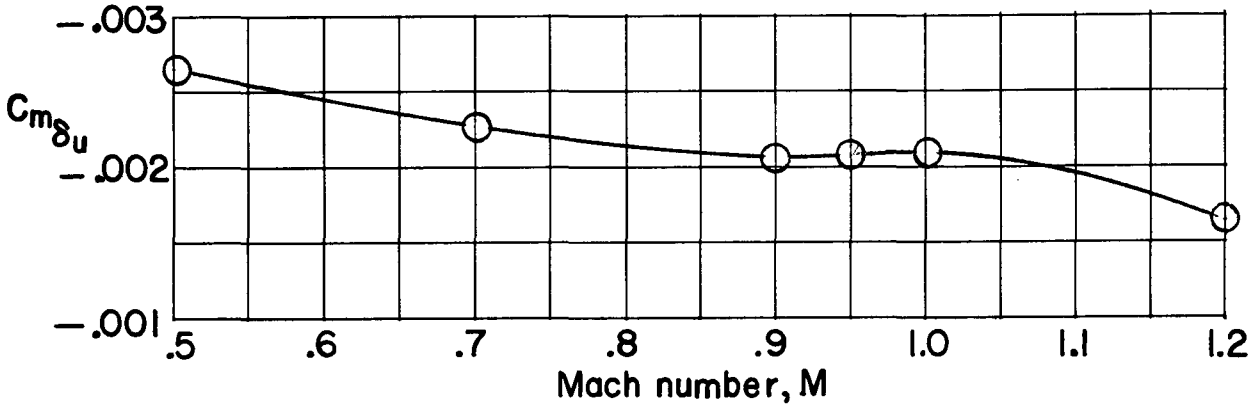

(a) Upper flaps; $\delta_l = 20^\circ$.

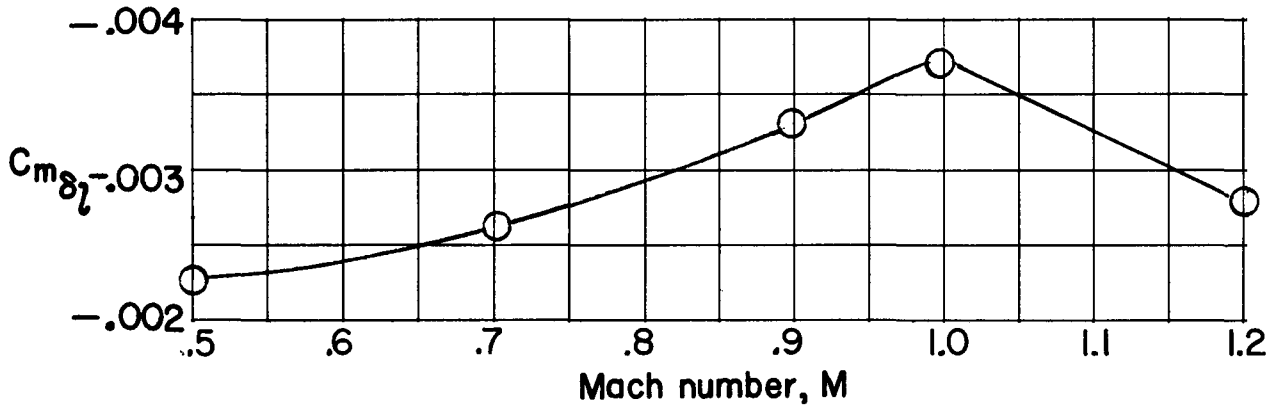

(b) Lower flaps; $\delta_u = -30^\circ$.

Figure 22.- Pitch effectiveness of upper and lower flaps. Configuration 3 (basic outboard and central vertical tails on, canopy on); $\delta_r = 0^\circ$; $\alpha = 15^\circ$.

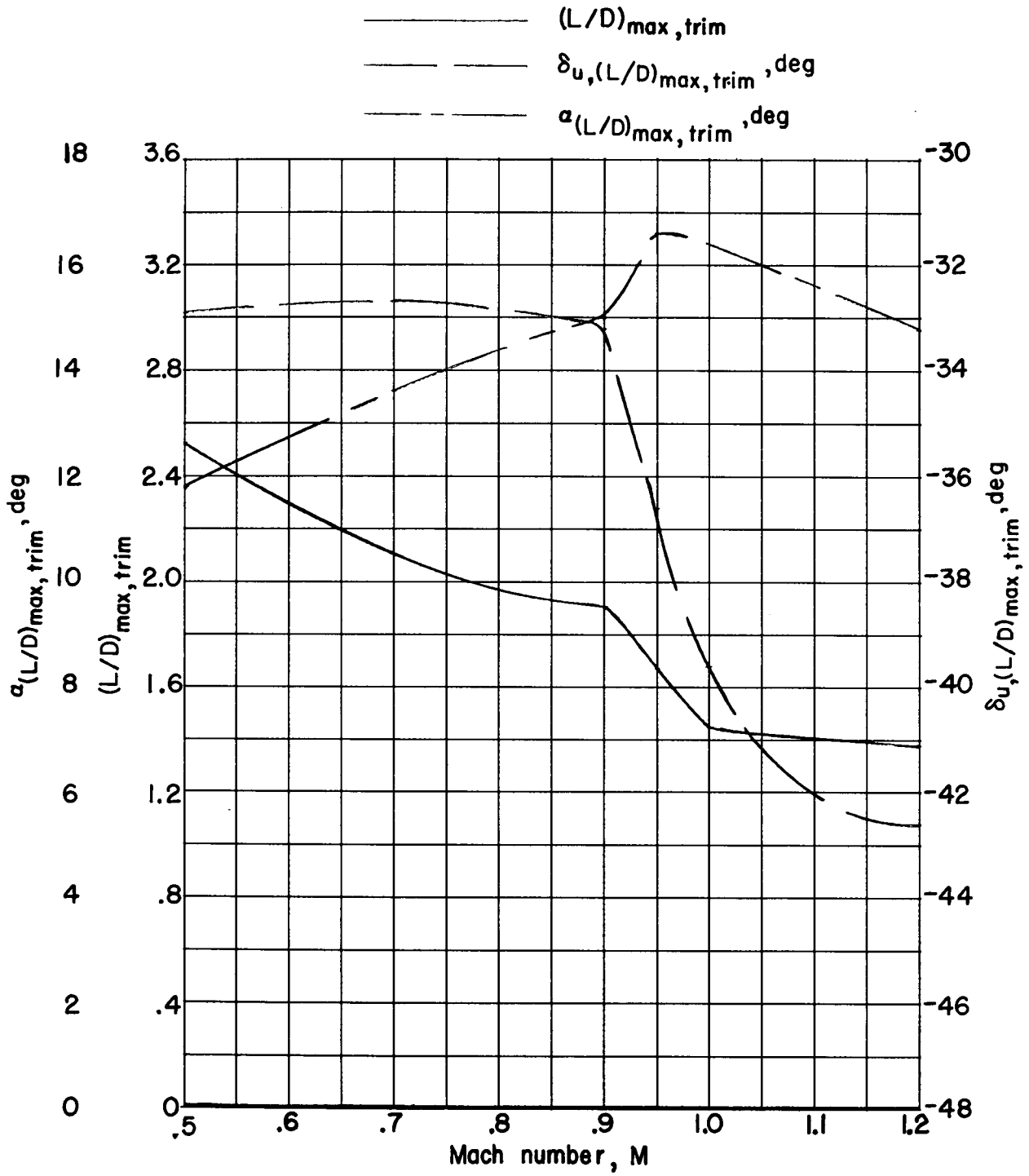

Figure 23.- Maximum lift-drag ratio at trim conditions when upper flaps are used for obtaining trim. Configuration 3 (basic outboard and central vertical tails on, canopy on); $\delta_l = 20^\circ$; $\delta_r = 0^\circ$.

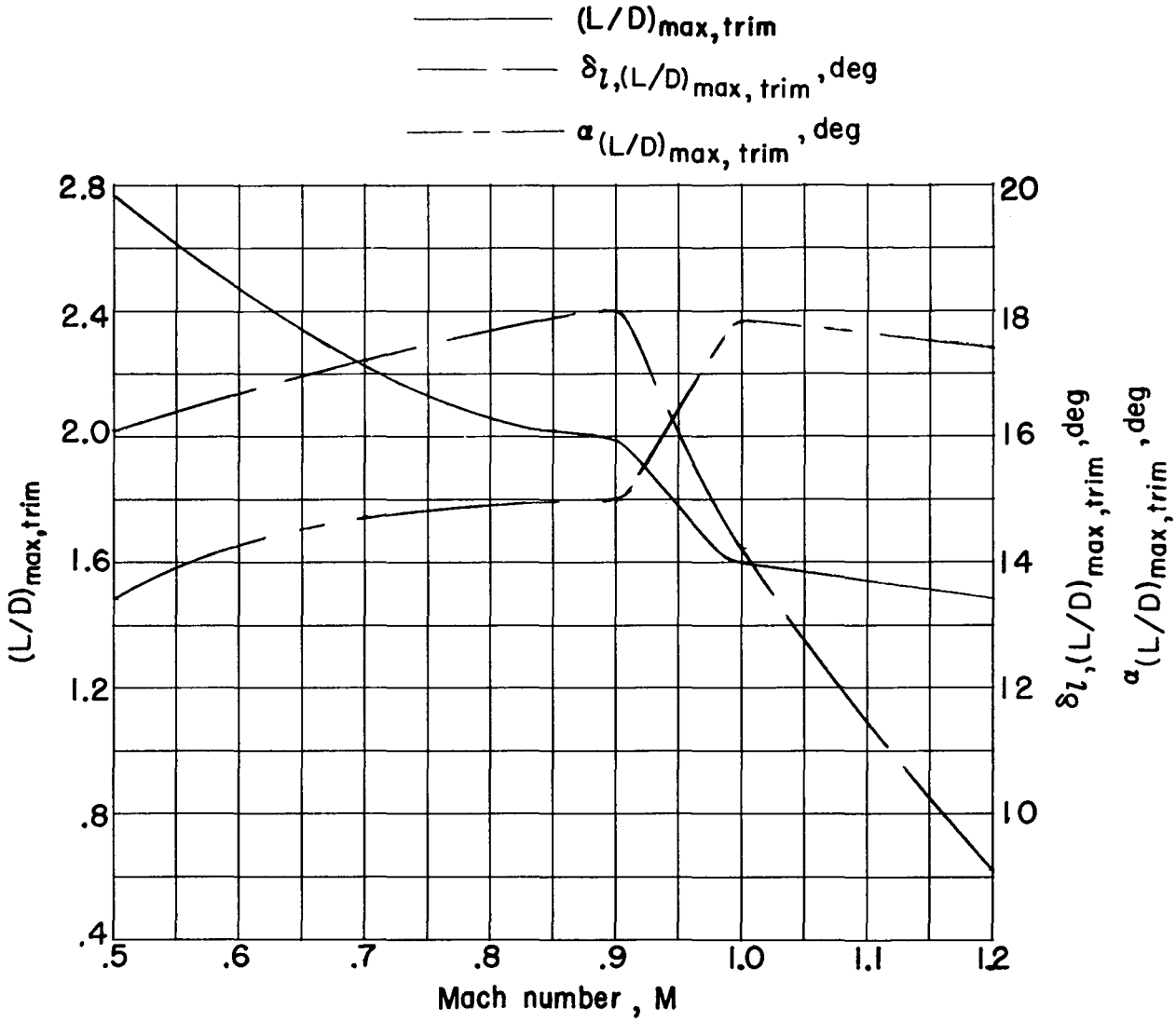

Figure 24.- Maximum lift-drag ratio at trim conditions when lower flaps are used for obtaining trim. Configuration 3 (basic outboard and central vertical tails on, canopy on); $\delta_u = -30^\circ$; $\delta_r = 0^\circ$.

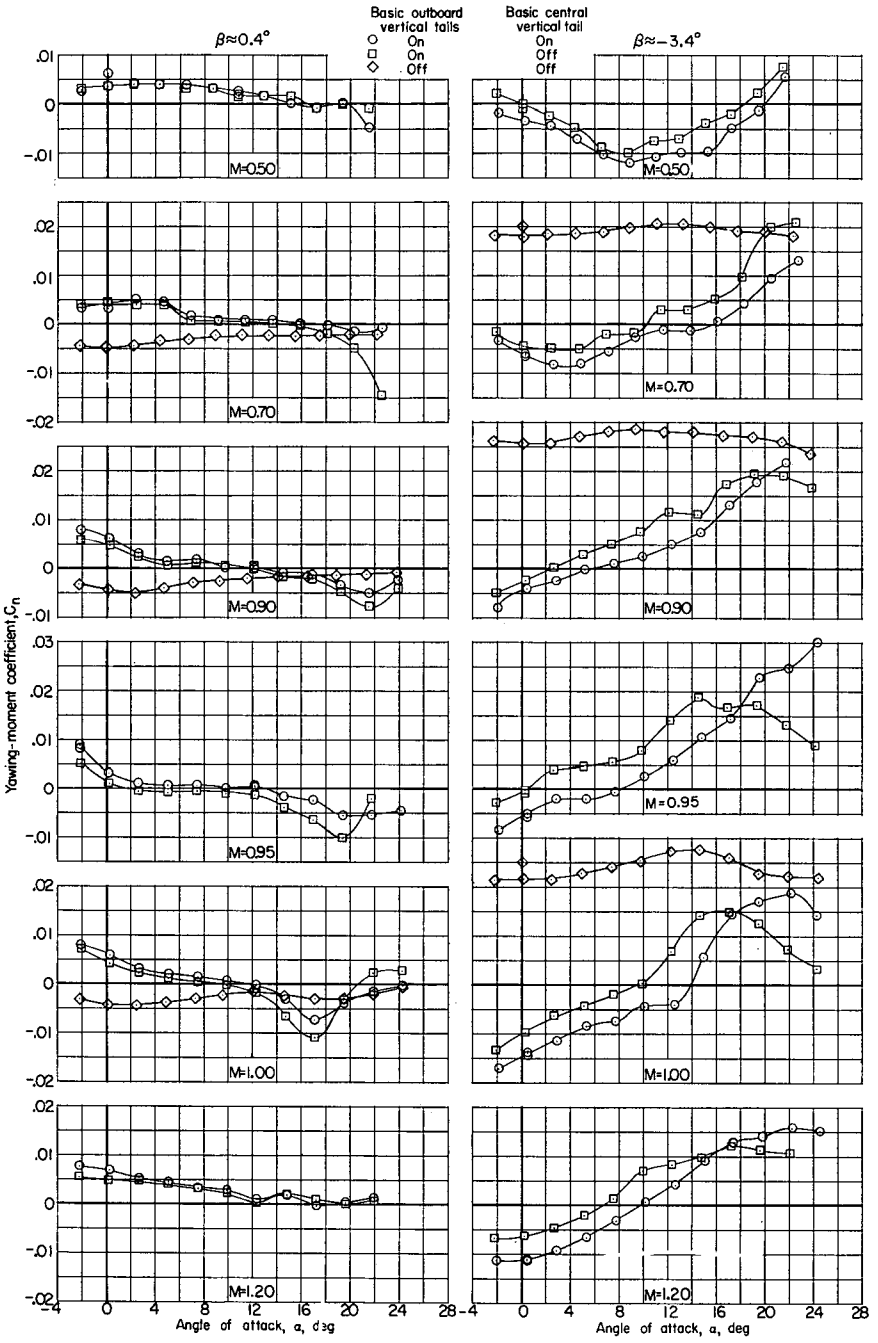

(a) C_n against α.

Figure 25.- Effect of basic outboard and central vertical tails on lateral aerodynamic characteristics. Configurations 1, 2, and 3 (canopy on); $\delta_u = -30^\circ$; $\delta_l = 20^\circ$; $\delta_r = 0^\circ$.

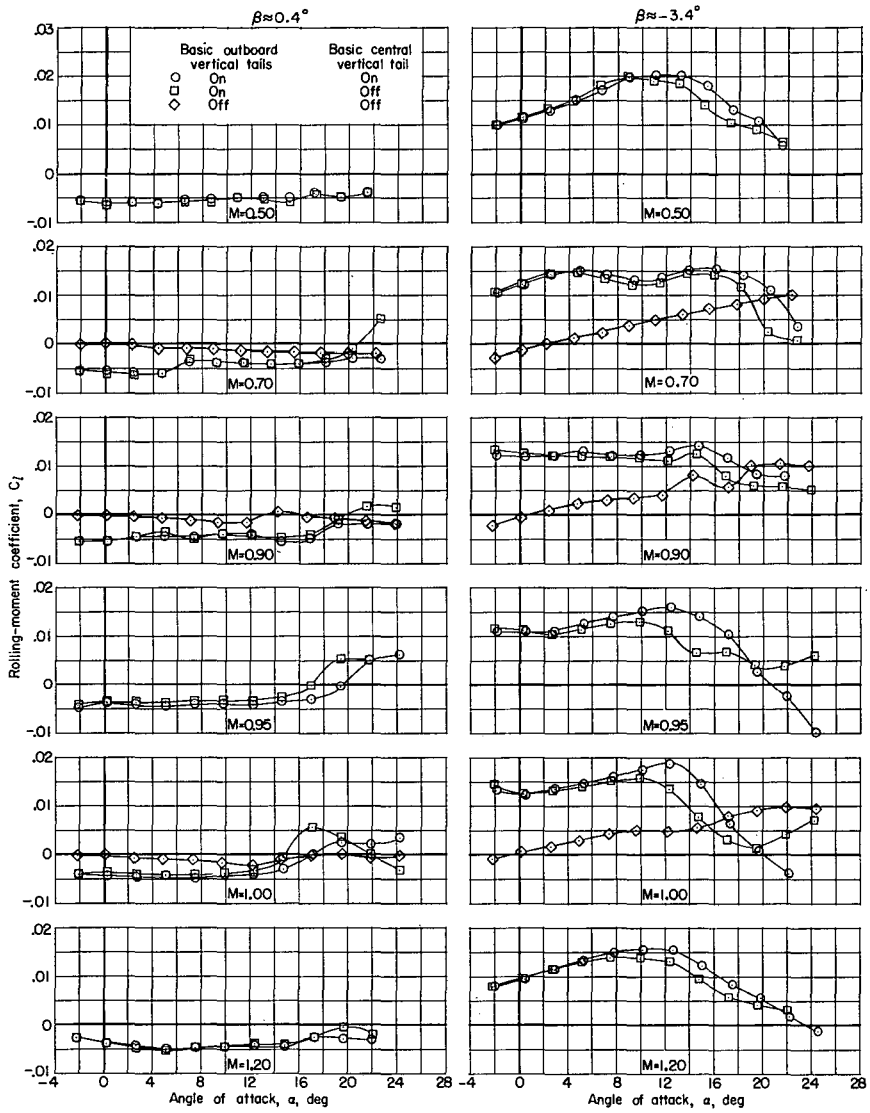

(b) C_l against α.

Figure 25.- Continued.

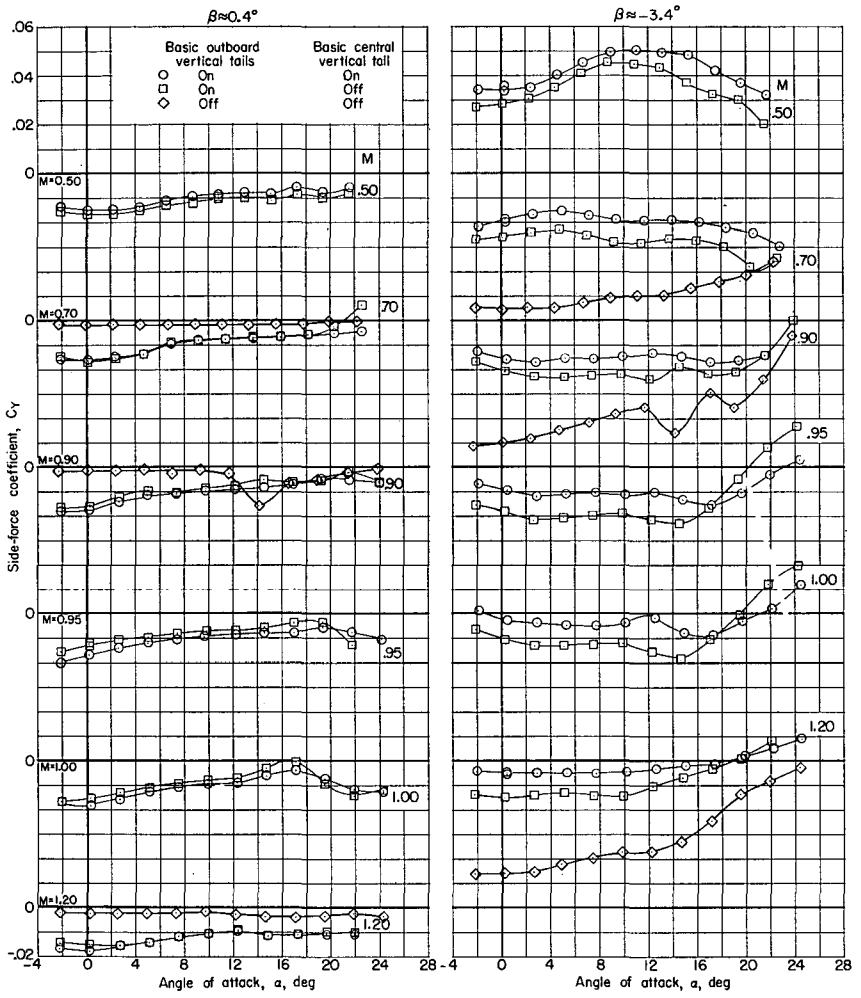

(c) C_Y against α.

Figure 25.- Concluded.

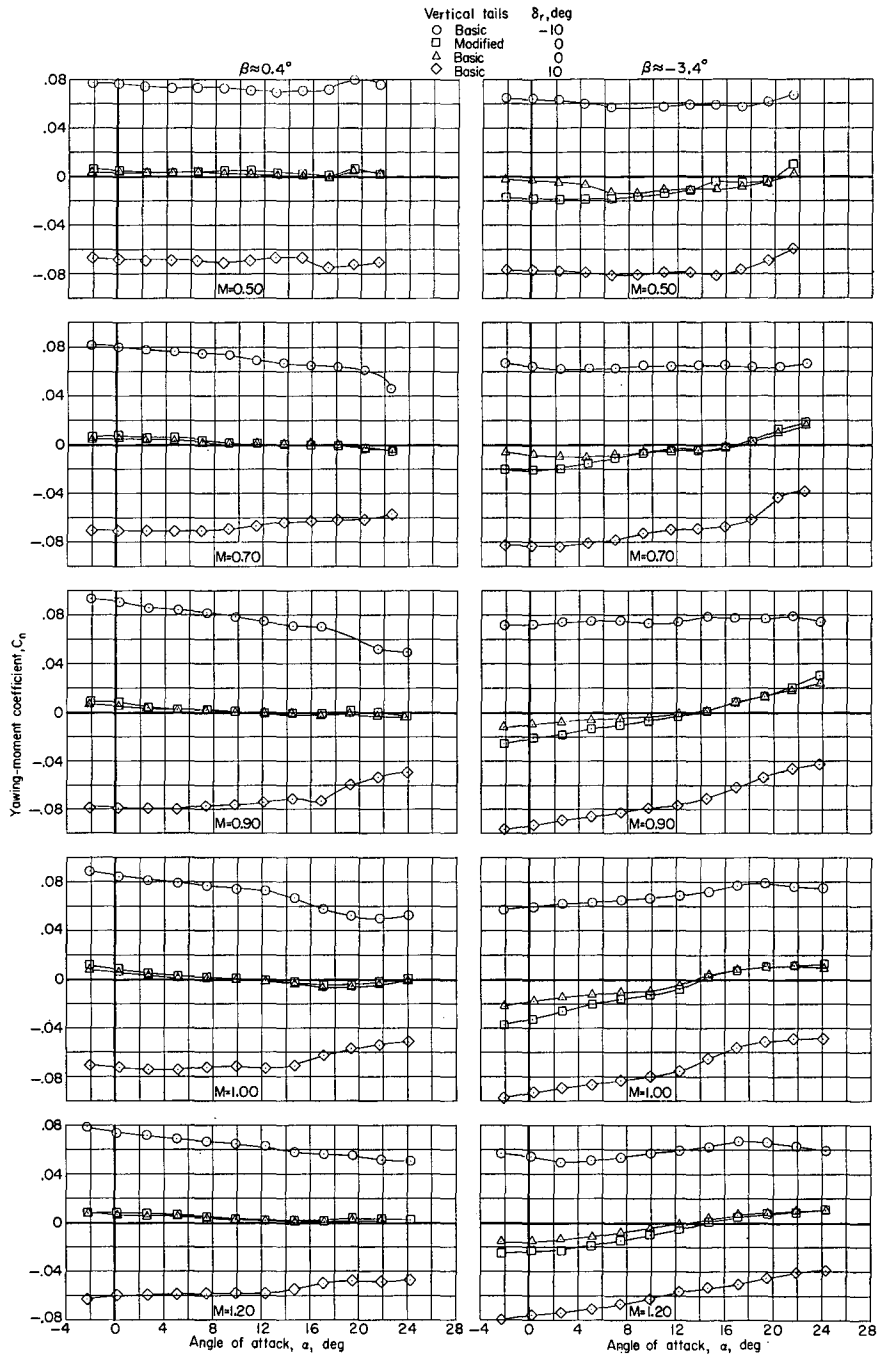

(a) C_n against α.

Figure 26.- Effect of modified outboard and central vertical tails and rudder deflection on lateral aerodynamic characteristics. Configurations 4 and 5 (canopy off); $\delta_u = -30^\circ$; $\delta_l = 20^\circ$.

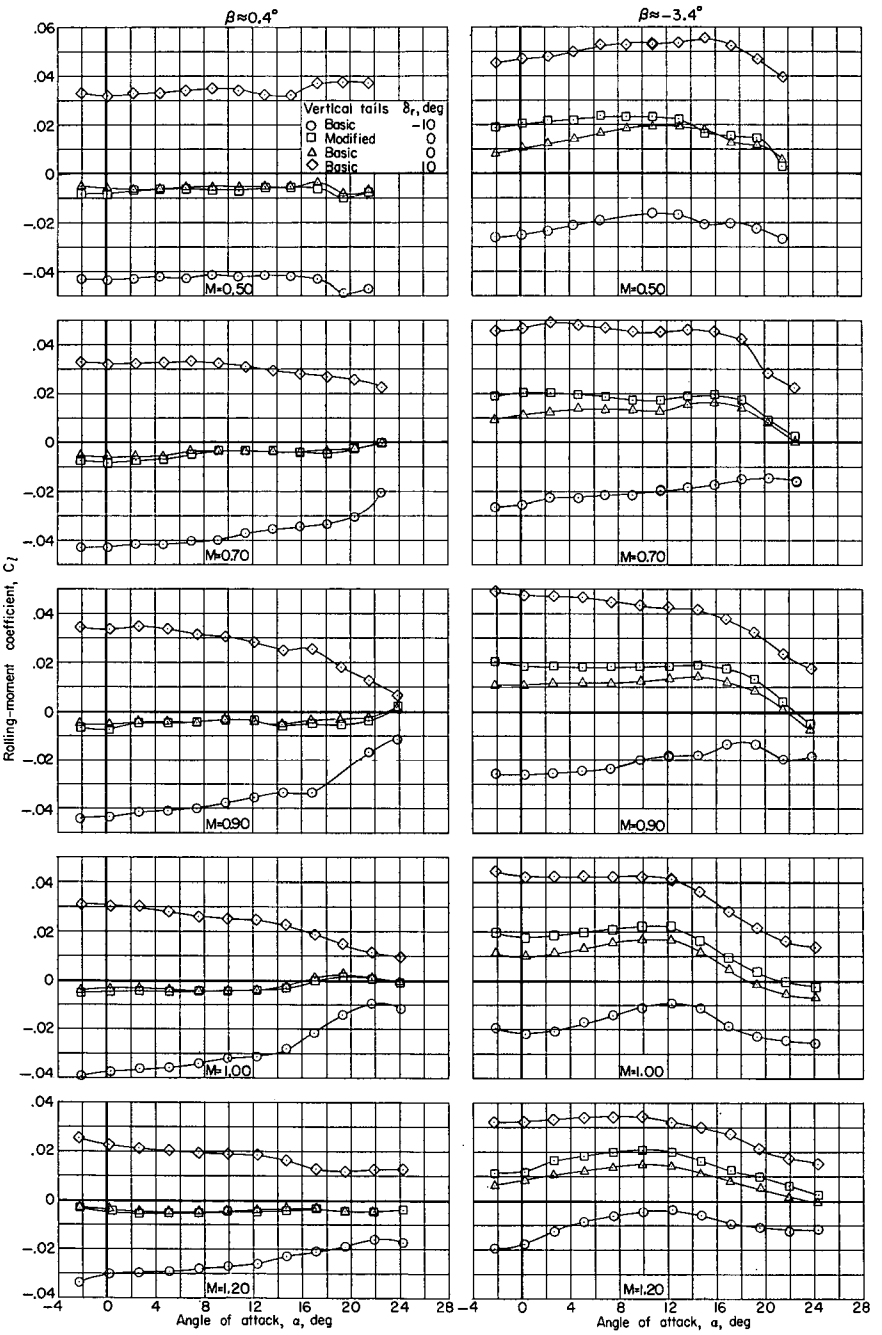

(b) C_l against α.

Figure 26.- Continued.

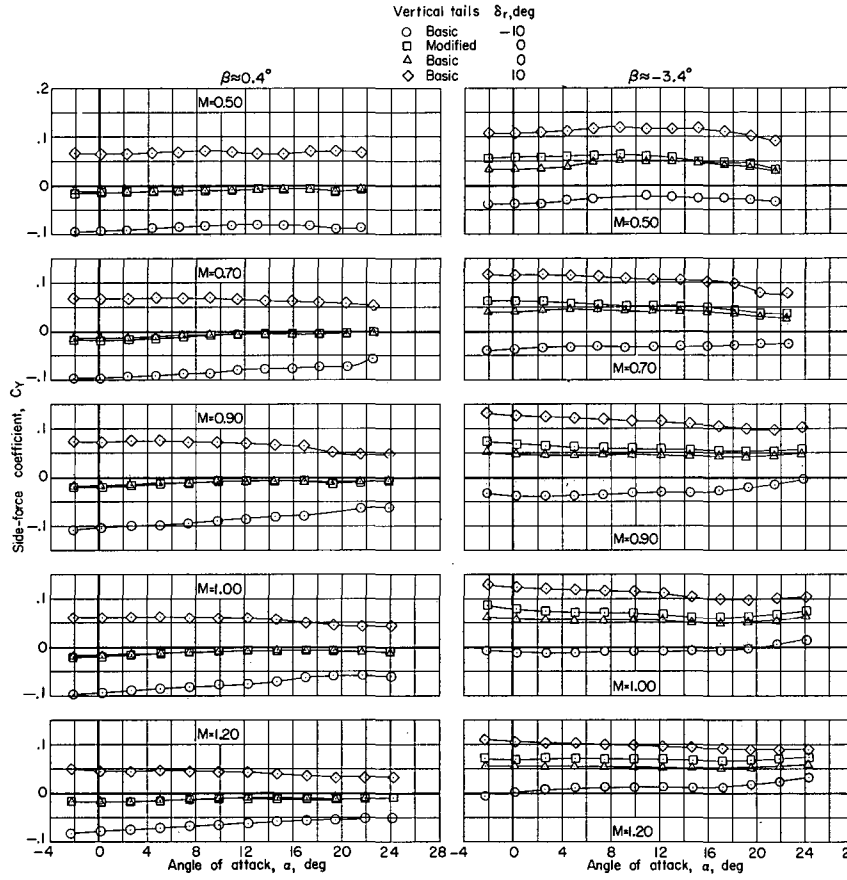

(c) C_Y against α.

Figure 26.- Concluded.

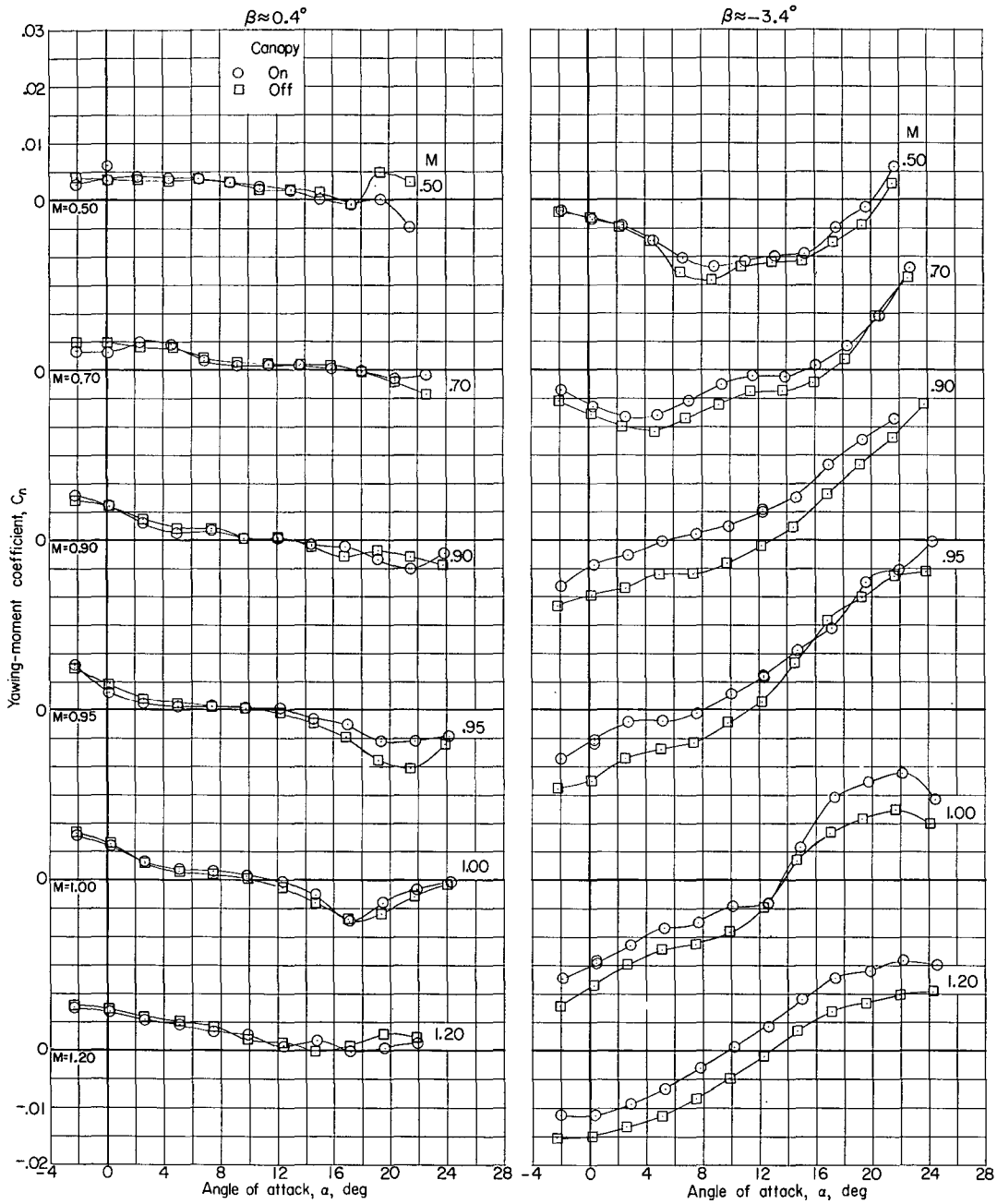

(a) C_n against α.

Figure 27.- Effect of canopy on lateral aerodynamic characteristics. Configurations 3 and 4 (basic outboard and central vertical tails on); $\delta_u = -30^\circ$; $\delta_l = 20^\circ$; $\delta_r = 0^\circ$.

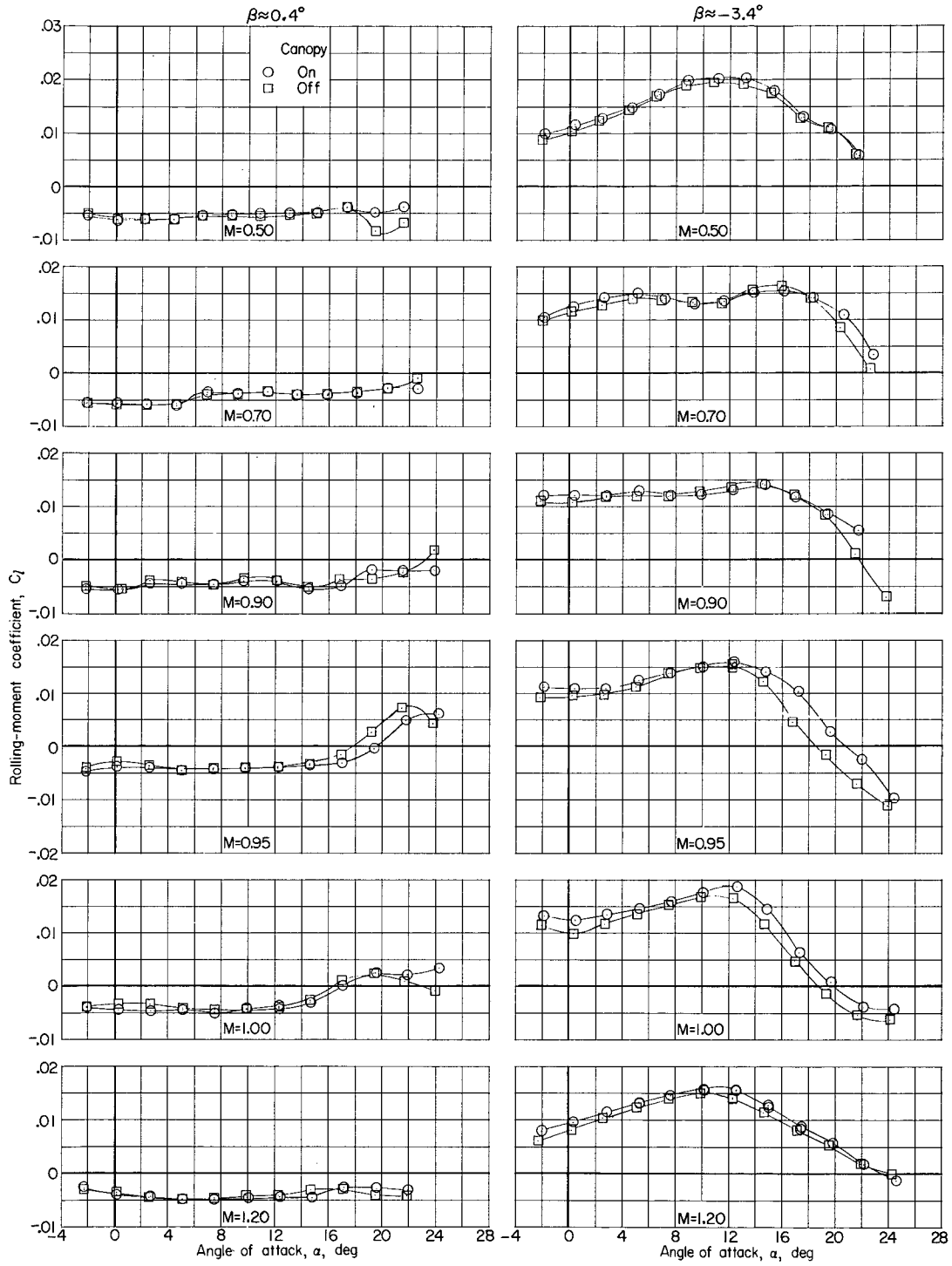

(b) C_l against α.

Figure 27.- Continued.

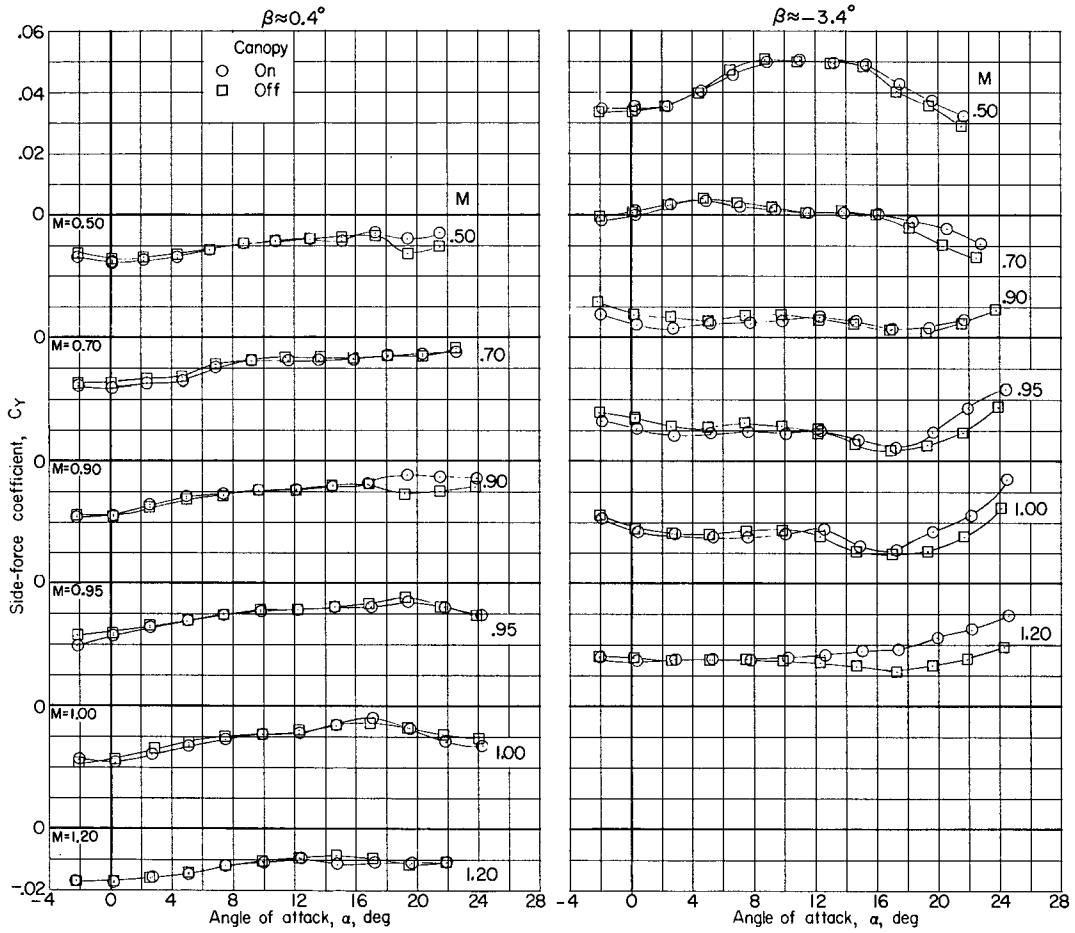

(c) C_Y against α.

Figure 27.- Concluded.

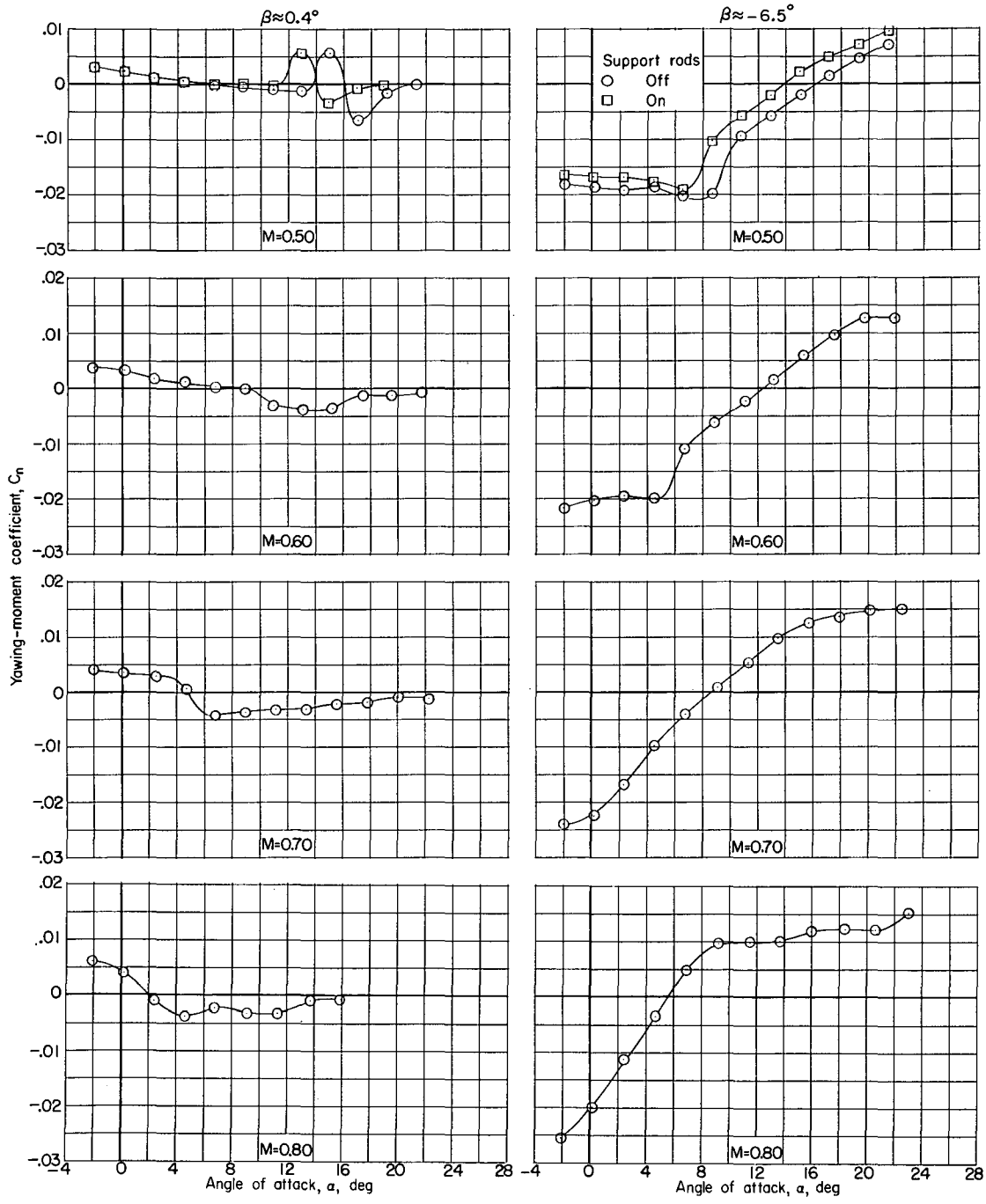

(a) C_n against α.

Figure 28.- Effect of external dummy support rods on lateral aerodynamic characteristics. Configurations 4 and 6 (basic outboard and central vertical tails on, canopy off); $\delta_u = -10^\circ$; $\delta_l = 0^\circ$; $\delta_{r,L} = -10^\circ$; $\delta_{r,R} = 10^\circ$.

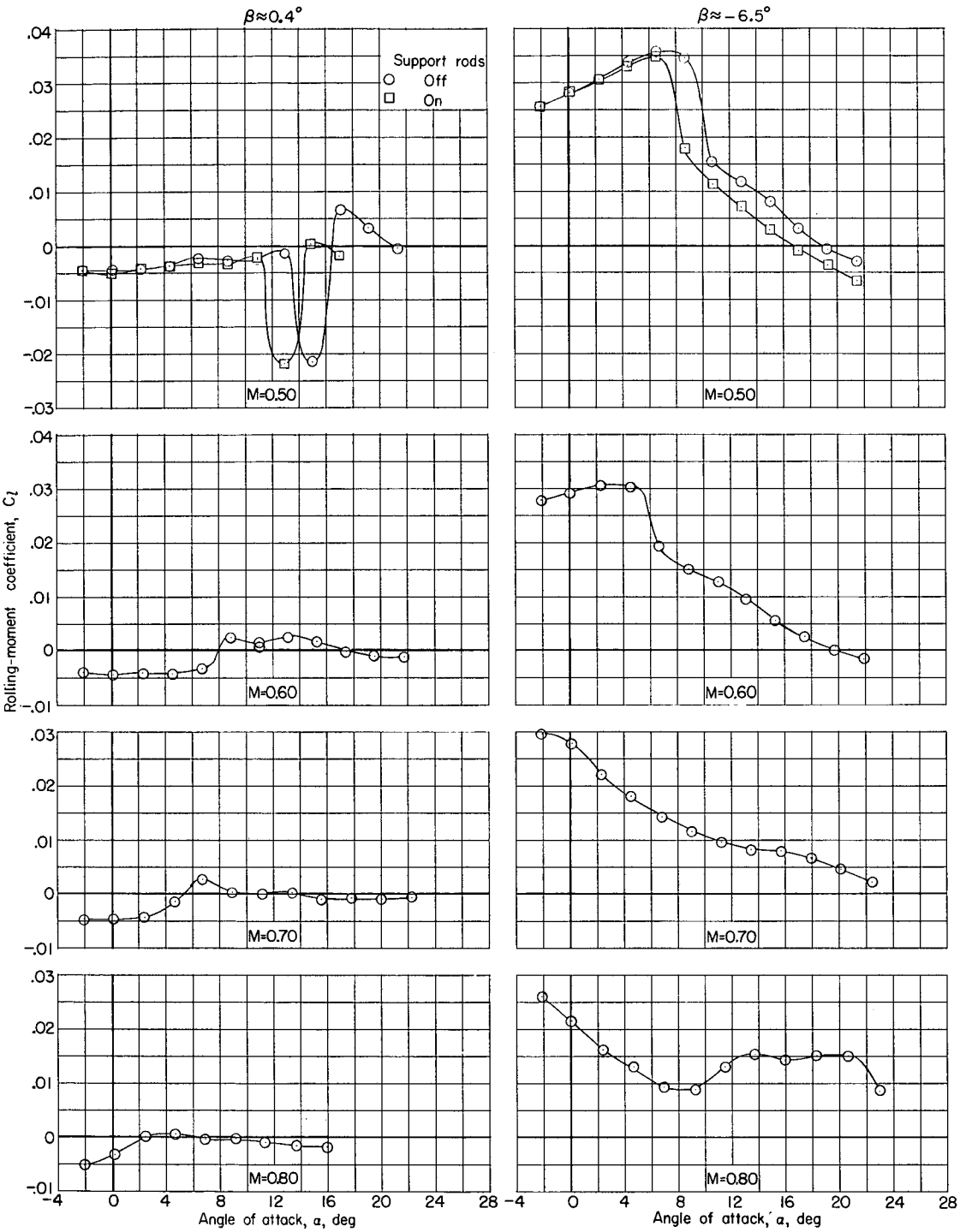

(b) C_l against α.

Figure 28.- Continued.

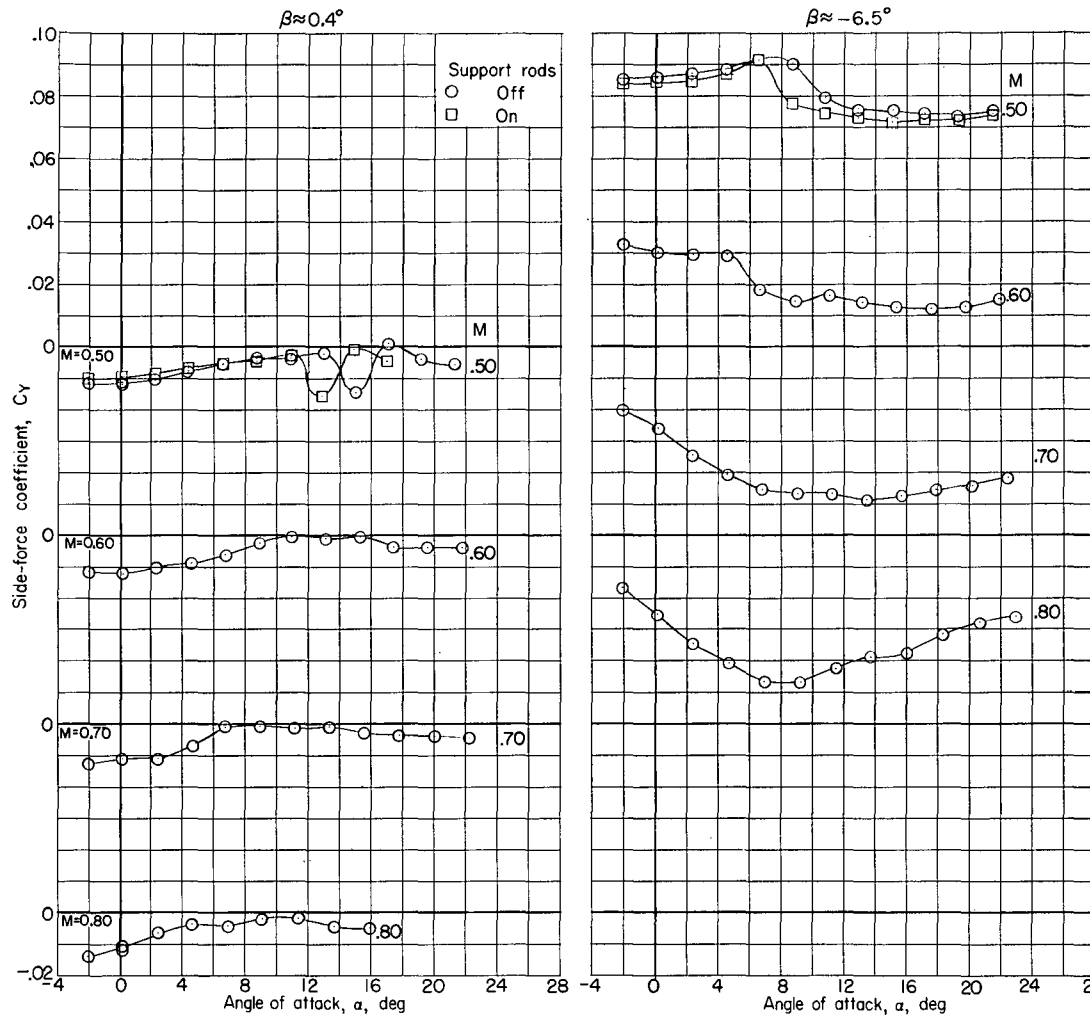

(c) C_Y against α.

Figure 28.- Concluded.

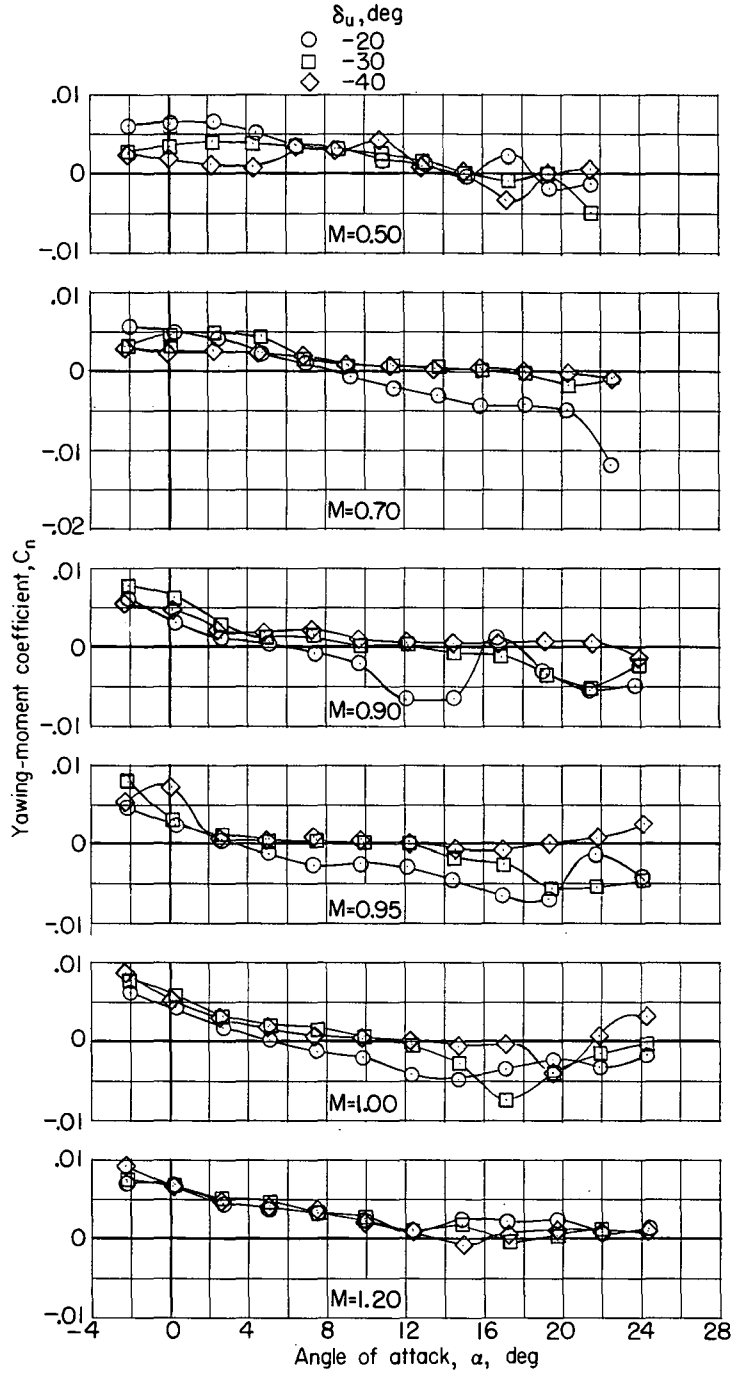

(a) C_n against α.

Figure 29.- Effect of upper-flap deflection on lateral aerodynamic characteristics. Configuration 3 (basic outboard and central vertical tails on, canopy on); $\delta_l = 20^\circ$; $\delta_r = 0^\circ$; $\beta \approx 0.4^\circ$.

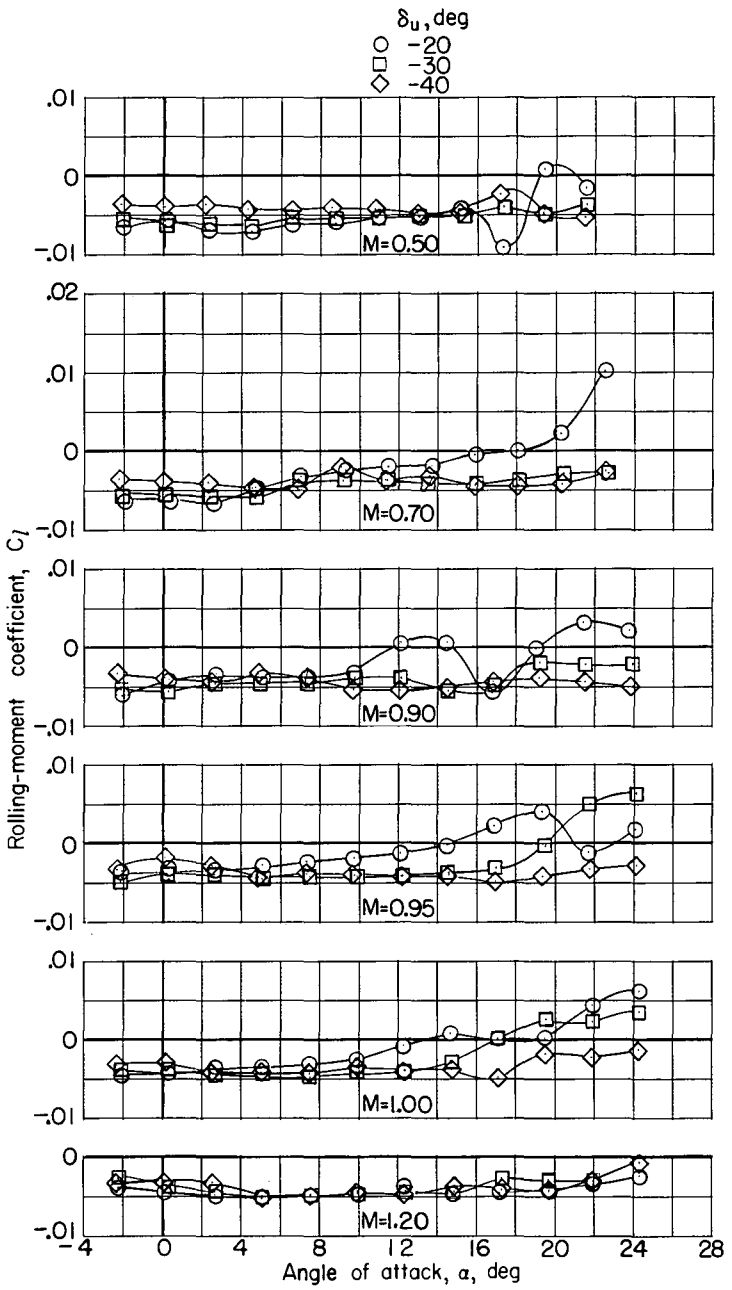

(b) C_l against α.

Figure 29.- Continued.

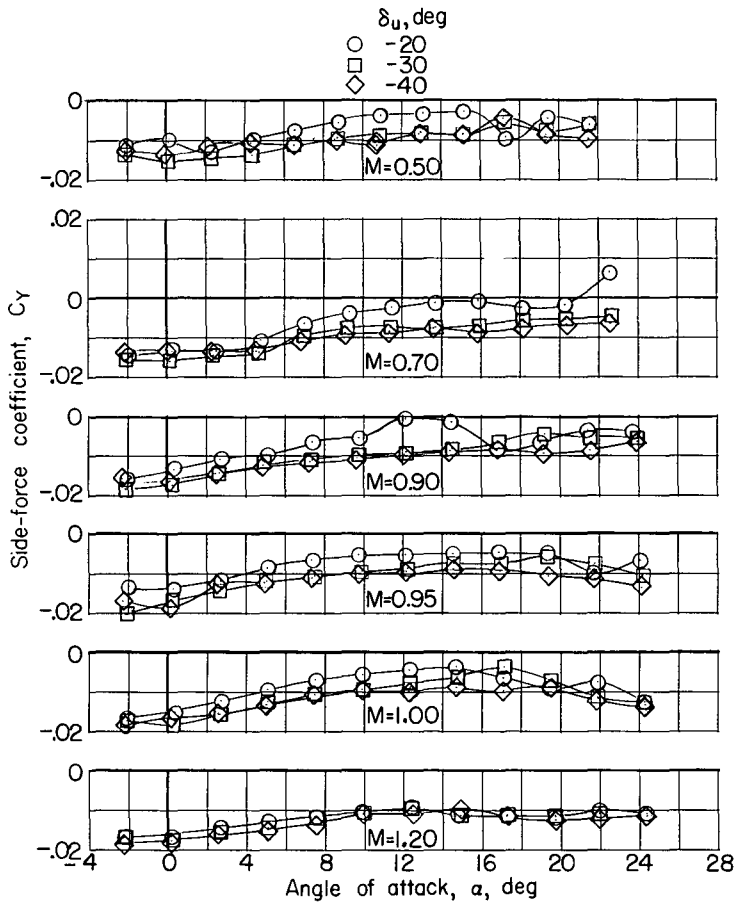

(c) C_Y against α.

Figure 29.- Concluded.

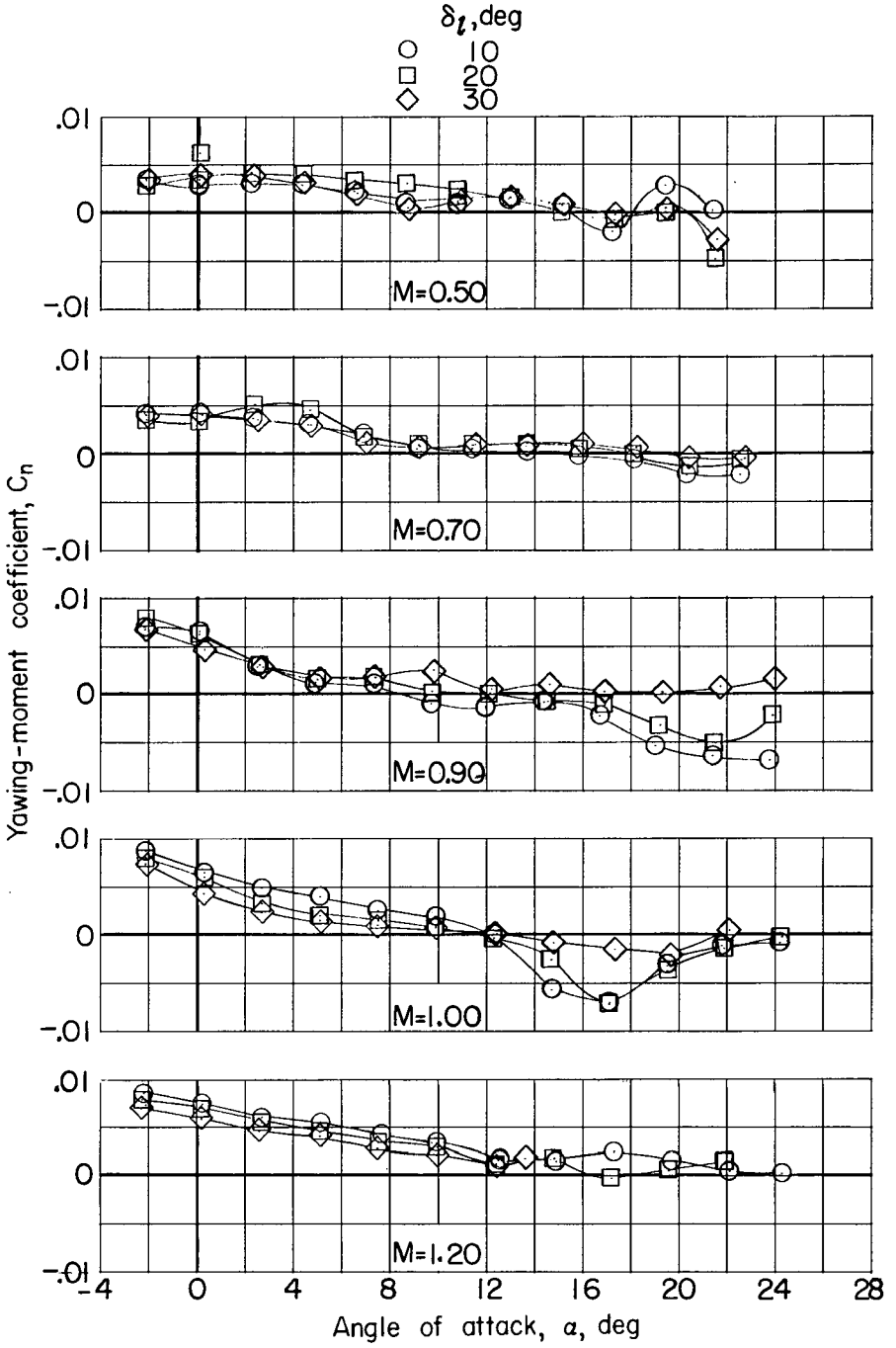

(a) C_n against α.

Figure 30.- Effect of lower-flap deflection on lateral aerodynamic characteristics. Configuration 3 (basic outboard and central vertical tails on, canopy on); $\delta_u = -30^\circ$; $\delta_r = 0^\circ$; $\beta \approx 0.4^\circ$.

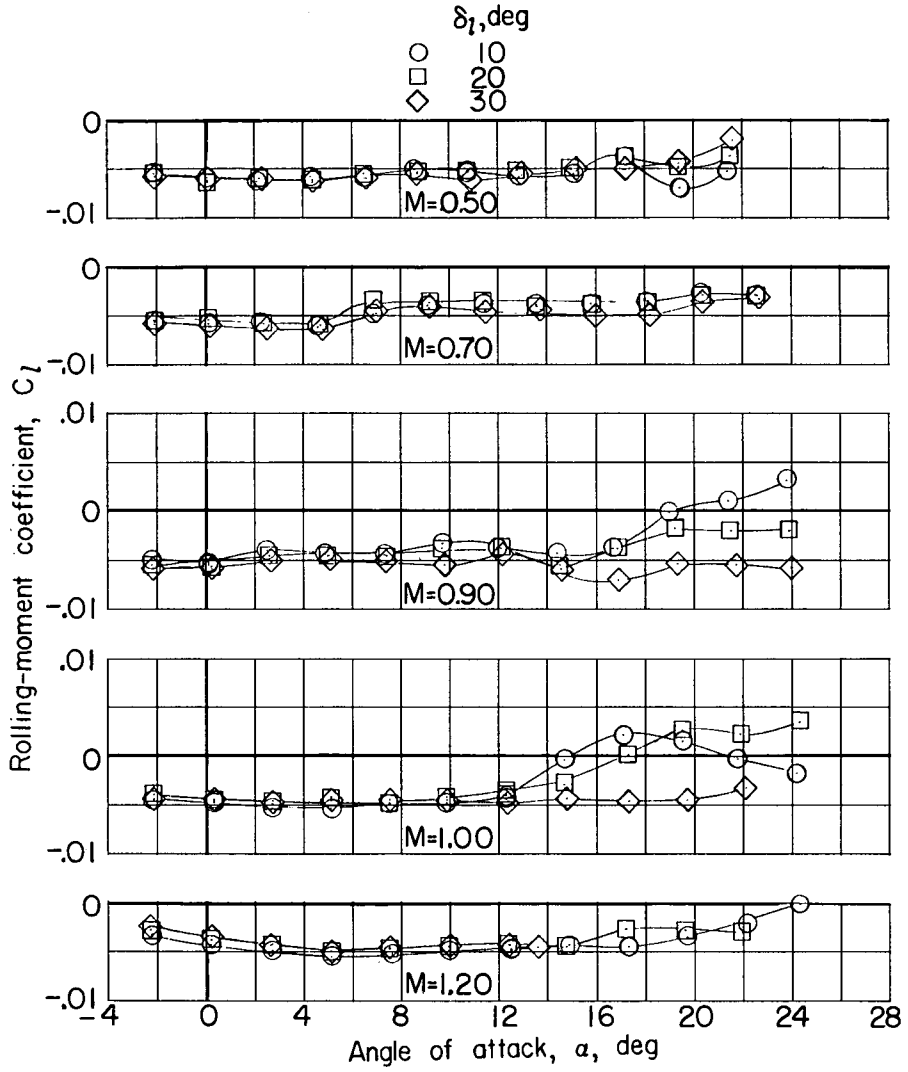

(b) C_l against α.

Figure 30.- Continued.

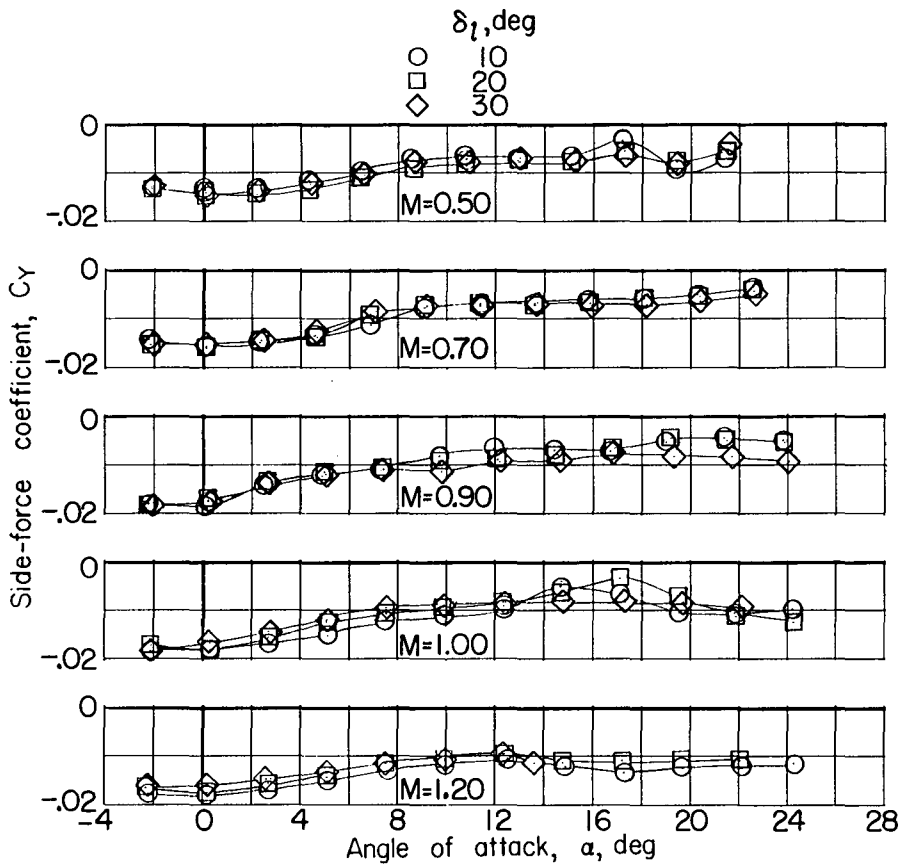

(c) C_Y against α.

Figure 30.- Concluded.

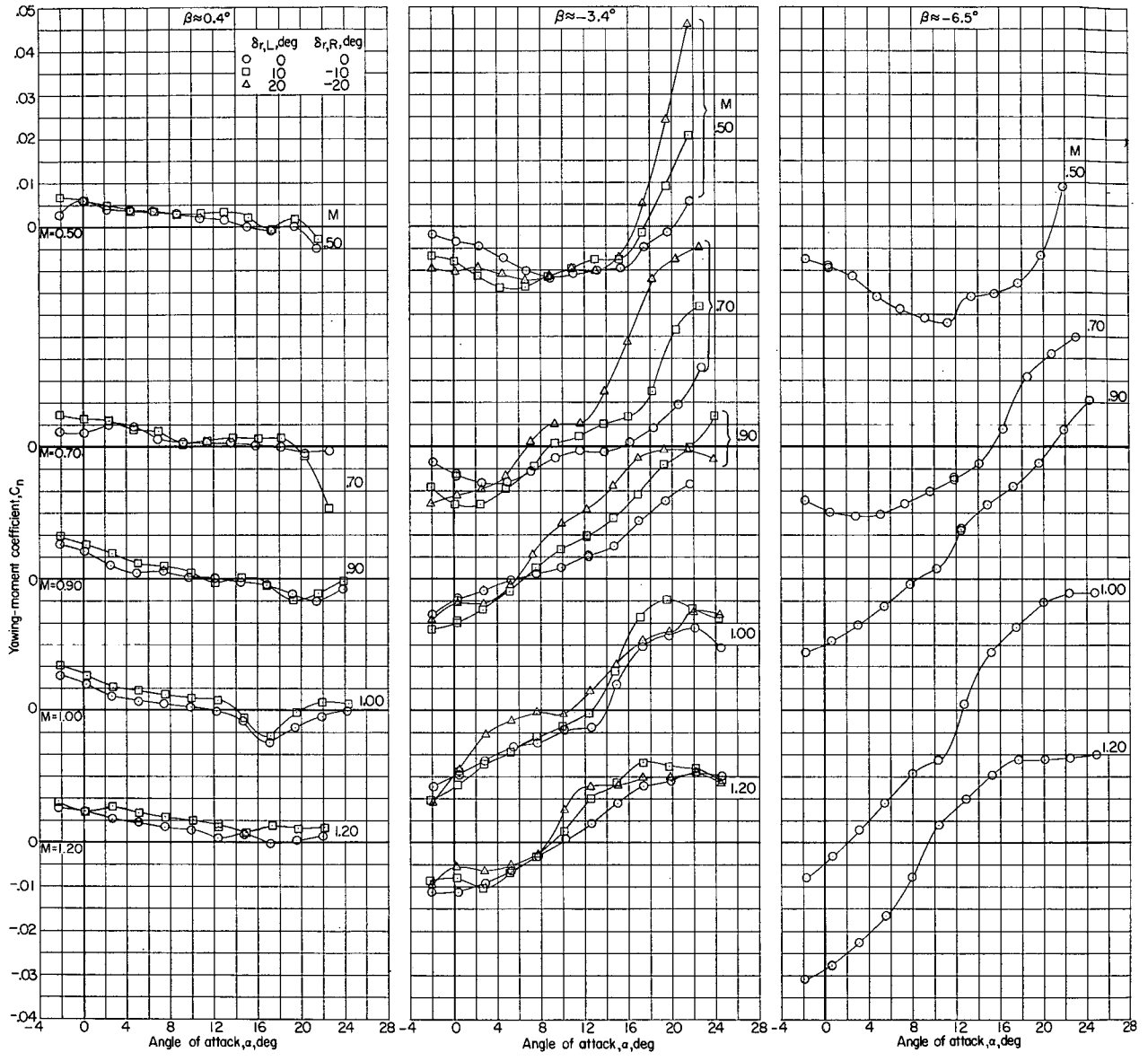

(a) C_n against α.

Figure 31.- Effect of differential rudder deflection on lateral aerodynamic characteristics. Configuration 3 (basic outboard and central vertical tails on, canopy on); $\delta_u = -30^\circ$; $\delta_l = 20^\circ$.

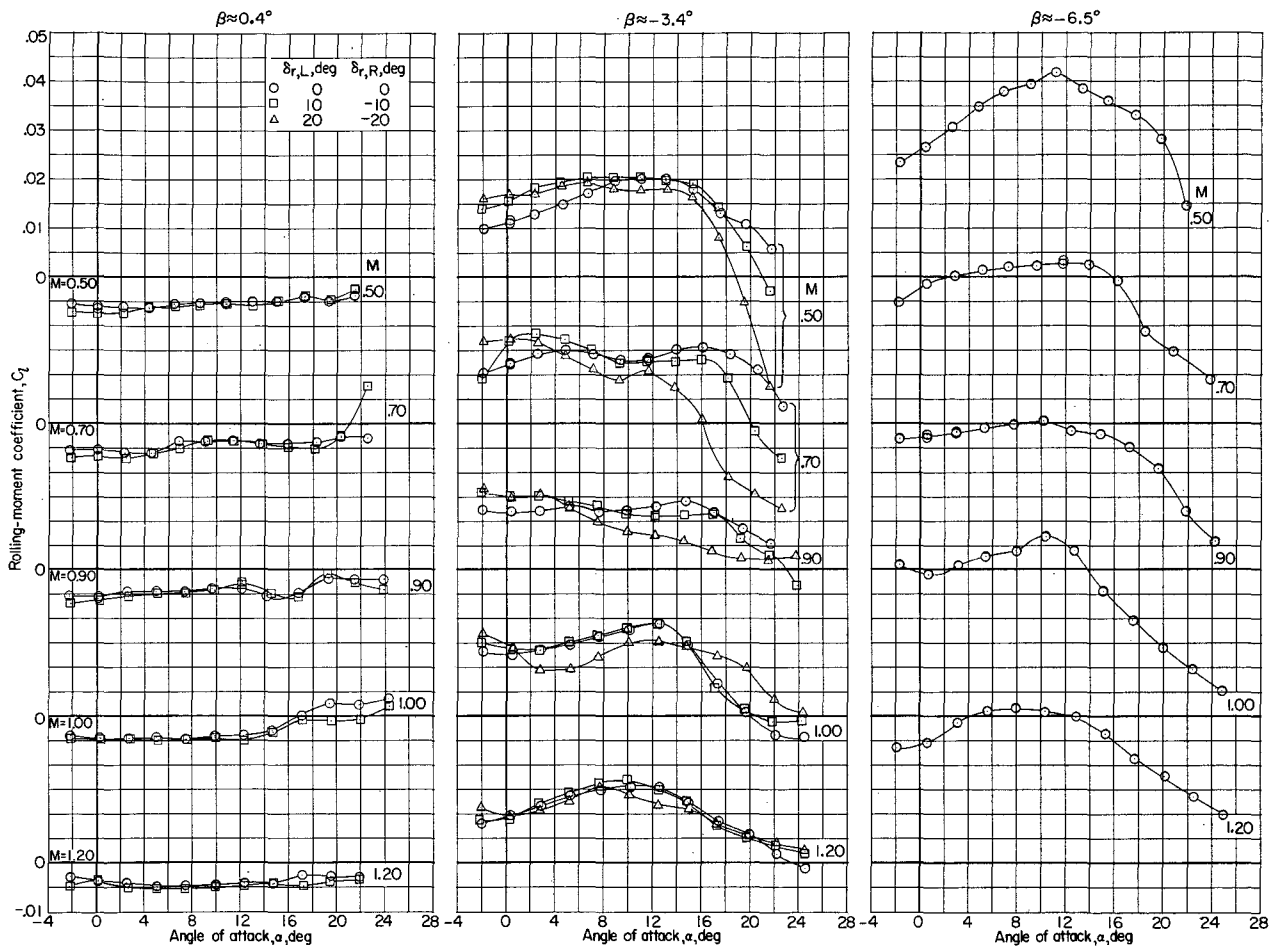

(b) C_l against α.

Figure 31.- Continued.

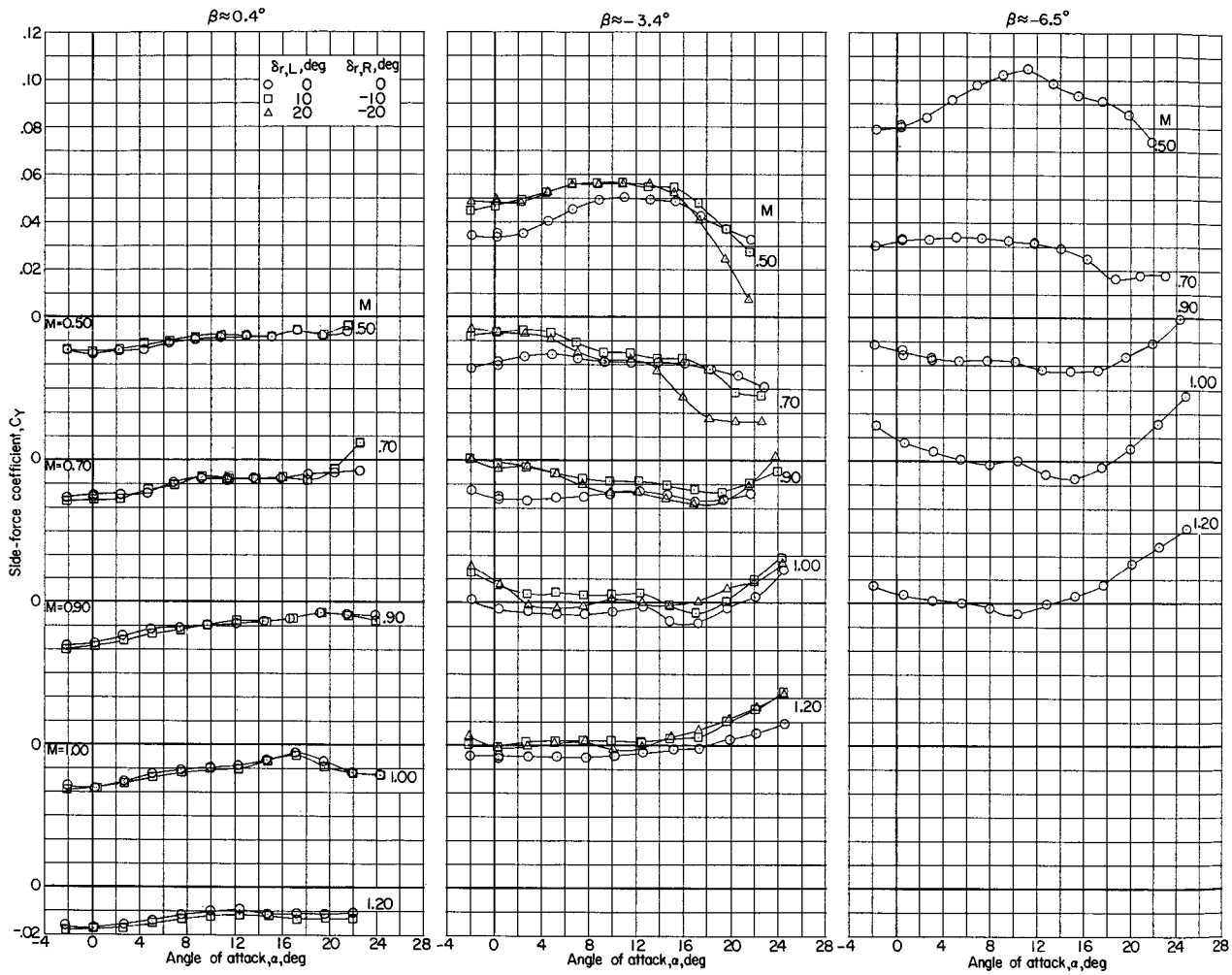

(c) C_Y against α.

Figure 31.- Concluded.

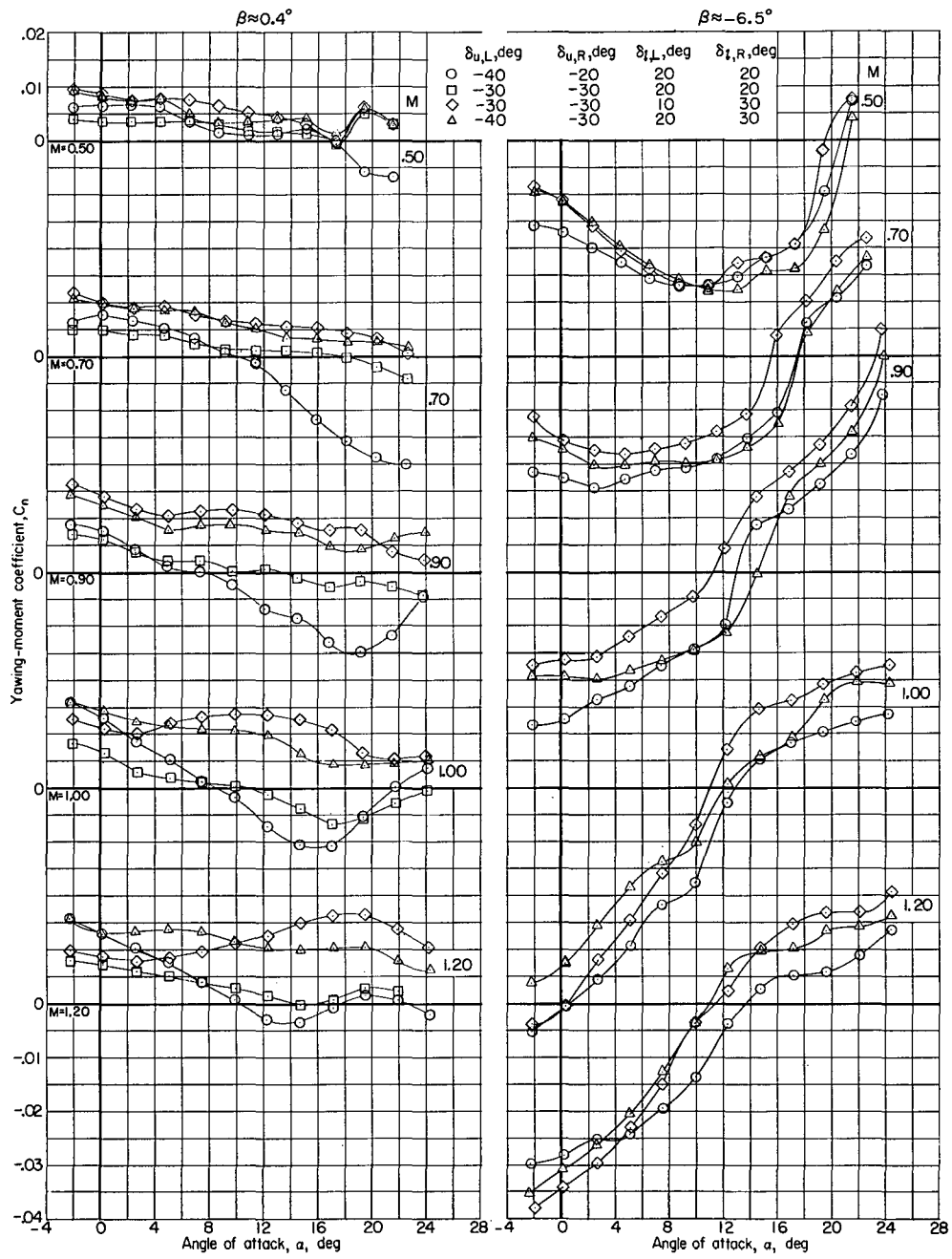

(a) C_n against α.

Figure 32.- Effect of differential flap deflection on lateral aerodynamic characteristics. Configuration 4 (basic outboard and central vertical tails on, canopy off); $\delta_r = 0^\circ$.

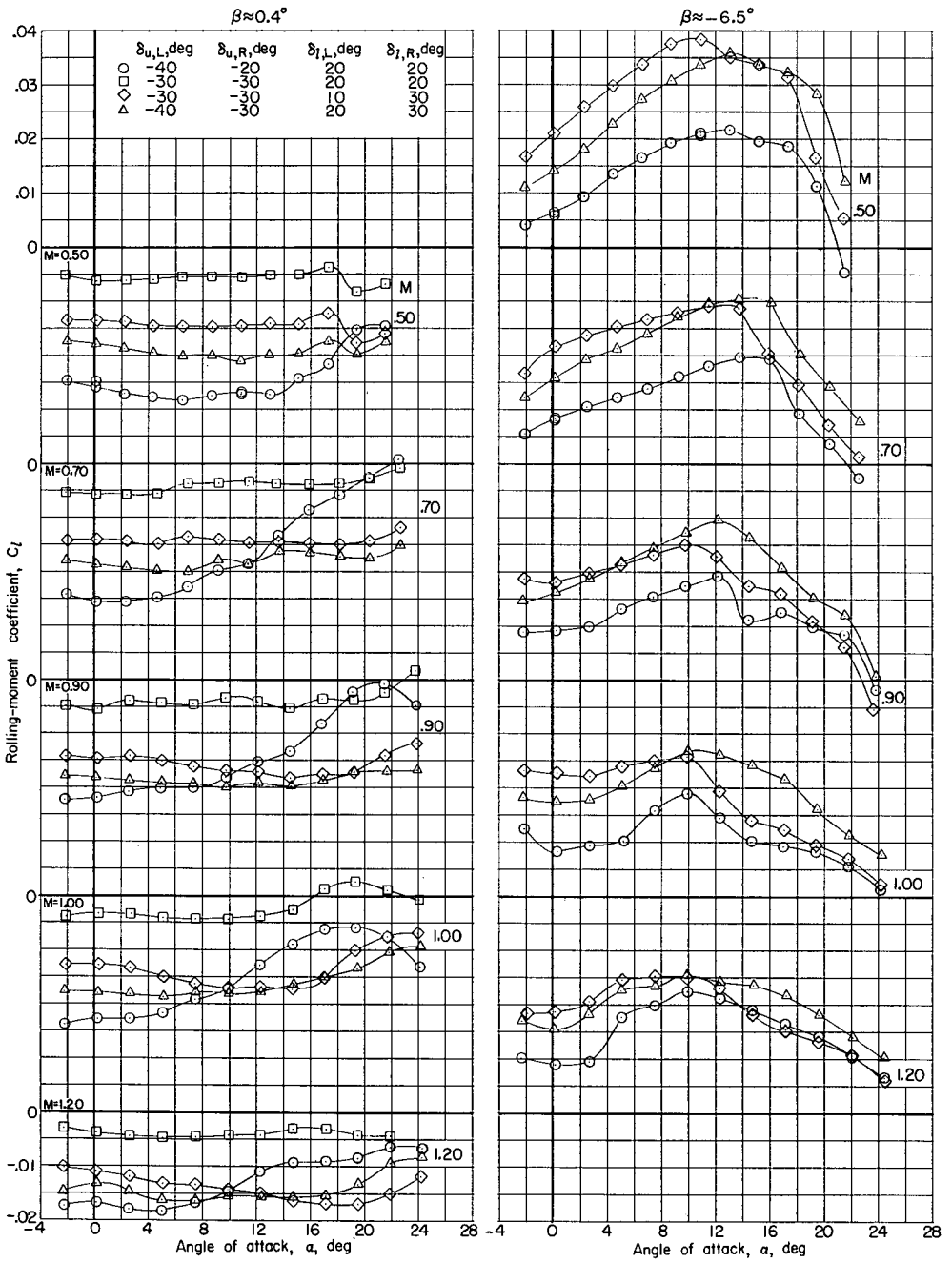

(b) C_l against α.

Figure 32.- Continued.

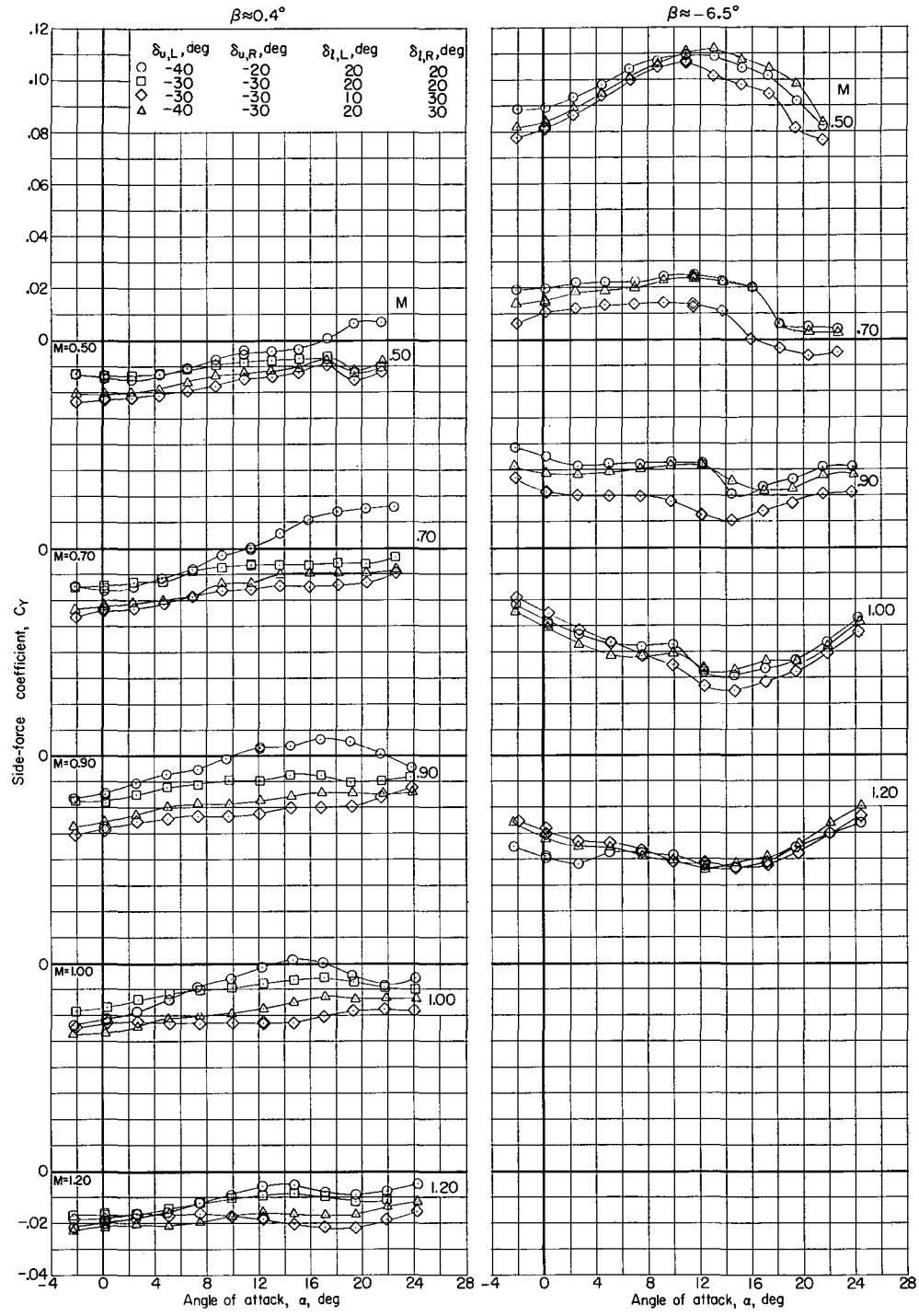

(c) C_Y against α.

Figure 32.- Concluded.

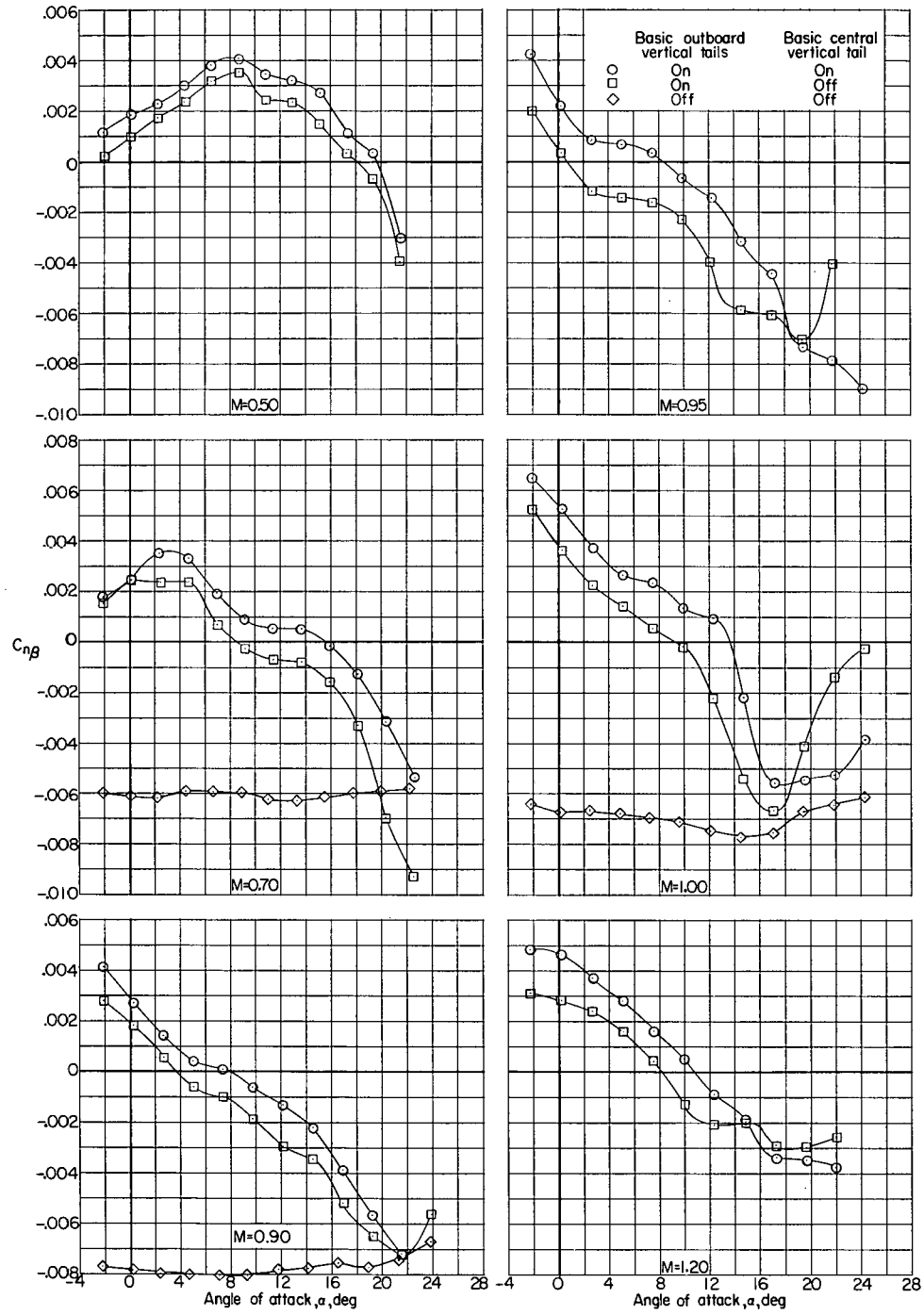

(a) C_{n_β} against α.

Figure 33.- Effect of basic outboard and central vertical tails on lateral-stability derivatives. Configurations 1, 2, and 3 (canopy on); $\delta_u = -30^\circ$; $\delta_l = 20^\circ$; $\delta_r = 0^\circ$.

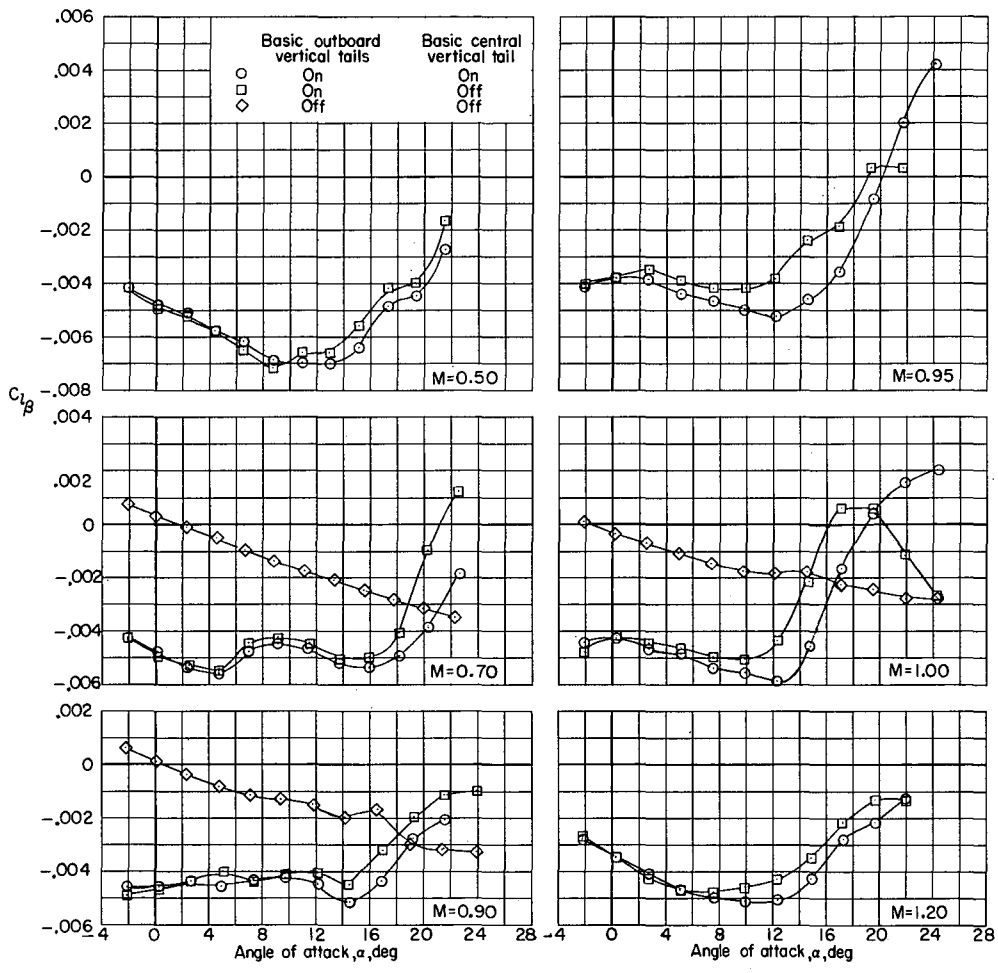

(b) C_{l_β} against α.

Figure 33.- Concluded.

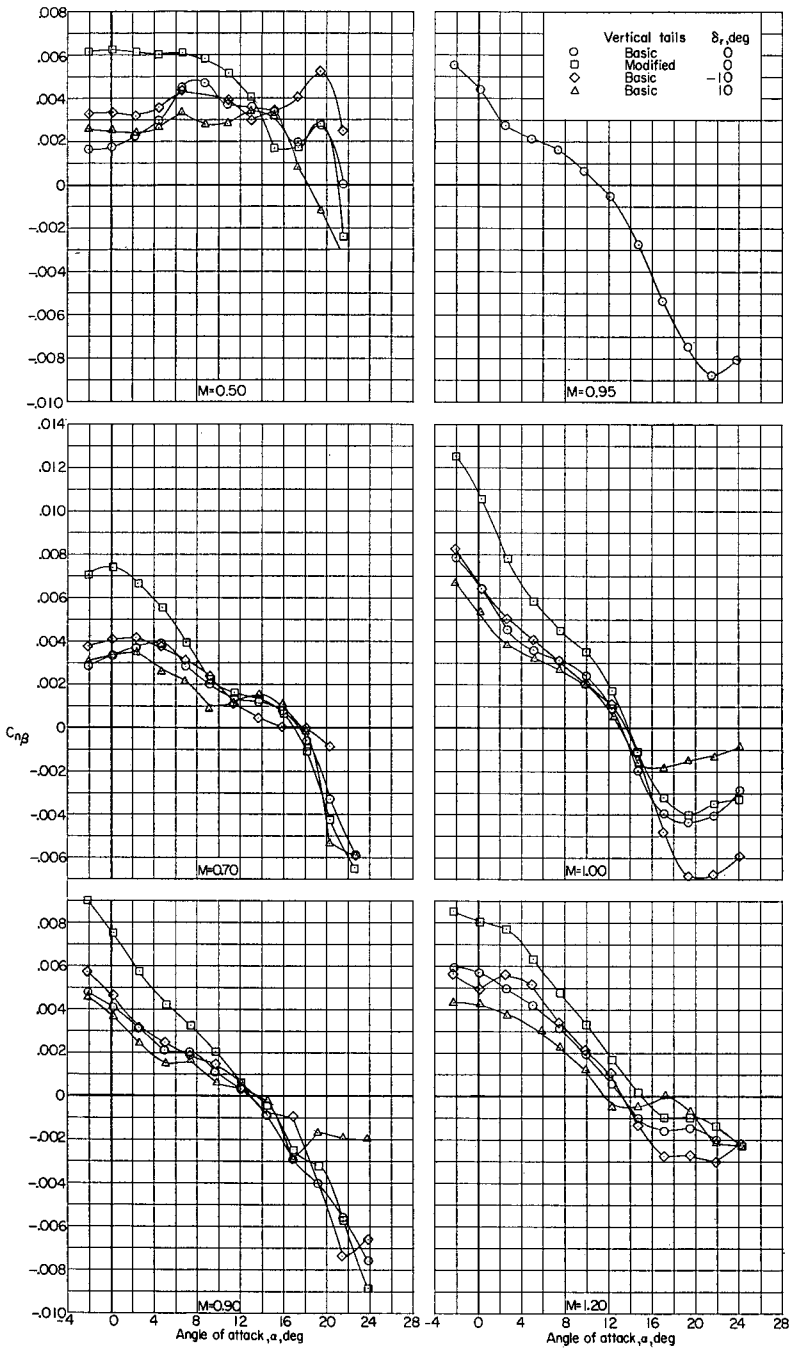

(a) C_{n_β} against α.

Figure 34.- Effects of modified outboard and central vertical tails and rudder deflection on lateral-stability derivatives. Configurations 4 and 5 (canopy off); $\delta_u = -30^\circ$; $\delta_l = 20^\circ$; $\delta_r = 0^\circ$.

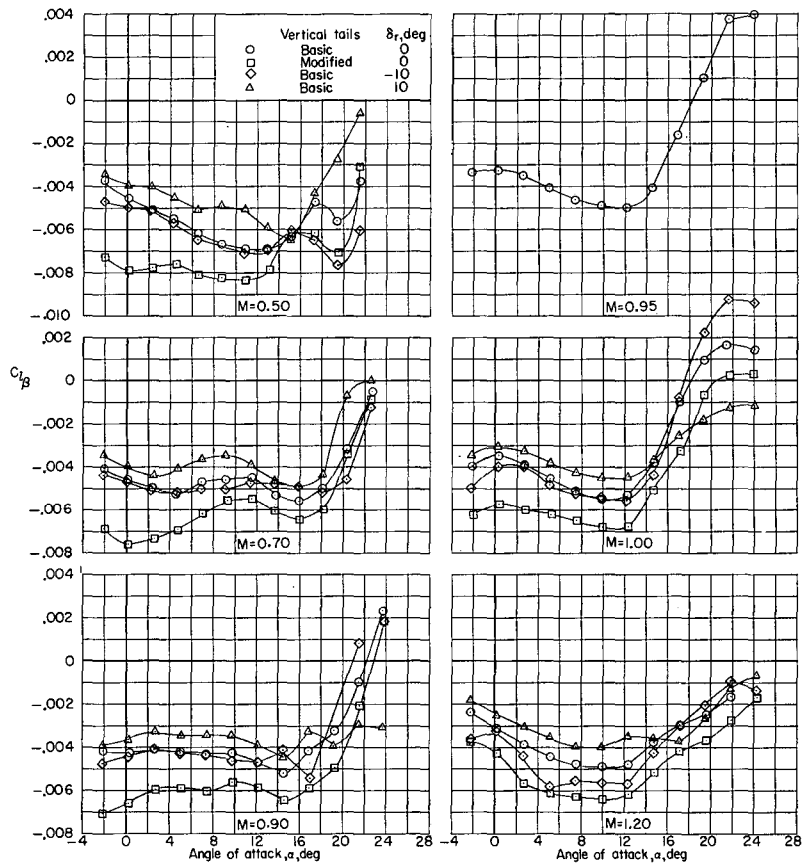

(b) C_{l_β} against α.

Figure 34.- Concluded.

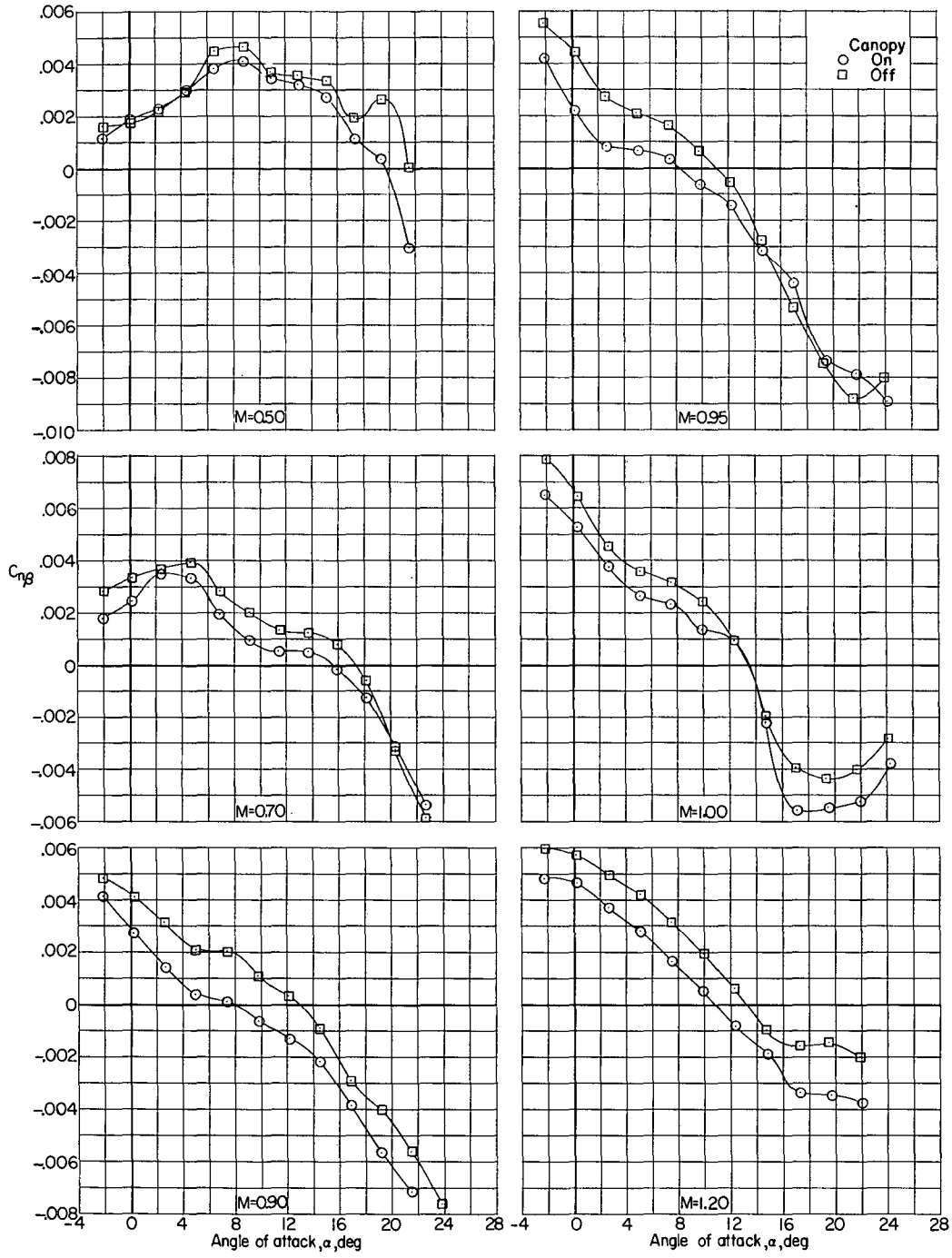

(a) C_{n_β} against α.

Figure 35.- Effect of canopy on lateral-stability derivatives. Configurations 3 and 4 (basic outboard and central vertical tails); $\delta_u = -30^\circ$; $\delta_l = 20^\circ$; $\delta_r = 0^\circ$.

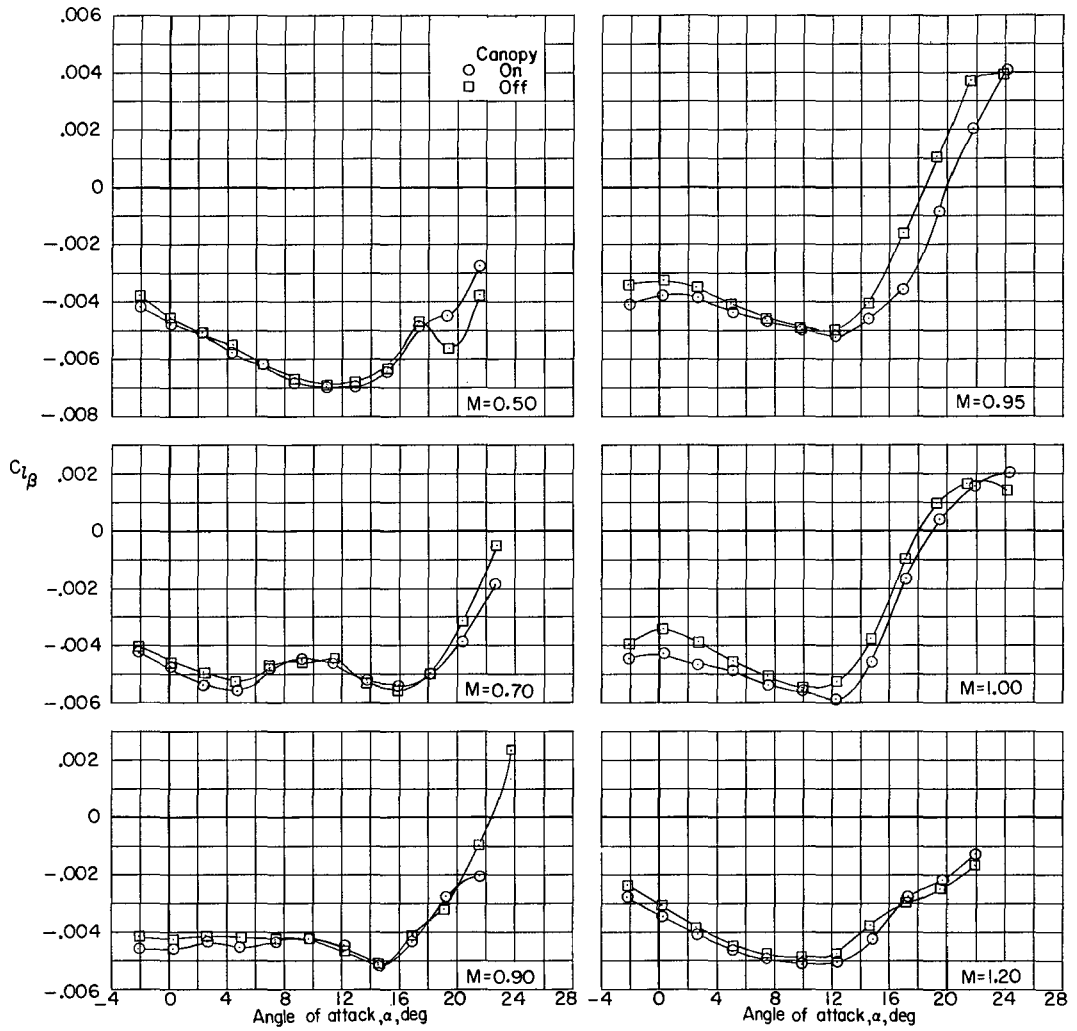

(b) C_{l_β} against α.

Figure 35.- Concluded.

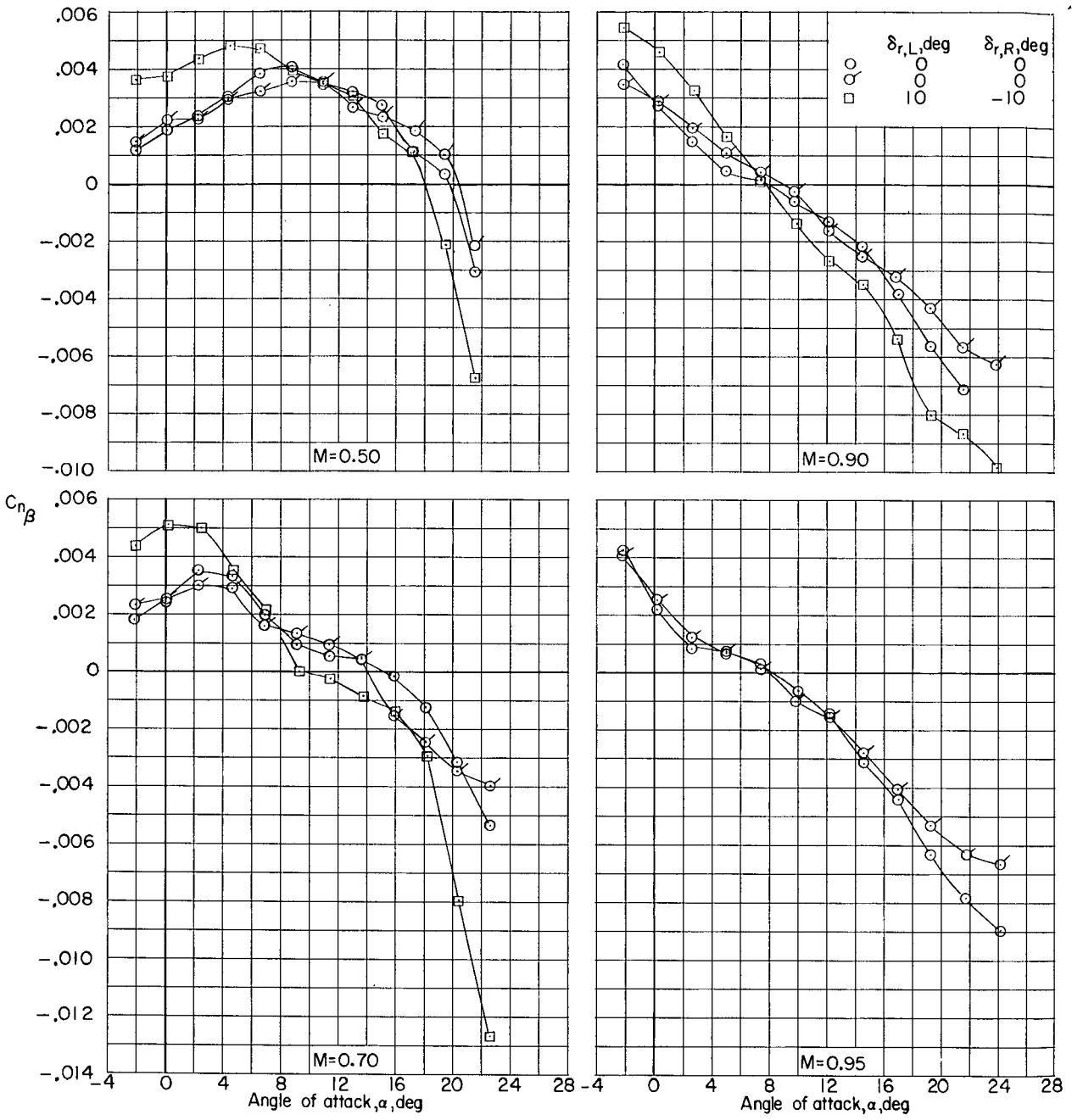

(a) C_{n_β} against α.

Figure 36.- Effect of differential rudder deflection on lateral-stability derivatives. Configuration 3 (basic outboard and central vertical tails on, canopy on); $\delta_u = -30^\circ$; $\delta_l = 20^\circ$. (The plain symbols indicate average slope values from $\beta \approx -3.4^\circ$ to $\beta \approx 0.4^\circ$, the flagged symbols, from $\beta \approx -6.5^\circ$ to $\beta \approx 0.4^\circ$.)

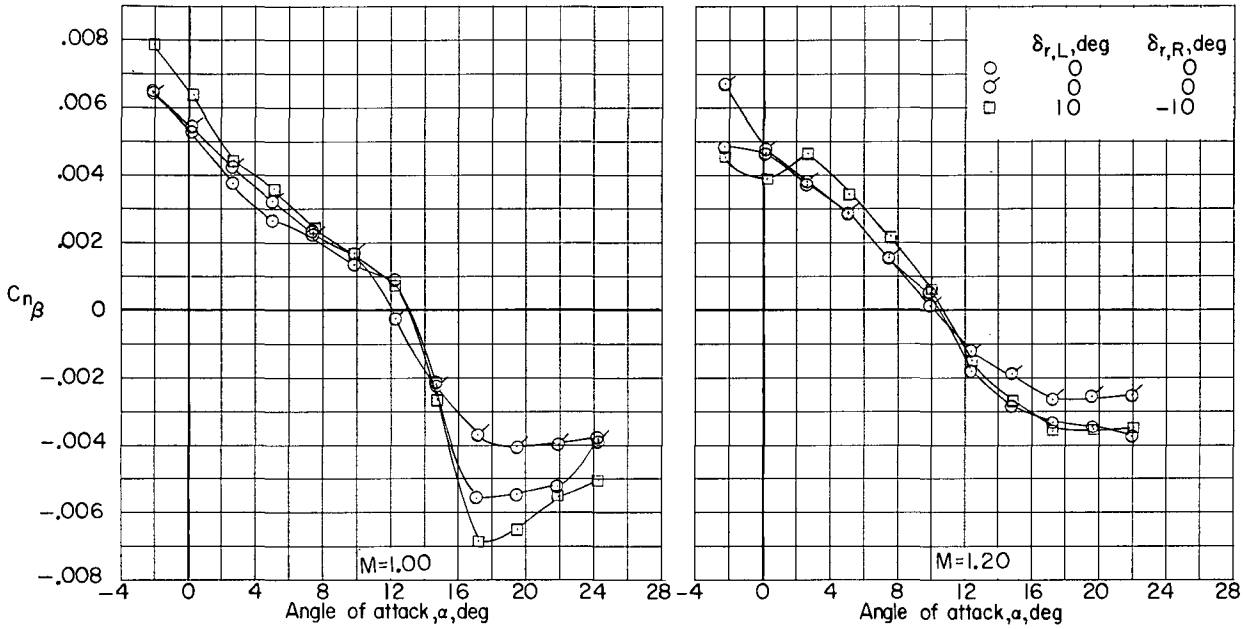

(a) Concluded.

Figure 36.- Continued.

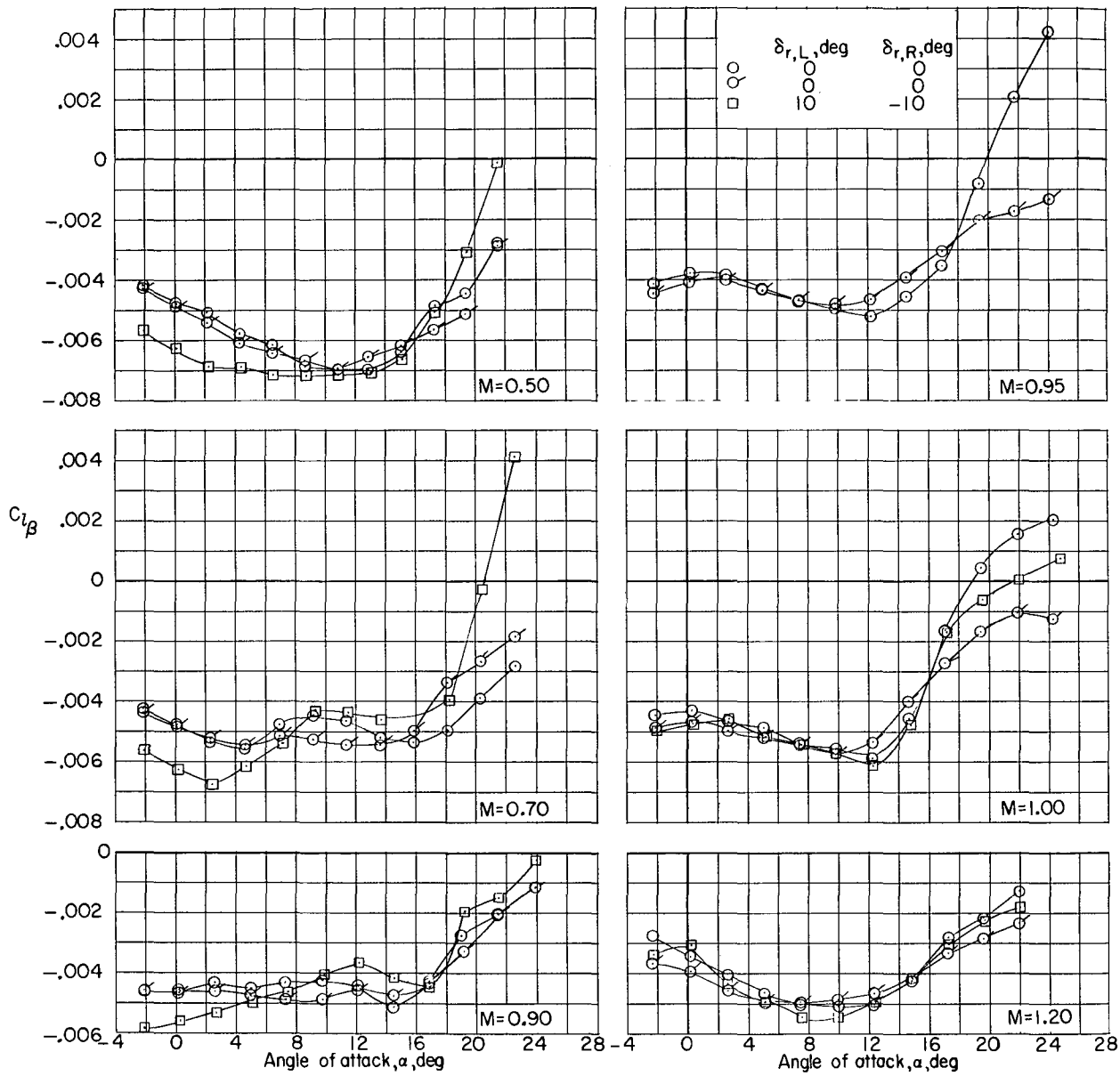

(b) C_{l_β} against α.

Figure 36.- Concluded.

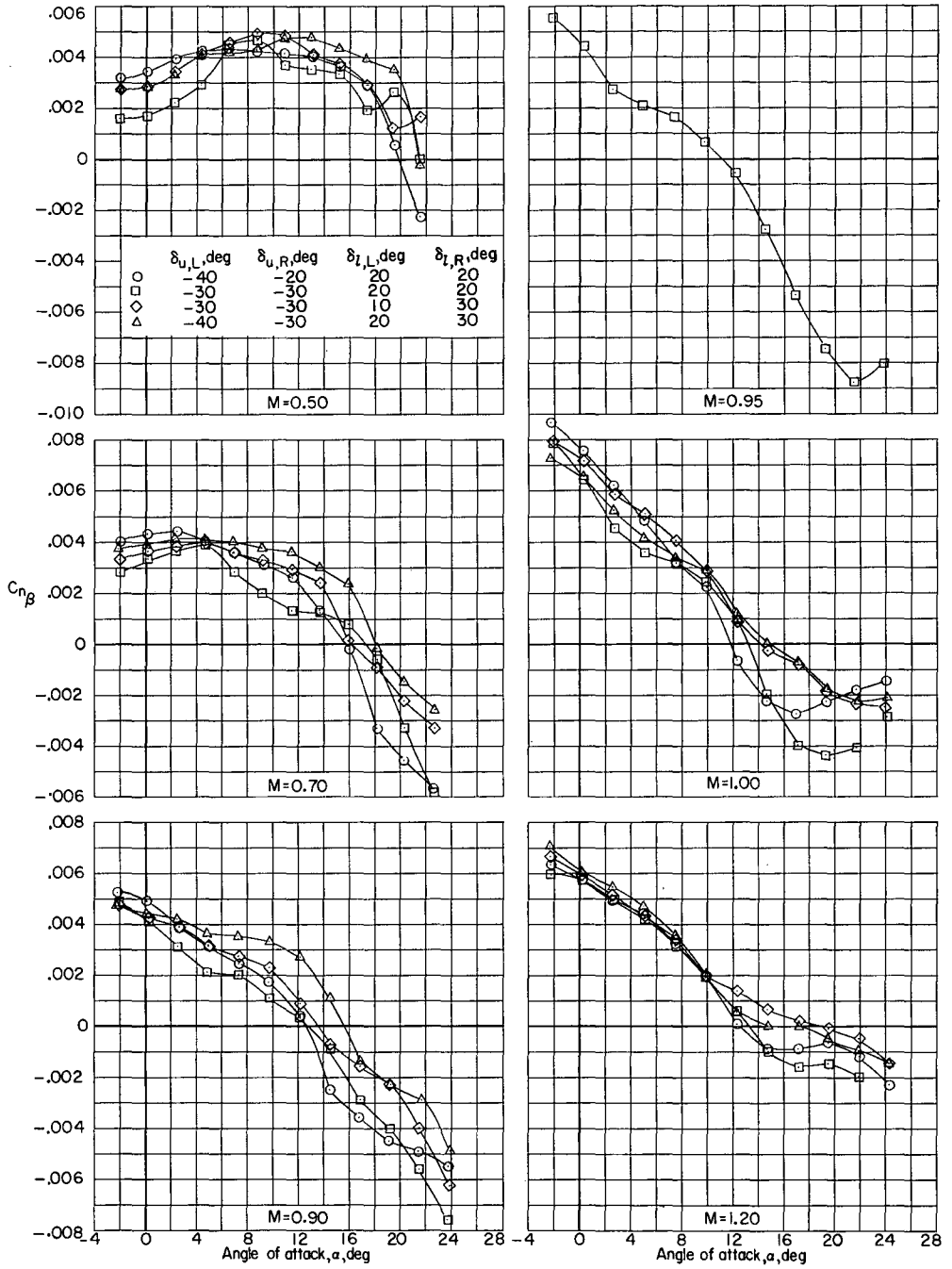

(a) C_{n_β} against α.

Figure 37.- Effect of differential flap deflection on lateral-stability derivatives. Configuration 4 (basic outboard and central vertical tails on, canopy off); $\delta_r = 0^o$.

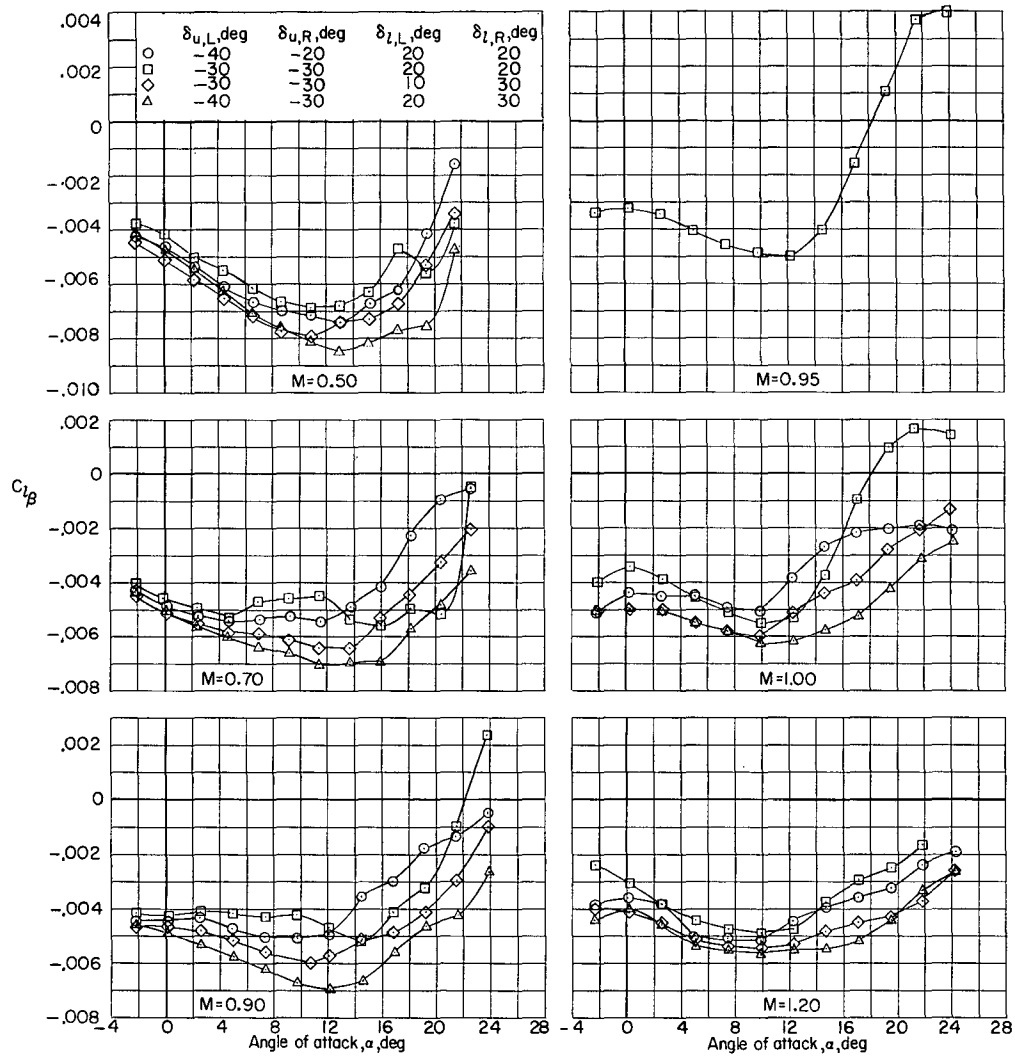

(b) C_{l_β} against α.

Figure 37.- Concluded.

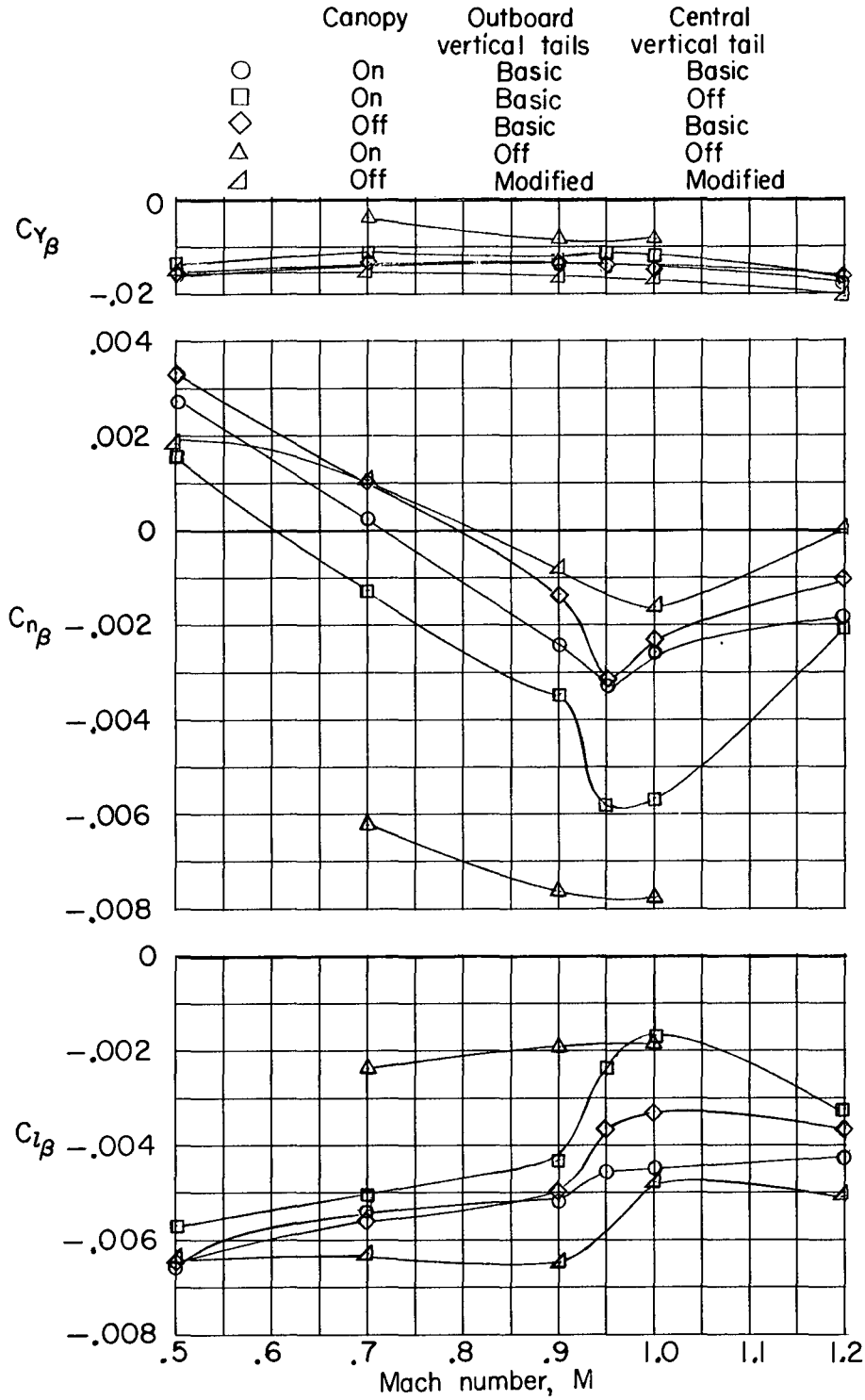

Figure 38.- Effect of model components on lateral-stability derivatives. Configurations 1 to 5; $\delta_u = -30^\circ$; $\delta_l = 20^\circ$; $\delta_r = 0^\circ$; $\alpha = 15^\circ$.

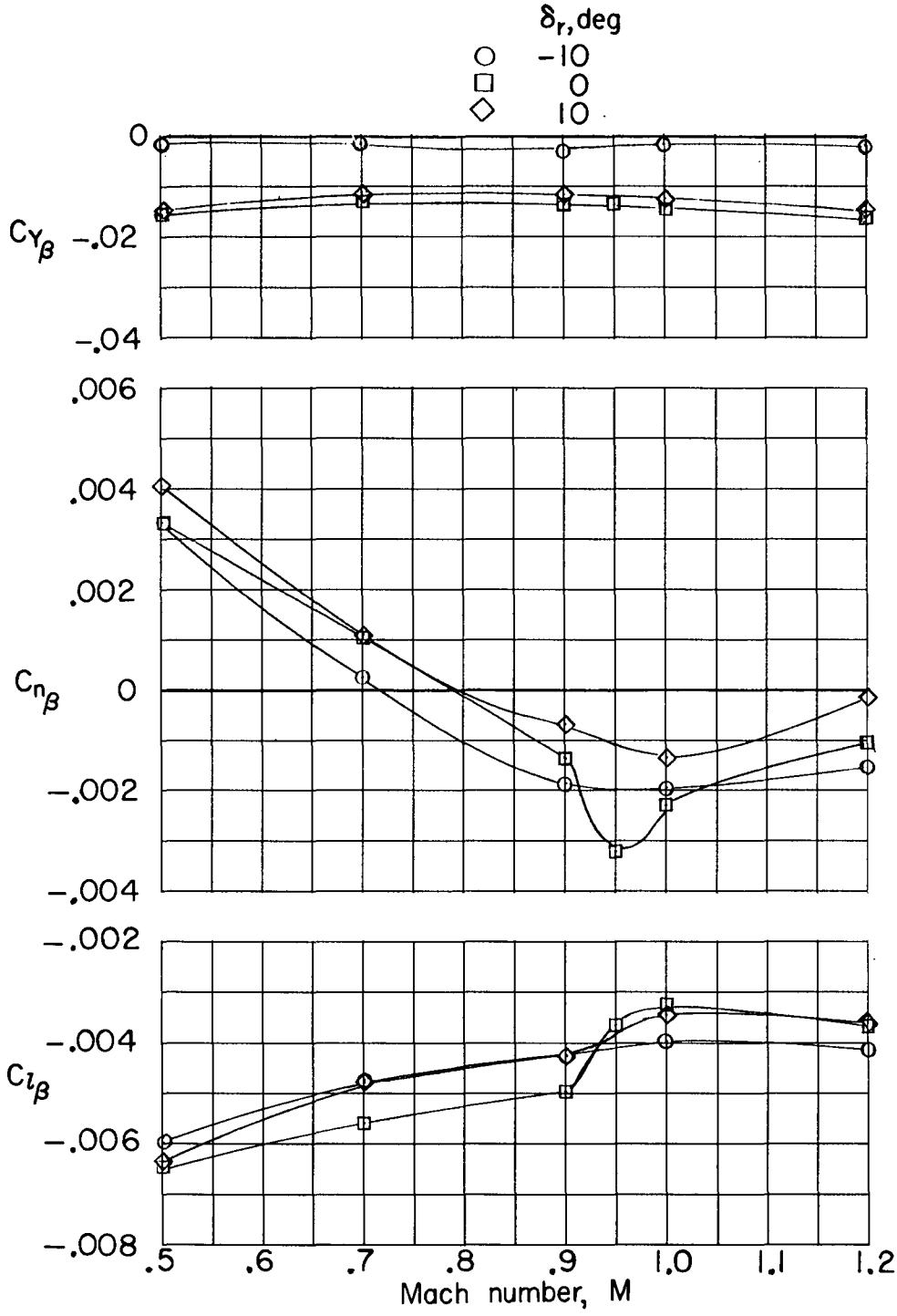

Figure 39.- Effect of rudder deflection on lateral-stability derivatives. Configuration 4 (basic outboard and central vertical tails on, canopy off); $\delta_u = -30^\circ$; $\delta_l = 20^\circ$; $\alpha = 15^\circ$.

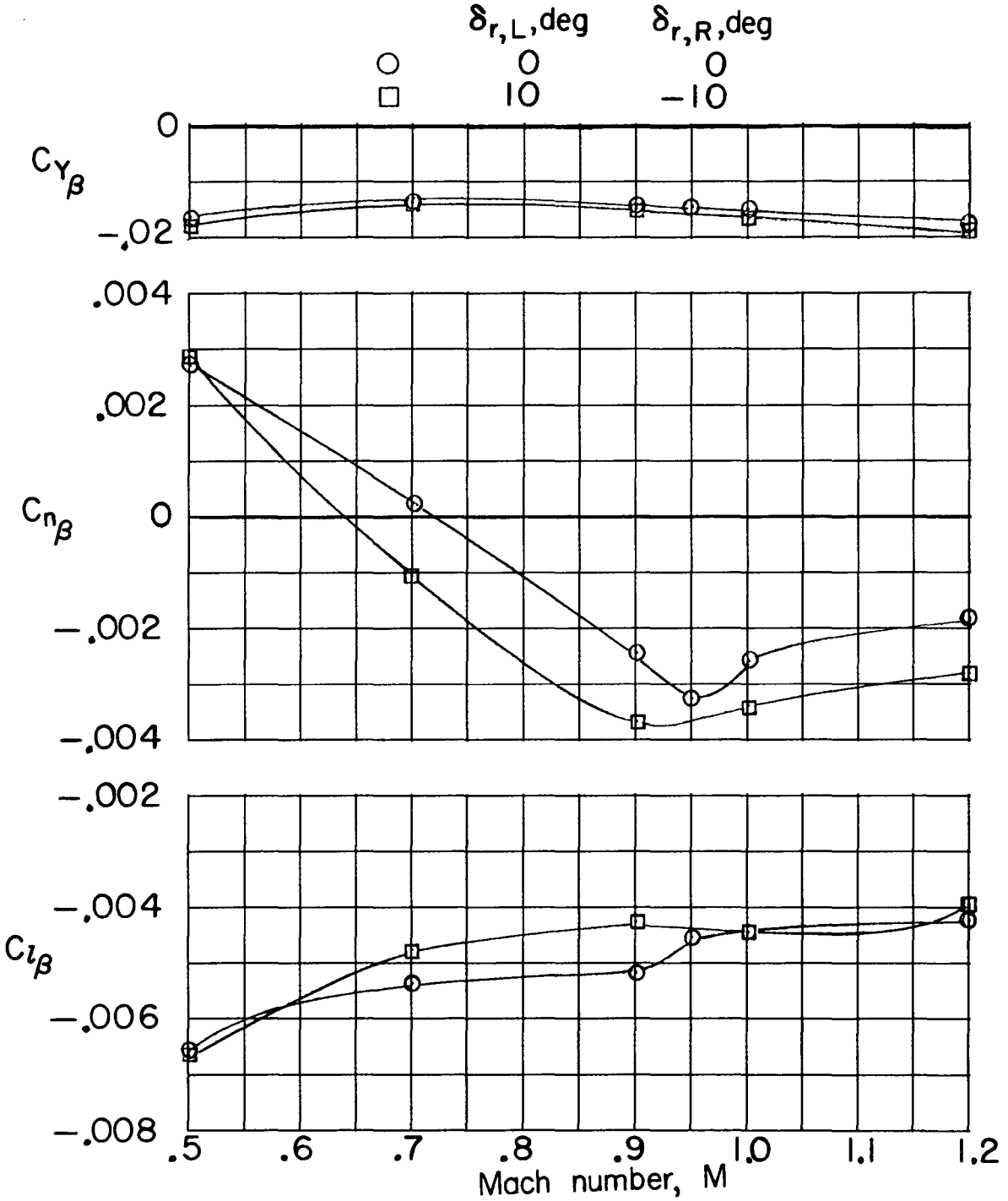

Figure 40.- Effect of differential rudder deflection on lateral-stability derivatives. Configuration 3 (basic outboard and central vertical tails on, canopy on); $\delta_u = -30^\circ$; $\delta_l = 20^\circ$; $\alpha = 15^\circ$.

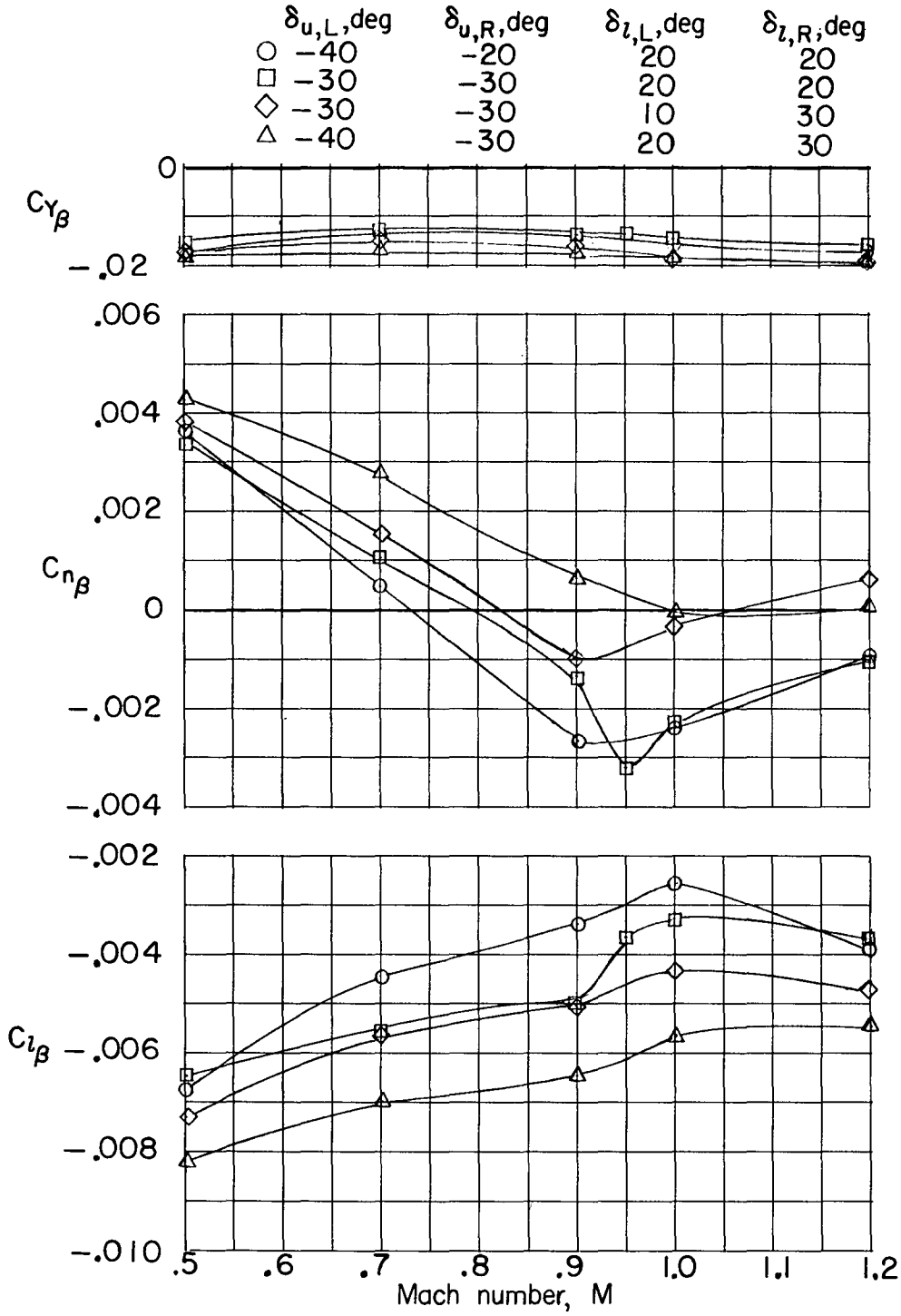

Figure 41.- Effect of differential flap deflection on lateral-stability derivatives. Configuration 4 (basic outboard and central vertical tails on, canopy off); $\delta_r = 0^\circ$; $\alpha = 15^\circ$.